https://ntrs.nasa.gov/search.jsp?R=19930002828 2020-03-17T09:48:16+00:00Z

IN-09
128401
P.64

NASA
Technical
Paper
3274

November 1992

Acoustical Evaluation of the NASA Lewis 9- by 15-Foot Low Speed Wind Tunnel

Milo D. Dahl
and Richard P. Woodward

(NASA-TP-3274) ACOUSTICAL EVALUATION OF THE NASA LEWIS 9 BY 15 FOOT LOW SPEED WIND TUNNEL (NASA). 64 p

N93-12016

Unclas

H1/09 0128401

462 602

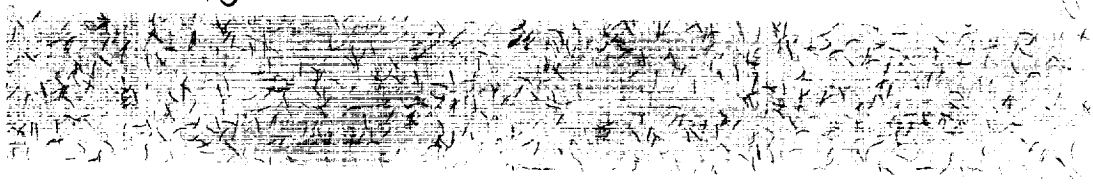

NASA

NASA Technical Paper 3274

1992

Acoustical Evaluation of the NASA Lewis 9- by 15-Foot Low Speed Wind Tunnel

Milo D. Dahl
and Richard P. Woodward
Lewis Research Center
Cleveland, Ohio

National Aeronautics and Space Administration
Office of Management
Scientific and Technical Information Program

Trade names or manufacturers' names are used in this report for identification only. This usage does not constitute an official endorsement, either expressed or implied, by the National Aeronautics and Space Administration.

Summary

The test section of the NASA Lewis 9- by 15-Foot Low Speed Wind Tunnel was acoustically treated to allow the measurement, under simulated free-field conditions, of acoustic sources within the tunnel test section. The treatment was designed to absorb sound at frequencies above 250 Hz and to withstand tunnel airflow velocities up to Mach 0.2. Nominal treatment depth was 34.4 cm; however, small regions of the treatment were made shallower to accommodate tunnel structural members. Evaluation tests with no tunnel airflow were conducted in the test section to assess the performance of the installed treatment. The low-speed airflows during test section operation would not significantly affect the results from the static acoustic evaluation measurements. Thus, these results were representative of the acoustic treatment performance at Mach 0.2. Evaluation tests included using time-delay spectrometry (TDS) to measure the effects of early and late reflections on the measurement of the incident signal and using decay with distance measurements to determine the extent of the acoustic free field. The early reflections were those that arrived at a microphone in the test section after reflecting off the treated and untreated surfaces in the test section. The late reflections were those that arrived at a microphone after leaving the test section, reflecting off some part of the tunnel structure upstream or downstream of the test section, and returning to the test section. Decay with distance measurements were performed with both broadband and pure-tone noise sources.

The early reflections (from within the test section) created interference patterns in the frequency response of the incident signal from the acoustic source. The interference ripple about the incident signal for five measurement setups varied on average from 1.7 to 3.2 dB wide from minimum to maximum level for measurements over a 500- to 5150-Hz frequency range. Using time-delay spectrometry, the early reflections were identified as coming from specific locations on the treatment, and their effects depended on the behavior of the treatment at those locations. Late reflections, from upstream and downstream of the test section, were insignificant for measurements at a microphone well within the test section; especially if the frequency resolution of the acoustic analysis is greater than 10 Hz. For acoustic sources with low directivity characteristics, decay with distance measurements in the test section show that incident free-field behavior can be measured on average with an accuracy of ± 1.5 dB or better at source frequencies from 400 Hz to 10 kHz. The free-field variations are typically much smaller with an omnidirectional source.

Introduction

The acoustic characteristics of wind tunnel test sections are an important consideration in the measurement of model aircraft propulsion system noise. Under simulated flight conditions, it is desirable to measure the acoustic field magnitude and directivity to characterize the noise source fully. This is not possible if acoustic reflections from the wind tunnel walls interfere with the direct sound from the test model. The solution for reducing interfering reflections has been to line the test section walls with an acoustic material that absorbs the incident sound waves and minimizes the level of any reflections.

The NASA Lewis 9- by 15-Foot Low-Speed Wind Tunnel was designed for determining the aerodynamic performance of aircraft propulsion systems and components at both takeoff and approach conditions. Since community noise is an important consideration during takeoff and approach, the wind tunnel test section was lined with acoustic material which permitted the measurement of the acoustic characteristics of propulsion systems at these conditions. The tunnel test section was originally lined with 3.8-cm-thick fiberglass acoustic material to allow for the measurement of the directivity of the inlet noise from turbofan engines (ref. 1). The lining was designed to reduce acoustic reflections above frequencies of 1000 Hz. When interest was renewed in high-speed turboprop propulsion systems and new-general aviation propellers, it became necessary to redesign the acoustic treatment of the tunnel test section in order to accommodate the lower frequency noise generated by the propellers. The treatment design goals were to improve the treatment absorption coefficients at low frequencies to 0.97 or higher and to reduce reflections so that measurements could be made in the test section at frequencies above 250 Hz. To meet this goal, the treatment depth was increased, where possible, from 3.8 to 34.4 cm, and the fiberglass was replaced with a bulk fibrous material that could withstand the environmental conditions in the test section without breaking down and dispersing into the flow. This design was developed with the aid of both an analytical bulk-absorber treatment model (to predict treatment impedances and absorption coefficients) and low-frequency absorption measurements of treatment samples (ref. 2). To verify that the

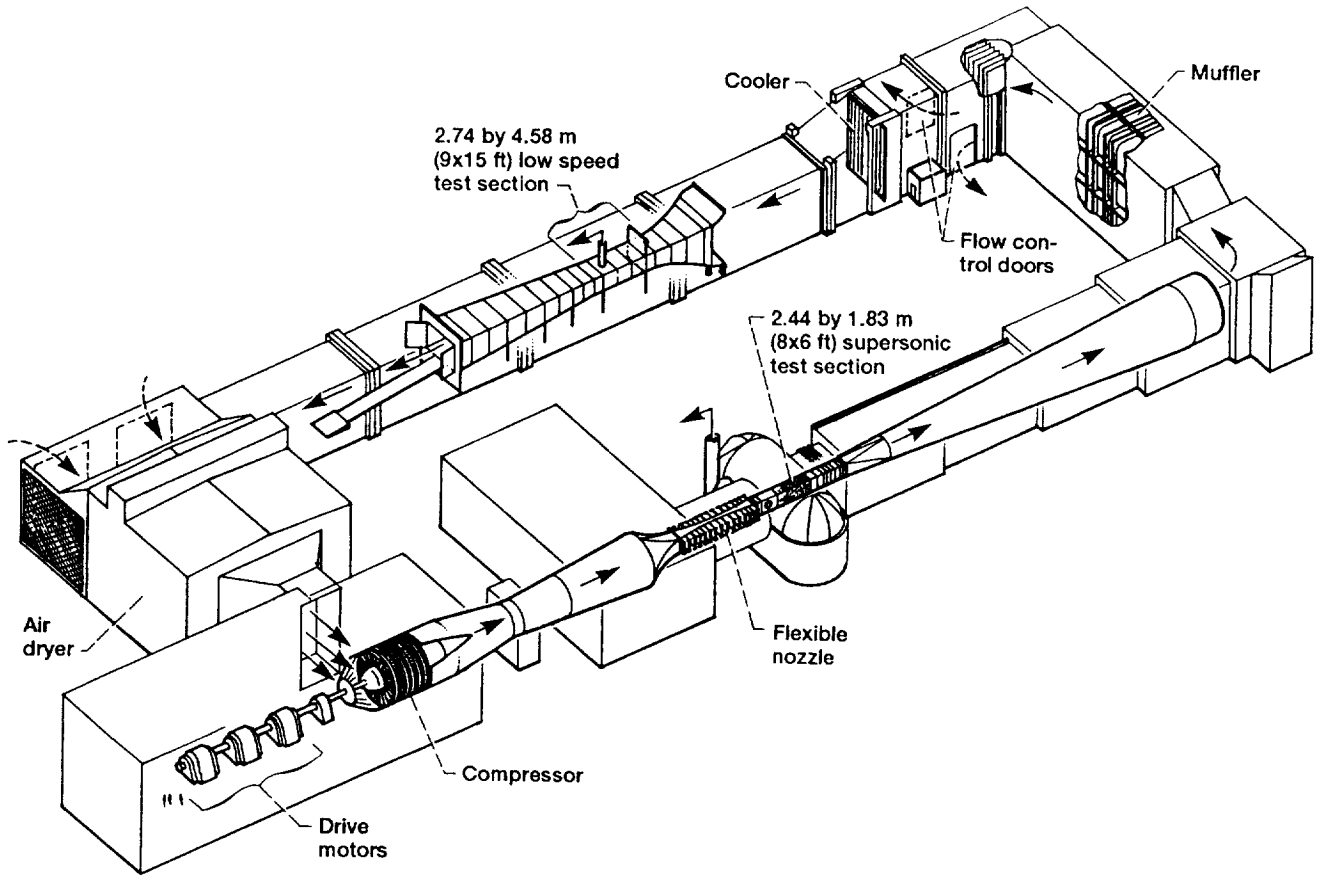

(a)

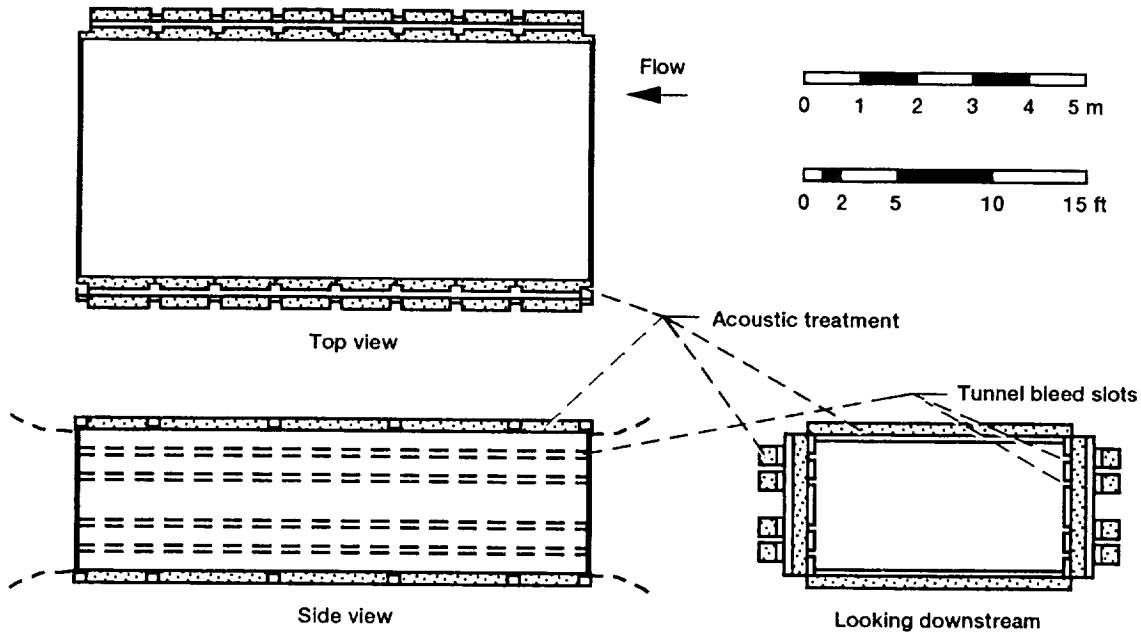

(b)

(a) NASA Lewis 9- by 15-Foot and 8- by 6-Foot Wind Tunnels.
(b) Sectional views of the 9- by 15-Foot Low-Speed Wind Tunnel test section.

Figure 1.—Design of NASA Lewis anechoic wind tunnel.

treatment design goals were achieved, the impedances and the absorption coefficients of the treatment were measured after the treatment was installed in the test section. The results presented in reference 3 showed that the installed acoustic treatment had absorption coefficients greater than 0.95 over the frequency range from 250 Hz to 4 kHz. These results were in good agreement with the predictions from the analytical model. What remained, however, was the measurement of the acoustic field characteristics of the treated test section, which is the subject of this report.

Acoustically treated wind tunnel test sections are commonly evaluated to assess the performance of the installed treatment. The data from such tests typically include measurements of the extent of the acoustic free field from a noise source (refs. 1 and 4 to 8) (also commonly called the decay of sound with distance from the source), the reverberation time (refs. 1, 5, and 7), the levels of the first early reflections from the treated test section walls (refs. 7 to 9), and measurements of a calibrated source in the test section (refs. 4 and 10). The acoustical evaluation of the tunnel test section involved measurements of the extent of the acoustic free field (from both broadband and pure-tone acoustic sources) and of the levels of the first early reflections; however, no measurements were made of the reverberation time nor were measurements taken using a calibrated source. The measurement of reverberation time requires that the sound field be statistically well-mixed, a condition that does not exist in the 9- by 15-ft test section, an open-ended test section with highly absorbent walls. In addition to early reflections, measurements were made of possible late reflections that may enter the test section due to sound from a source in the test section reflecting off a tunnel structure upstream or downstream of the test section.

After the test section and treatment are described, the first set of measurements which acoustically evaluate the test section for the effects of early and late reflections are discussed. This is followed by a summary of the results of the acoustic evaluation using steady acoustic sources and using measurements of the decay of sound with distance from the source. In appendixes A to C, detailed results are given of the measurements.

Description of Test Section and Acoustic Treatment

The test section of the 9- by 15-Foot Low-Speed Wind Tunnel is located in the low-speed return leg of the 8- by 6-Foot Supersonic Wind Tunnel (fig. 1(a)). The test section is 2.74-m high by 4.58-m wide by 8.75-m long. The airflow through the test section has a nominal maximum Mach number of 0.2. Four horizontal bleed slots, 10.1 cm wide, extend along each vertical wall for the full length of the test section. Further details on the tunnel may be found in reference 11.

Sectional views of the test section with treatment are shown in figure 1(b). The floor and ceiling are completely treated except where model supports would protrude through the treatment. For the walls additional treatment is located behind the bleed slots in order to reduce reflections from sound entering the slots from the test section.

The acoustic treatment consists of boxes with perforated-plate facing to hold the acoustic bulk-absorber material, called Kevlar. A typical example is shown in figure 2. The boxes were designed to fit among, and be supported by, the structural beams of the wind tunnel. Consequently, the boxes near structural beams were shallower than 34.4 cm. Approximately 95 percent of the thin treatment had a depth of 5.1 cm. The remaining thin treatment boxes had customized depths to enable the boxes to fit among the structural beams. For the typical full depth of 34.4 cm, the treatment consisted of two layers of bulk absorber, each 17.2 cm thick. As can be seen in figure 2, the structure of the treatment from the front facing to the hard metal backing was (1) perforated facing plate, (2) 20-mesh screen (1.3-mm center-to-center wire spacing), (3) first layer of bulk absorber (nominal bulk density, 6.4 kg/m^3), (4) perforated separator plate, and (5) a second layer of bulk absorber (nominal bulk density, 17.7 kg/m^3). The facing and the separator plates were 0.16 cm thick and were perforated with 0.32-cm-diameter holes creating an open area of 40 percent. The front perforated plate was backed by a 20-mesh screen, used as an additional measure to prevent any fibers from the bulk absorber from getting into the flow stream. A varnish spray was used to attach the screen to the first sheet of bulk-absorber material. For acoustic boxes near structural beams, the treatment was less deep than the 17.2 cm of the first bulk-absorber layer but of the same nominal bulk density. The example box in figure 2 shows the 5.1-cm depth treatment at both ends of the box. Finally, tube spacers with tie bolts were passed through the treatment (1) to add structural support, (2) to help keep the bulk-absorber material from sagging, and (3) to keep the separator plate in place (fig. 2).

Acoustic Evaluation—Early and Late Reflections

The acoustical evaluation of the tunnel test section was conducted with no airflow through the test section. As stated previously, the test section was designed to accommodate an airflow of Mach 0.2. Airflows of this amount, or less, would not significantly affect the results of the static acoustic evaluation measurements taken here. However, the airflow would increase the background noise that a microphone would measure in the test section. This is a separate limitation on the ability to measure a low level acoustic source in the test section in addition to the effects of reflections off wind tunnel surfaces.

The acoustic source for these measurements was a low-frequency acoustic driver with and without an attached exponential horn. The driver had a usable frequency response from 150 Hz to about 7 kHz. The exit of the driver and the

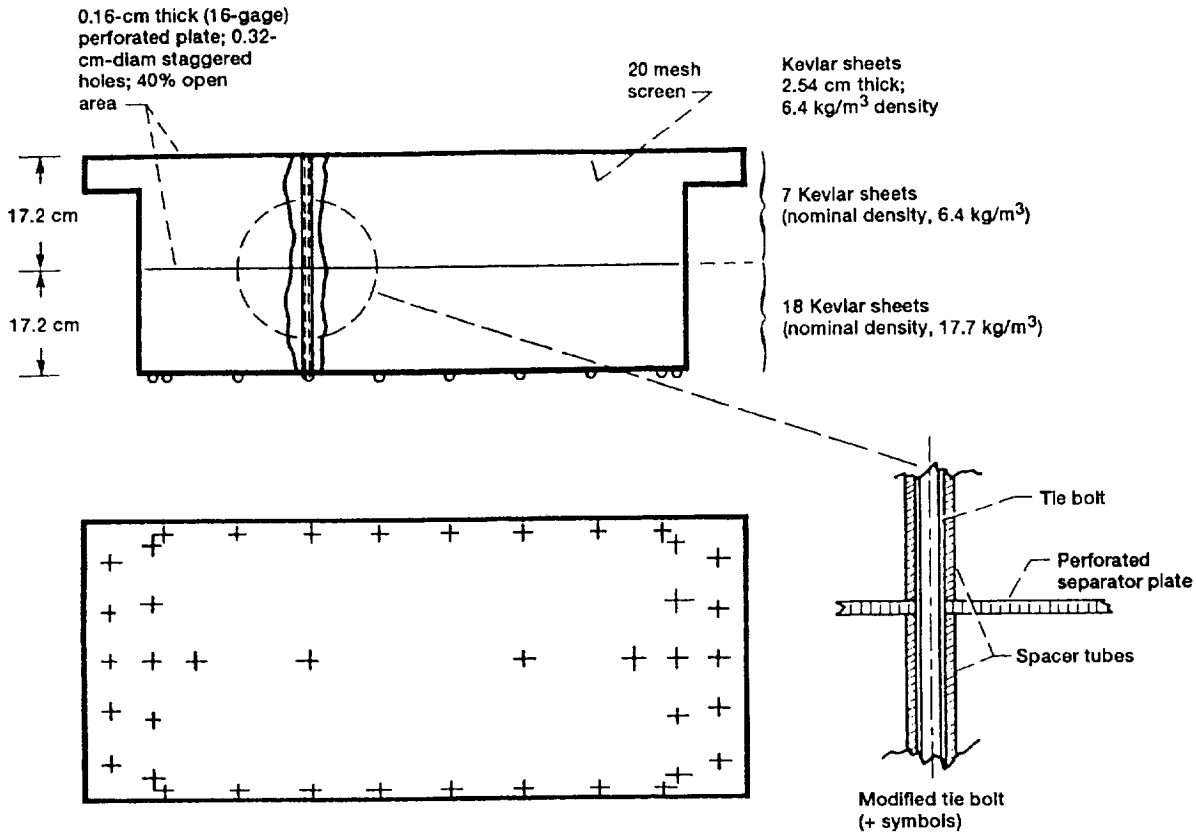

Figure 2.—Typical acoustic treatment box for the 9- by 15-Foot Wind Tunnel test section.

throat of the exponential horn had a diameter of 8.1 cm. The horn mouth, or exit, was 17.8- by 17.8-cm square. The sound produced by this source was measured with a 0.64-cm-diameter condenser microphone.

Measurement Technique

The first set of evaluation measurements was conducted to determine the effects of early and late reflections on the measurement of the incident signal from an acoustic source in the test section. The early reflections were those that arrived at a microphone in the test section after reflecting off the treated and untreated surfaces in the test section. The late reflections were those that arrived at a microphone after leaving the test section, reflecting off some part of the tunnel structure upstream or downstream of the test section, and returning to the test section. The measurements of the effects of early and late reflections were made using time-delay spectrometry (TDS), a swept frequency technique that allowed the measurements to be made in both the time and frequency domains.

The fundamental concepts of TDS are shown in figure 3. Based on the work of Heyser (ref. 12), TDS uses a linear, swept-frequency sine wave to excite the system under test. The source signal illustrated in figure 3(a) is for a sweep from a higher frequency to a lower frequency. Figure 3(b) shows the idealized instantaneous frequency plot for this time signal. The plot represents a single frequency spike moving with time across the frequency spectrum at a constant sweep rate S (in hertz per second). (Symbols are defined in appendix E.) When the sweep signal is applied to the system with the geometry schematically shown in the figure, it travels simultaneously through each of the paths to the receiver. Because each path length is different and assuming a constant propagation velocity c, the signals arrive at different times. If the incident path i is used as a reference, then each reflected path signal arrives at a time $\Delta d_{ij}/c$ later than the incident signal, where Δd_{ij} is the path length difference between the incident path i and the particular reflected path j. In essence, TDS converts these time delays into frequency shifts, as shown in figure 3(c), for the receiver signal. For instance, by the time the first reflected signal arrives, the incident signal has shifted by an amount $\Delta f_{i1} = S\Delta d_{i1}/c$. This frequency shift allows us to apply a tracking filter that moves with the desired signal at the same sweep rate. The bandwidth B of the tracking filter is set such that the desired signal (or signals) is measured and the effects of all the other signals are eliminated. Figure 3(d) shows an example in which a tracking filter (represented by the dashed lines) is applied to the incident signal and all the reflected

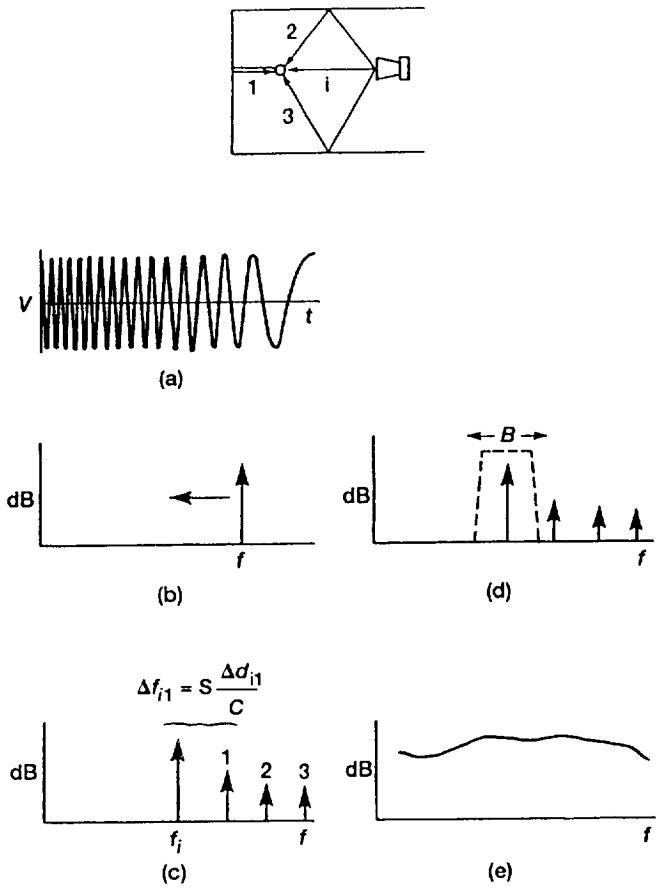

(a) Input time signal.
(b) Instantaneous frequency.
(c) Receiver signal. Δf_{i1} denotes time delay converted to frequency shift.
(d) Tracking filter applied.
(e) Filter output. Frequency resolution, $\Delta f = 1/T = S/B$.

Figure 3.—Fundamental concepts of time delay spectrometry.

signals are suppressed. For this case the output of the tracking filter is the frequency response (magnitude and phase) of the source with frequency resolution $\Delta f = S/B$ (fig. 3(e)).

In addition to the frequency response, TDS can provide the time domain response for the system shown in figure 3. The instantaneous system time response is represented by figure 3(c). If this signal is multiplied by the source signal (fig. 3(b)) at every instant of the sweep, then we get a set of signals at every instant that looks like figure 3(c), where, in each set, the spikes are stationary in time with some amplitude and phase. (This signal processing is called heterodyning or mixing.) The amplitude of the average of these sets of signals over the entire sweep is the time domain response of the system.

In measuring the effects of reflections, TDS used the tracking filter to create a time window through which only certain parts of the acoustic signal in the test section were measured. By using a small time window centered at the time of arrival of the incident signal from the source, the incident signal was measured, and all the reflections were filtered out of the measurement. This simulated the measurement of an acoustic source under anechoic conditions. By gradually opening up the time window, the effects of early reflections were detected in the measurement. The major effect of the reflections was to create an interference pattern in the frequency domain measurement due to positive and negative reinforcements of the reflections on the incident signal at the microphone. The deviations from the incident signal level were then a measure of the ability of the treatment to reduce the levels of reflections.

Effects of Early Reflections

Seven measurement setups were used to determine the effects of early reflections in the test section. The first two were used to make measurements in the center of the test section. Figure 4 schematically shows measurement setup 1. The acoustic source on the floor of the test section was aimed at the ceiling, with the microphone near the center of the test section. In measurement setup 2 (fig. 5) the acoustic source was located near one wall and aimed at the opposite wall. The microphone was, again, located near the center of the test section. The remaining five measurement setups were designed to simulate the effects of early reflections during typical sideline measurements of an acoustic source in the test section, such as a high-speed propeller (refs. 13 and 14). Figures 6 to 8 show measurement setups 3 to 5, where the line through the source and the microphone is 30°, 90°, and 135°, respectively, from the direction of airflow. In setups 3 and 5 the

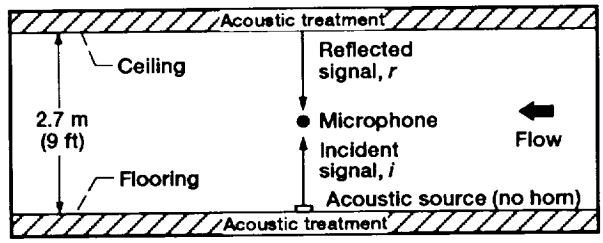

Figure 4.—Side view of measurement setup 1.

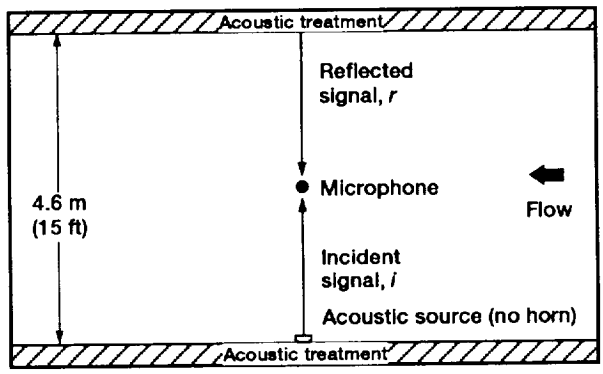

Figure 5.—Top view of measurement setup 2.

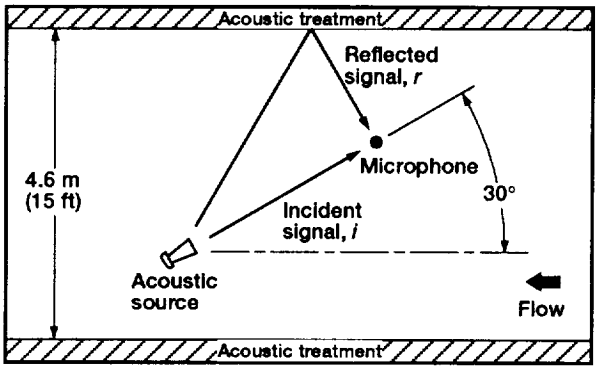

Figure 6.—Top view of measurement setup 3.

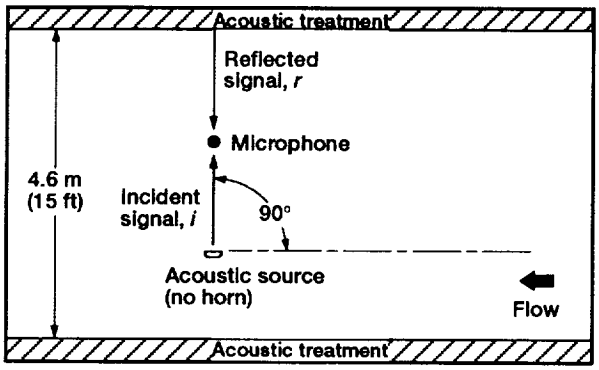

Figure 7.—Top view of measurement setup 4.

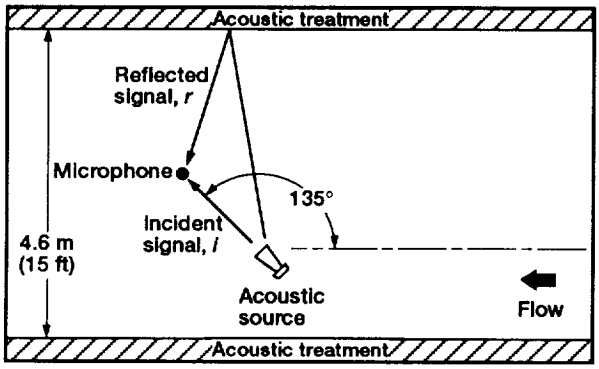

Figure 8.—Top view of measurement setup 5.

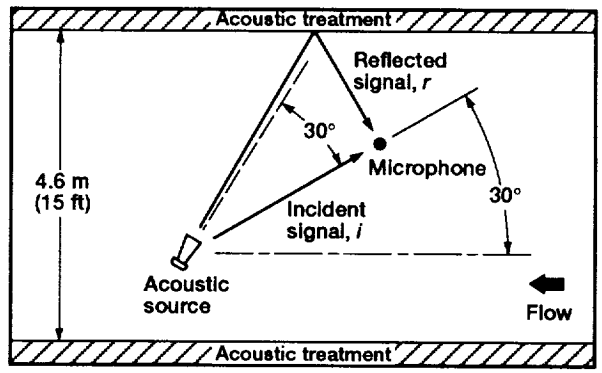

Figure 9.—Top view of measurement setup 6.

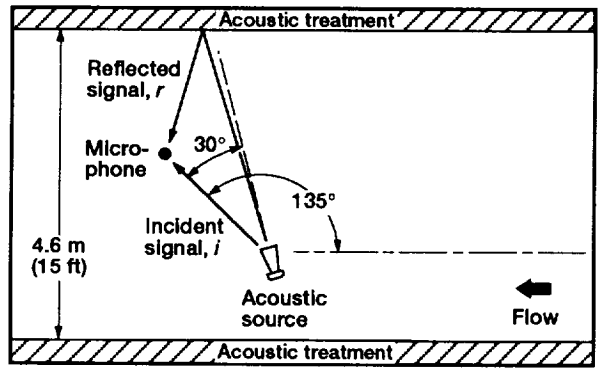

Figure 10.—Top view of measurement setup 7.

TABLE I.—LOCATION OF ACOUSTIC SOURCE AND MICROPHONE FOR ACOUSTIC EVALUATION MEASUREMENTS

Setup number	Location of center of microphone, cm			Location of exit center of acoustic source, cm			Angle of source axis with flow direction, deg
	x	y	z	x	y	z	
1	435.9	129.5	228.6	435.9	8.4	228.6	90
2	435.9	129.5	228.6	435.9	129.5	8.4	90
3	308.5	129.5	300.7	546.1	129.5	163.6	30
4	546.1	129.5	300.7	546.1	129.5	163.6	90
5	683.3	129.5	300.7	546.1	129.5	163.6	135
6	308.5	129.5	300.7	546.1	129.5	163.6	60
7	683.3	129.5	300.7	546.1	129.5	243.8	105
8	17.1	129.5	243.8	382.9	129.5	243.8	0
9	435.9	129.5	213.4	588.3	129.5	213.4	0
10	854.6	129.5	243.8	488.8	129.5	243.8	180
11	435.9	129.5	213.4	283.5	129.5	213.4	180

acoustic driver had a horn attached to it, and the axis of the horn was pointed at the microphone. Measurement setups 6 and 7 (figs. 9 and 10) were designed for off-axis measurements, with the axis of the horn pointed 30° toward the sidewall from the line through the driver and the microphone. Table I summarizes the locations of both the microphone and the acoustic source in each setup with respect to the axes shown in figure 11. The angle between the axis of the acoustic source and the direction of airflow is also shown for each setup in the table. It should be noted that the angle in setup 1 is in a plane parallel to the *xy*-plane shown in figure 11 and that all the remaining setups have angles in the horizontal plane, parallel to the *xz*-plane. The location of the acoustic source was identified as the center of the exit opening from which the sound emanated.

The frequency range for the early reflection measurements was from 150 to 5150 Hz. This 5-kHz range was adequate to cover the frequencies of interest for a high-speed propeller sound source (refs. 13 and 14) that the test section treatment was designed to absorb. The sweep rate S for these measurements was chosen to be 200 Hz/sec by trial and error, based on how clearly the early reflections were identifiable.

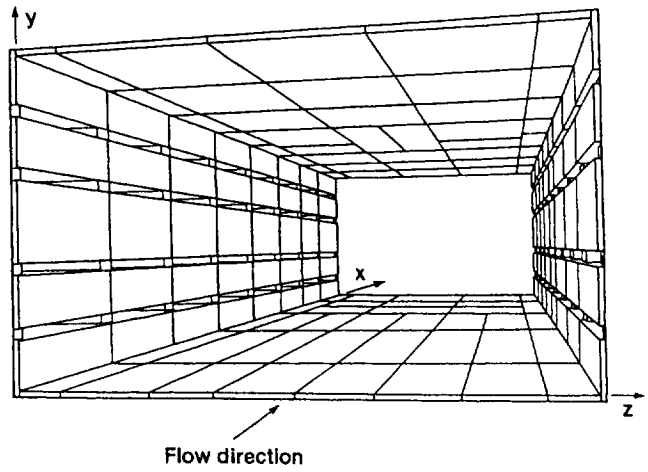

Figure 11.—Perspective view of treated test section showing axes used to identify locations in measurement setups.

The measured effects of early reflections in each setup are shown in figures 12 to 18. Each figure consists of a time domain plot and a frequency domain plot. The time domain plots show the magnitude of the acoustic energy that arrives at the microphone at a certain time after leaving the source. This energy magnitude is an integrated result over the frequency range of the TDS sweep. Typically, the energy magnitude versus time plots show a large incident signal that arrives at the microphone after traveling over the direct path between the acoustic source and the microphone. The incident signal is followed in time by lower level signals that traveled longer paths to get to the microphone. Most of these signal paths include the effects of one or more reflections off surfaces in the test section. For example, the incident path *i* and a reflected path *r* are drawn in each of the setups shown in figures 4 to 10. The reflected path was determined by the method of images. The path direct from the image source to

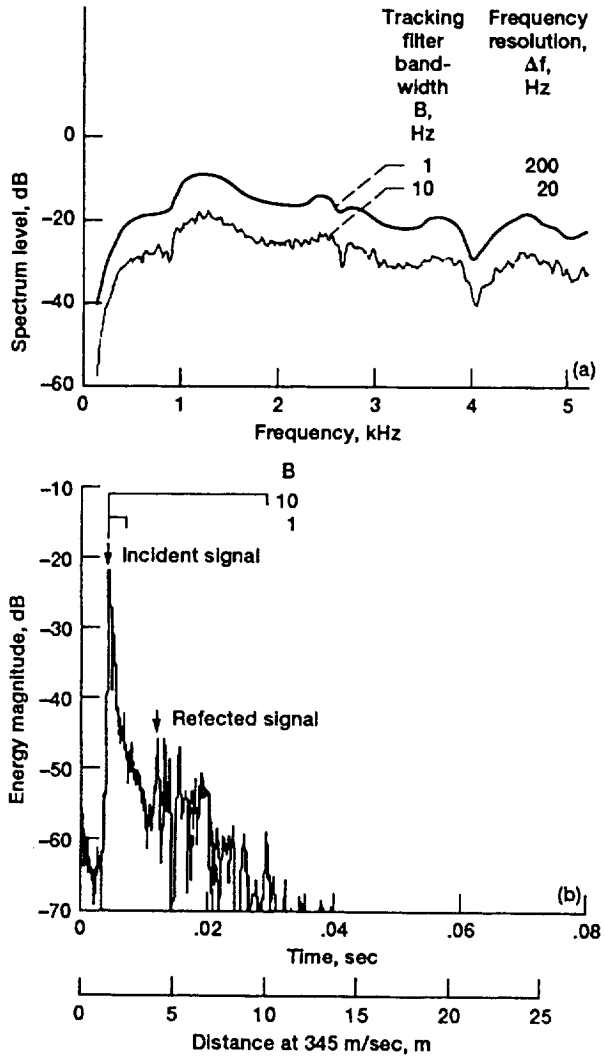

(a) Frequency domain measurement. Tracking filter with bandwidth B corresponds to time window shown on time domain plot.
(b) Time domain measurement. Signals from paths shown in fig. 4.

Figure 12.—Early reflection effects measured in setup 1.

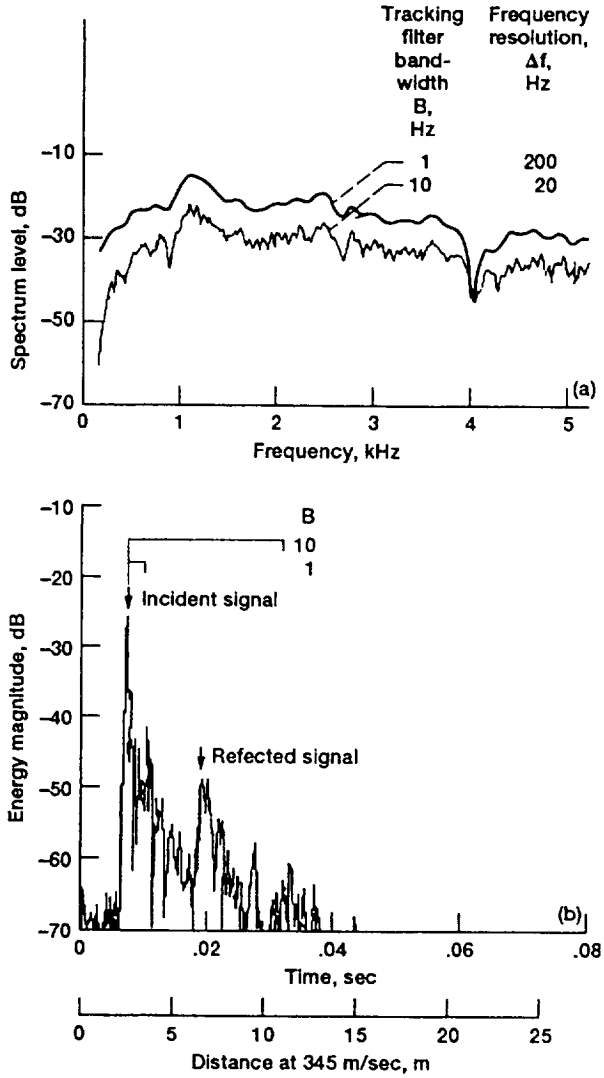

(a) Frequency domain measurement. Tracking filter with bandwidth B corresponds to time window shown on time domain plot.
(b) Time domain measurement. Signals from paths shown in fig. 5.

Figure 13.—Early reflection effects measured in setup 2.

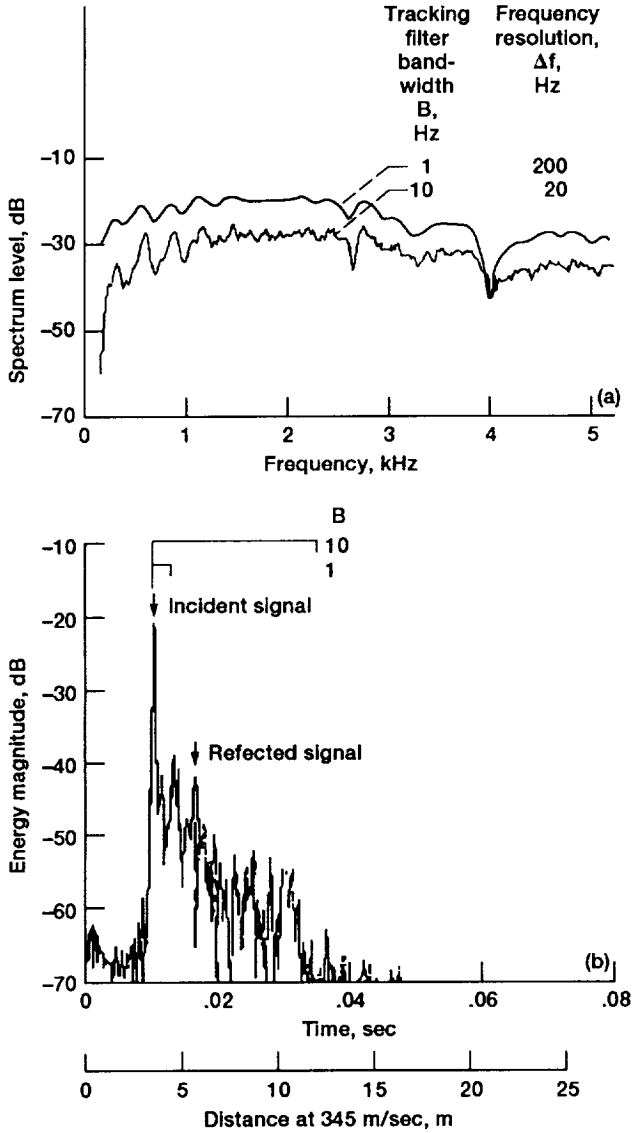

(a) Frequency domain measurement. Tracking filter with bandwidth B corresponds to time window shown on time domain plot.
(b) Time domain measurement. Signals from paths shown in fig. 6.

Figure 14.—Early reflection effects measured in setup 3.

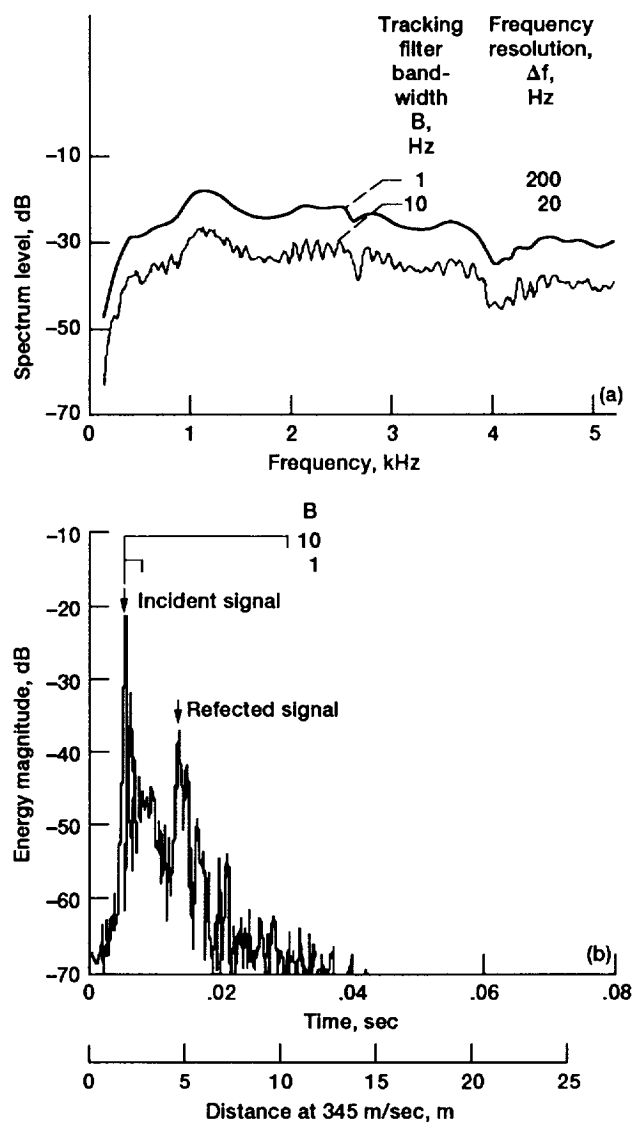

(a) Frequency domain measurement. Tracking filter with bandwidth B corresponds to time window shown on time domain plot.
(b) Time domain measurement. Signals from paths shown in fig. 7.

Figure 15.—Early reflection effects measured in setup 4.

the microphone intersects the reflecting surface, thus determining the point of reflection for the shown reflected path r on the reflecting surface. The resulting energy magnitudes of the signals that traveled over those paths are labeled on the time domain plots of figures 12 to 18.

The frequency domain plots were obtained in the manner described in relation to figure 3(e) (p. 5). The tracking filter was centered on the incident signal, and the filter bandwidth, B, was set to 1 Hz. Half the tracking filter bandwidth is shown on the time domain plots in figures 12 to 18 to indicate the amount of time signal included in the frequency spectrum. The resulting time window was 0.005 sec wide, and the spectrum frequency resolution was 200 Hz. For this case the frequency spectrum, labeled with the tracking filter bandwidth B equal to 1 Hz, is the frequency response of the acoustic source as if it was measured under anechoic conditions. To allow the effects of early reflections to enter the measurement, the tracking filter bandwidth was increased to 10 Hz. With the filter still centered on the incident signal, the time window was now 0.05 sec wide, and the spectrum frequency resolution was 20 Hz. The resulting frequency spectra, this time labeled with B equal to 10 Hz, show interference patterns represented by notches spaced at frequency intervals of $\Delta f_{int} = 1/(t_r - t_i)$. The notches become more prominent as the level of the reflection increases.

The frequency spectra are the results obtained after one TDS sweep. No averaging was done during or after the measurement to reduce incoherent noise or randomness in the

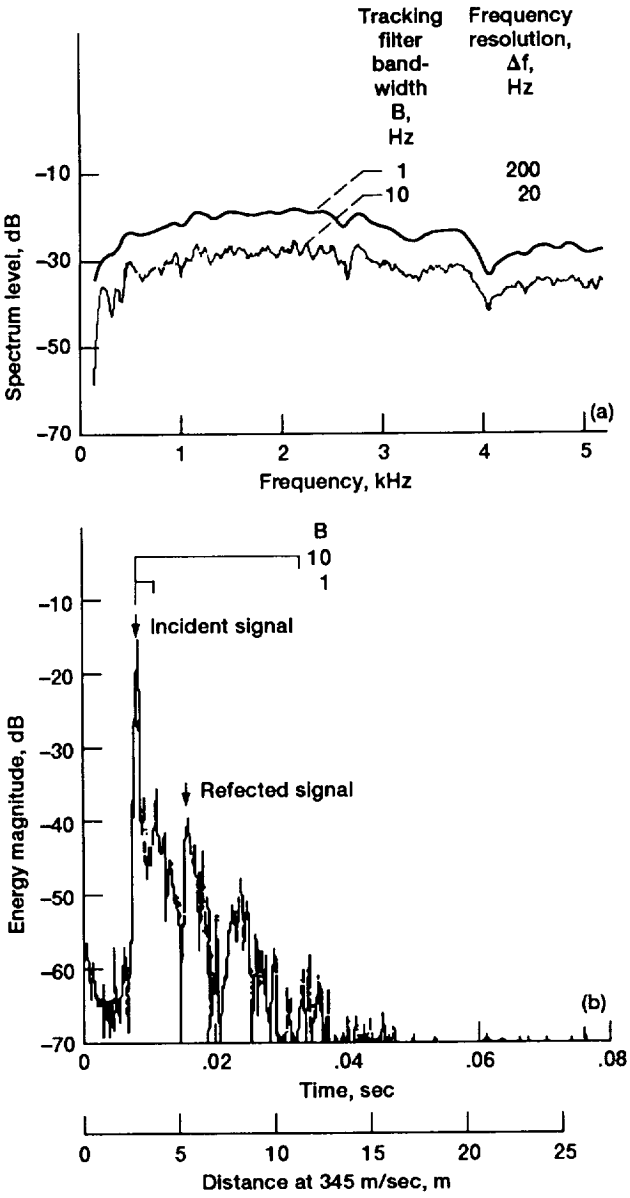

(a) Frequency domain measurement. Tracking filter with bandwidth B corresponds to time window shown on time domain plot.
(b) Time domain measurement. Signals from paths shown in fig. 8.

Figure 16.—Early reflection effects measured in setup 5.

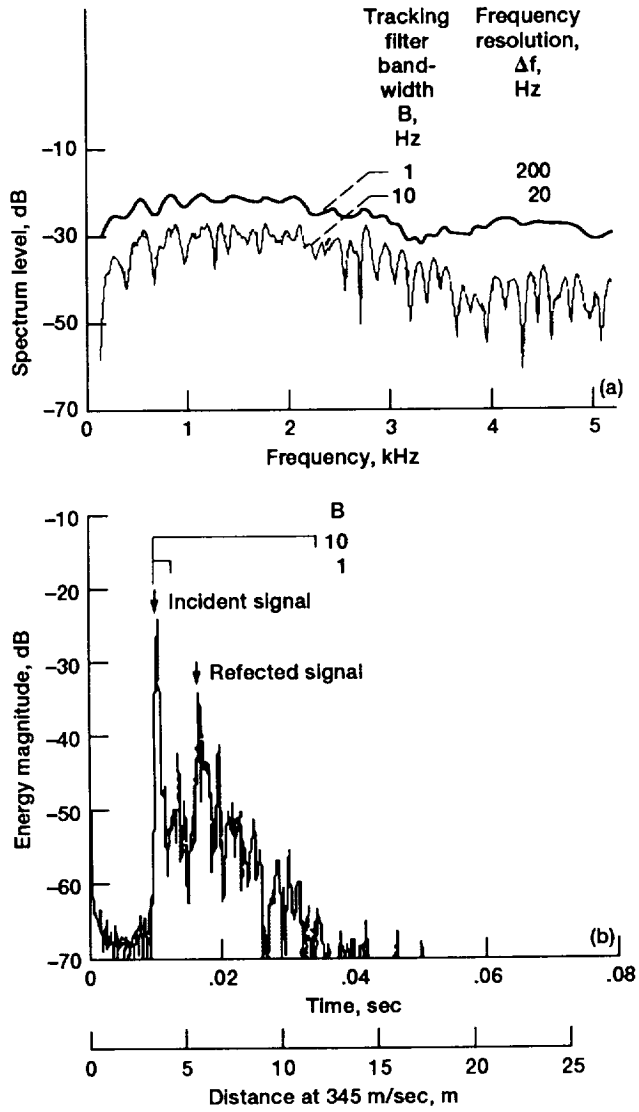

(a) Frequency domain measurement. Tracking filter with bandwidth B corresponds to time window shown on time domain plot.
(b) Time domain measurement. Signals from paths shown in fig. 9.

Figure 17.—Early reflection effects measured in setup 6.

frequency spectra. It is anticipated that sufficient averaging would reduce slightly the measured level of the interference pattern. With that in mind, the results for the effects of early reflections were summarized (see table II).

Using the geometry of the setups, the major reflection signals and reflecting surfaces were identified on the time domain plots. In some cases, reflections from the floor and ceiling were not separately identifiable. This is noted in the table. The change in energy magnitude was determined between the reflected signals and the incident signal. These results were then corrected for spherical spreading using the equation shown in table II. For most of the cases where the major axis of the acoustic source is pointed at the microphone (setups 1 to 5), the tunnel treated surfaces provided 15 to 19 dB of total attenuation over the frequency range from 150 to 5150 Hz as shown in the column labeled ΔdB_{corr} in table II. The first major reflected signal in setup 4, which was from the source nearest to and pointed directly at a wall, was only attenuated 10 dB by the wall treatment. Time-delay spectrometry had been used previously to measure the absorptive properties of localized areas of the absorbing treatment (ref. 3). In the same manner, TDS was used to identify the reflected signal in setup 4 as coming from an area with a thin layer of absorbing treatment.

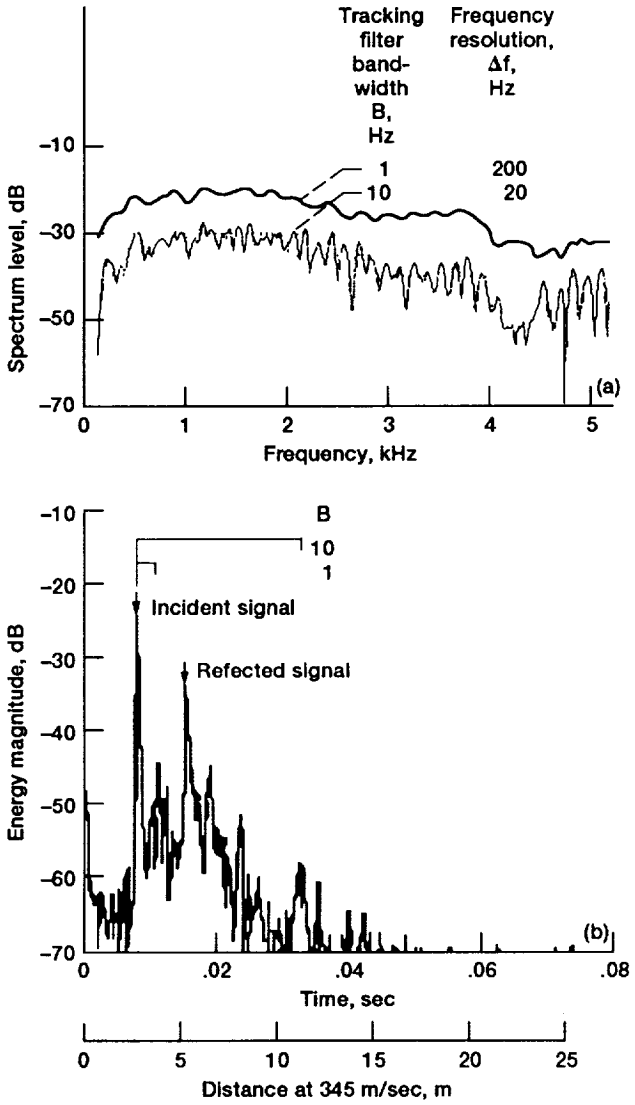

(a) Frequency domain measurement. Tracking filter with bandwidth B corresponds to time window shown on time domain plot.
(b) Time domain measurement. Signals from paths shown in fig. 10.

Figure 18.—Early reflection effects measured in setup 7.

The arrival times for the incident and reflected signals were used to identify the interference patterns in the frequency spectra measured using the 10-Hz tracking filter. The difference between a local maximum level and a local minimum level (in terms of decibels) of the interference pattern ripple was determined at various locations on the frequency spectra. No data were used below 500 Hz because of the rapid decrease in the frequency spectrum. Those difference values above 500 Hz were averaged to obtain an average value for the interference ripple. The results are listed in table II as an indicator of the effects of early reflections. For setups 1 to 5, the interference ripple about the incident signal varied on average from 1.7 to 3.2 dB wide from minimum to maximum level over the frequency range of 500 to 5150 Hz. Recall that

TABLE II.—SUMMARY OF EARLY REFLECTION EFFECTS SHOWN IN FIGURES 12 TO 18 FOR SETUPS 1 TO 7

[Total attenuation (dB) is over the frequency range 150 to 5150 Hz. Average interference ripple is over the frequency range 500 to 5150 Hz.]

Setup	Time of incident signal, t_i, msec	Time of major reflection signal, t_r, msec	Reflecting surface	Total attenuation ΔdB, dB	ΔdB_{corr} (a)	Interference pattern, Δf_{int}, Hz (b)	Average interference ripple, dB (c)
1	3.8	11.6	Ceiling	−28.4	−18.7	128.2	1.7±0.5
2	6.8	10.4	Floor/ceiling	−19.4	15.7	277.8	3.2±1.0
		19.2	Wall	−26.9	−17.9	80.6	2.3±0.8
3	9.6	12.8	Floor/ceiling	−21.0	−18.5	312.5	2.4±0.7
		16.0	Wall	−23.3	−18.9	156.3	2.3±0.8
4	4.4	13.0	Wall	−19.7	−10.3	116.3	2.9±1.2
5	7.4	10.6	Floor/ceiling	−21.9	−18.8	312.5	2.0±0.3
		15.4	Wall	−25.2	−18.8	125.0	2.4±0.7
6	9.8	16.0	Wall	−12.6	−8.3	161.3	10.2±5.3
7	7.6	15.0	Wall	−13.4	−7.5	135.1	7.9±3.5

[a] $\Delta dB_{corr} = \Delta dB + 20 \log(t_r/t_i)$
[b] Where $\Delta f_{int} = 1/(t_r - t_i)$ in Hz
[c] Interference ripple = 20 log (maximum level/minimum level)

for these setups the major axis of the acoustic source was pointed at the microphone. For setups 6 and 7, the source was pointed away from the microphone and toward the wall (figs. 9 and 10). The major axis of the source almost points along the wall reflection path. This increases the level of the reflected signal relative to the incident signal because of the directivity pattern of the acoustic source. The interference ripple is larger in these cases than for the on-axis cases, with standard deviations half the size of the average interference ripple.

Effects of Late Reflections

Nine measurement setups were used to determine the effects of late reflections in the test section. Figure 19(a) shows setup 8 where the microphone is located at the start of the test section and the acoustic source is near the center of the test section with the horn pointed upstream at the microphone. After this setup, the microphone was moved to the center of the test section, and the acoustic source was moved back towards the end of the test section as shown in figure 19(b) for setup 9. These two setups were repeated in the downstream direction. Setup 10 is shown in figure 20(a), where the microphone is located near the end of the test section, and figure 20(b) shows setup 11, where the microphone is near the center of the test section. The remaining five setups for determining the effects of late reflections were setups 1 to 5 described previously. The locations of the acoustic source and the microphone for these four additional setups are also listed in table I.

In order to measure the effects of late reflections using TDS, the time window must be large enough to include these late reflections. The time window T is equal to $n\Delta t = n/F$, where F is the frequency range of the TDS sweep and n is an integer. Thus, F must be small for T to be large when n is fixed. A frequency sweep over range F of 500 Hz provided a sufficiently large time window ($T \approx 0.8$ sec) that all major late reflections were included in the measurements. The maximum signal path length associated with this time window was then about 275 m. A consequence of this small F was

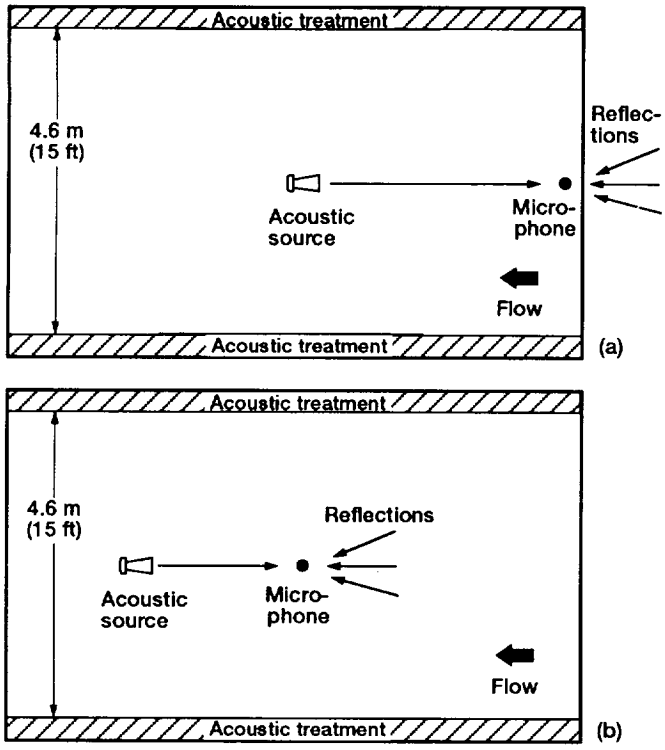

(a) Measurement setup 8. (b) Measurement setup 9.

Figure 19.—Top views of measurement setups for upstream late reflections.

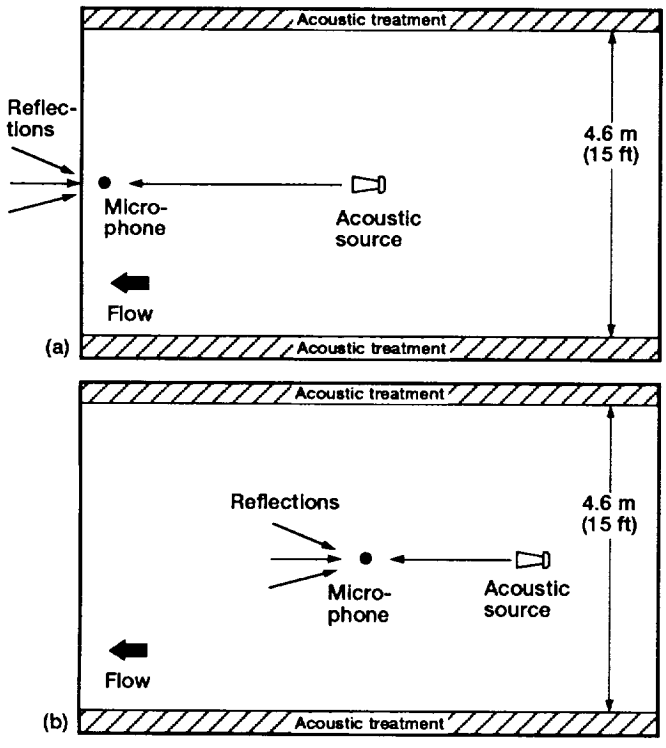

(a) Measurement setup 10. (b) Measurement setup 11.

Figure 20.—Top views of measurement setups for downstream late reflections.

that a large frequency range had to be covered in increments of 500 Hz. Since most of the effects of late reflections were in the lower frequencies, the time domain measurements were made in nine 500-Hz increments covering the frequency range from 200 to 4250 Hz.

The frequency domain measurements were made of the "incident" signal and the incident plus late reflected signals in the same manner as was done for early reflections. Setting the sweep rate S to 100 Hz/sec and the tracking filter bandwidth B to 2 Hz provided a time window T equal to 0.02 sec through which to measure the incident signal. It is clear from the early reflection results that this 0.02-sec window means that this incident signal includes the effects of early reflections. Figures 12 to 18 all show that the most prominent early reflections arrive at the microphone less than 0.02 sec after the incident signal. Thus, the late reflections are an additional interference effect on the incident signal, on top of the early reflections, which in this measurement are part of the incident signal. Now, to include the late reflections in the frequency domain measurements, both S and B were adjusted to make T large, where $T = B/S$. The settings $S = 5$ Hz/sec and $B = 2.2$ Hz gave T as 0.45 sec.

Setup 8, shown in figure 19(a), was designed to measure the acoustic reflections from tunnel structures upstream of the test section as they enter the test section. The most prominent structure upstream of the test section is the wind tunnel cooler, or heat exchanger (see fig. 1). It is located approximately 32.8 m from the start of the test section. The time domain results for setup 8 show a relatively large reflection, labeled "2" in figure 21, at about the time expected for a reflection to return from the cooler. Note that the incident signal is a large spike, at the left hand side of the time plot, which includes the unresolved early reflections. When the upstream reflection gets into the center of the test section (setup 9, fig. 19(b)), it is diminished in amplitude, as shown in figure 22. The frequency domain plots are shown for these two cases in figures 23 and 24 for the incident and the incident-plus-reflected signals in selected 500-Hz frequency bands centered at 450 Hz, 1 kHz, 2 kHz, and 4 kHz. The larger reflected signal at the start of the test section causes a larger interference ripple in the frequency response (up to 10.8 dB in fig. 23) than what is measured at the center of the test section (fig. 24).

An identical set of measurements was made in the downstream direction using setups 10 and 11. The main structural features downstream of the test section (fig. 1(a)) are (1) the point where the diffuser dumps into the back leg of the wind tunnel 20.7 m from the end of the test section, (2) the point where the inside of the corner begins before the air dryer 54.9 m from the end of the test section, and (3) the wall at the outer corner of the turn before the air dryer 76.2 m from the end of the test section. Reflections from these locations are identified in figure 25, the time domain plots for the signals entering the test section from reflections downstream. Clearly, the reflections begin at the point of discontinuity between the end of the diffuser and the wind tunnel outer structural shell.

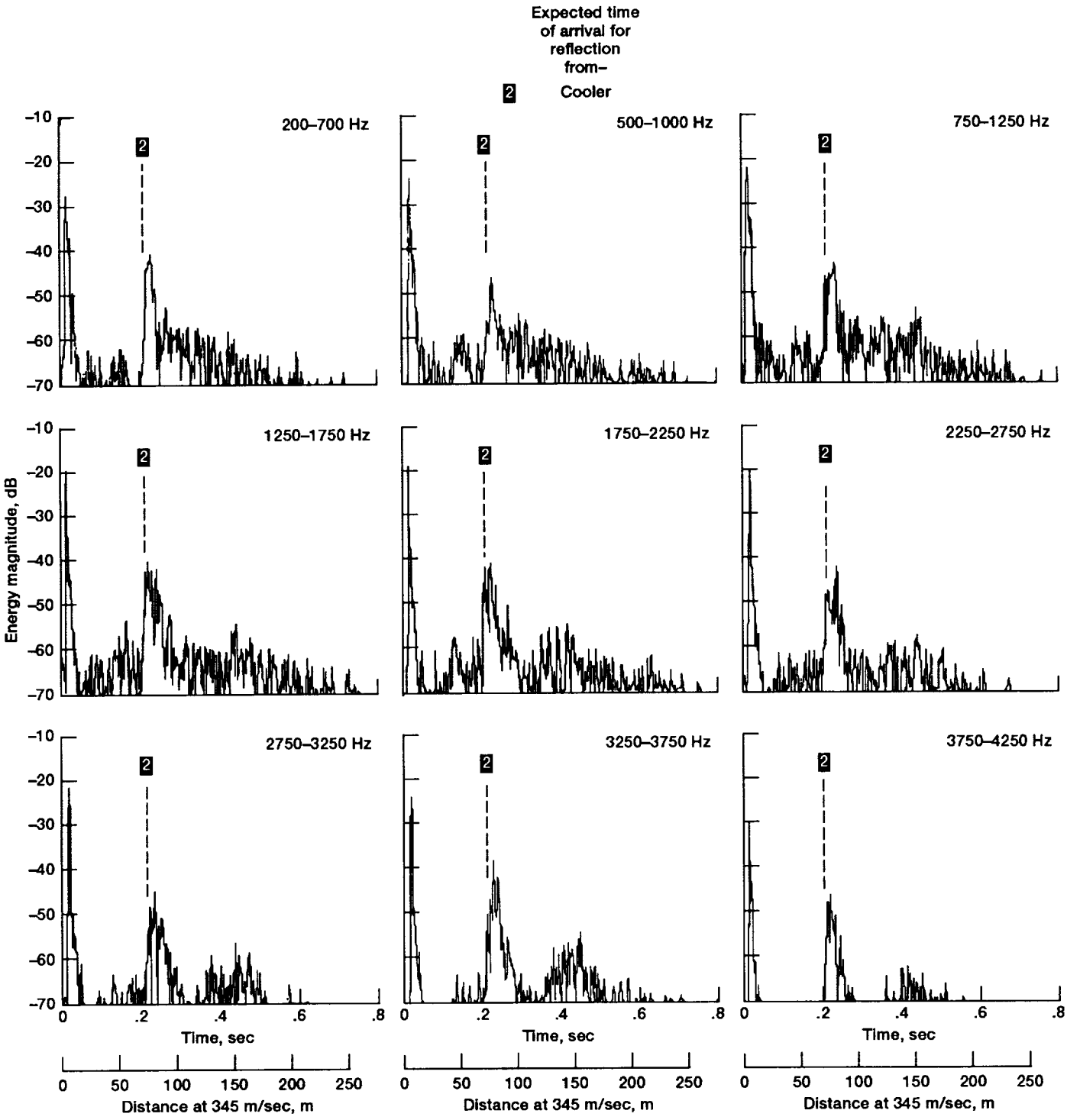

Figure 21.—Time domain measurements in 500 Hz intervals of late reflections from upstream of test section using setup 8.

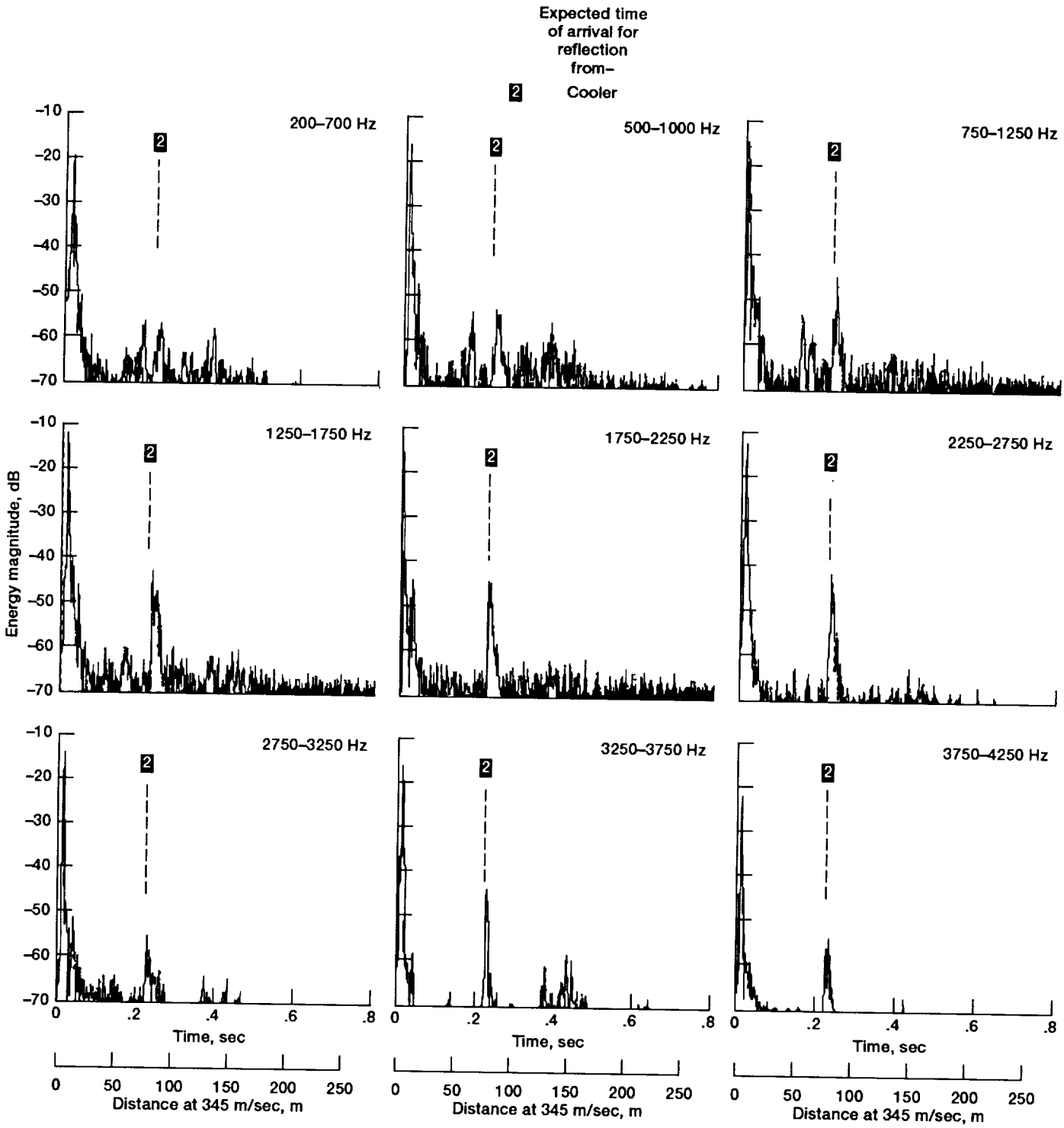

Figure 22.—Time domain measurements in 500 Hz intervals of late reflections from upstream of test section using setup 9.

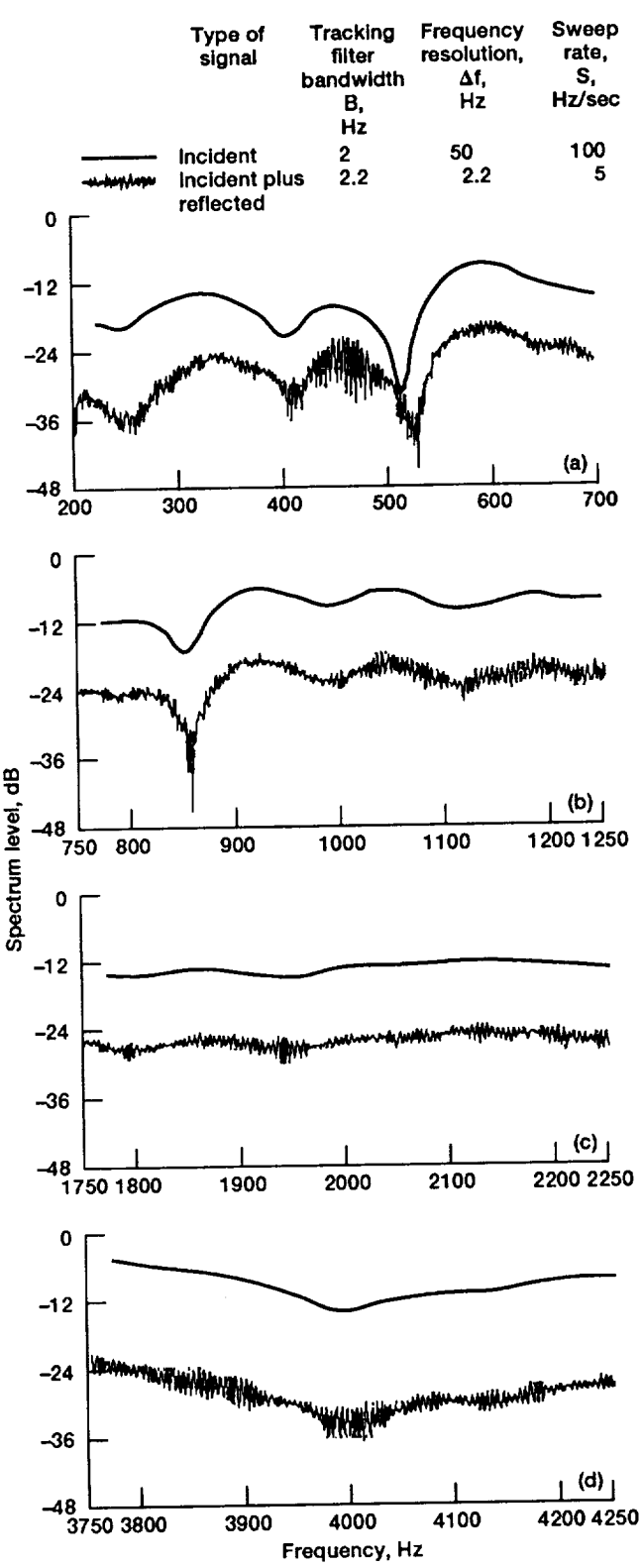

(a) Center frequency, 450 Hz.
(b) Center frequency, 1000 Hz.
(c) Center frequency, 2000 Hz.
(d) Center frequency, 4000 Hz.

Figure 23.—Frequency domain measurements in selected 500-Hz intervals of late reflections from upstream of test section using setup 8.

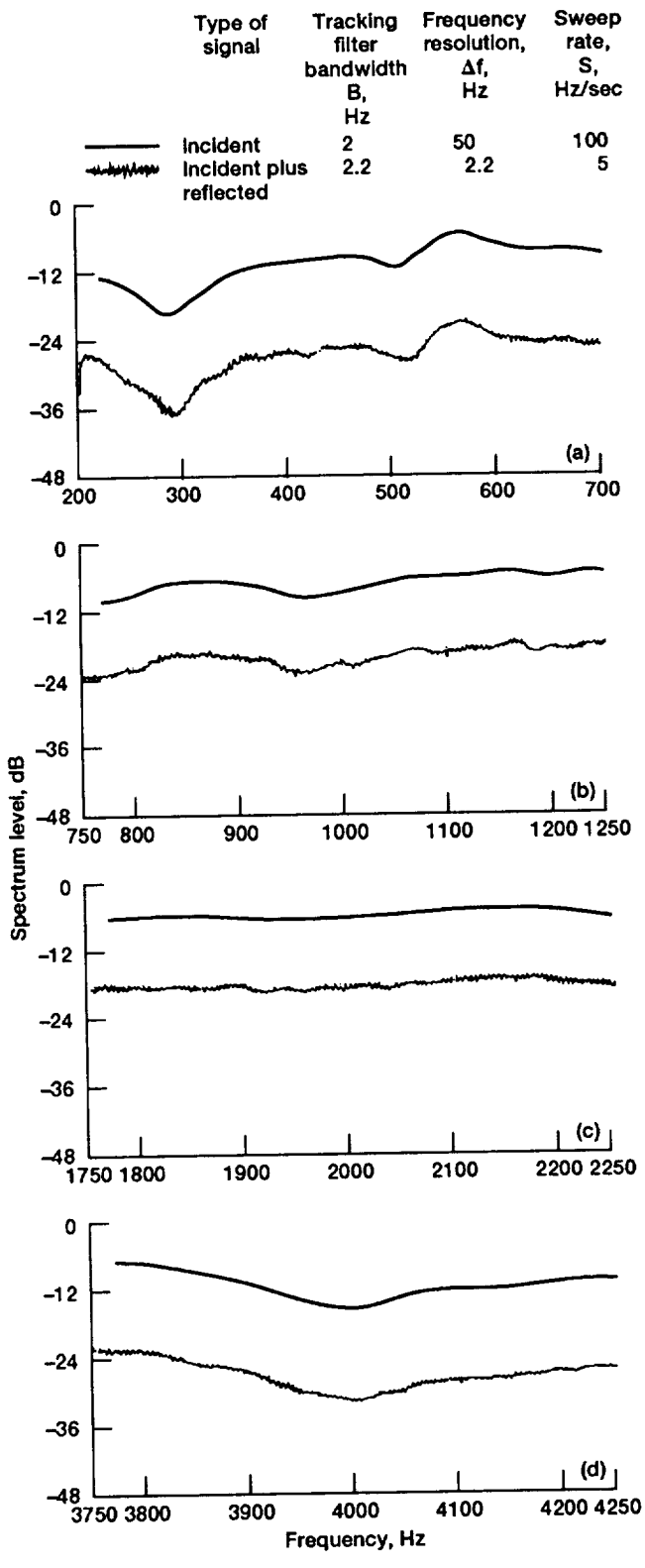

(a) Center frequency, 450 Hz.
(b) Center frequency, 1000 Hz.
(c) Center frequency, 2000 Hz.
(d) Center frequency, 4000 Hz.

Figure 24.—Frequency domain measurements in selected 500-Hz intervals of late reflections from upstream of test section using setup 9.

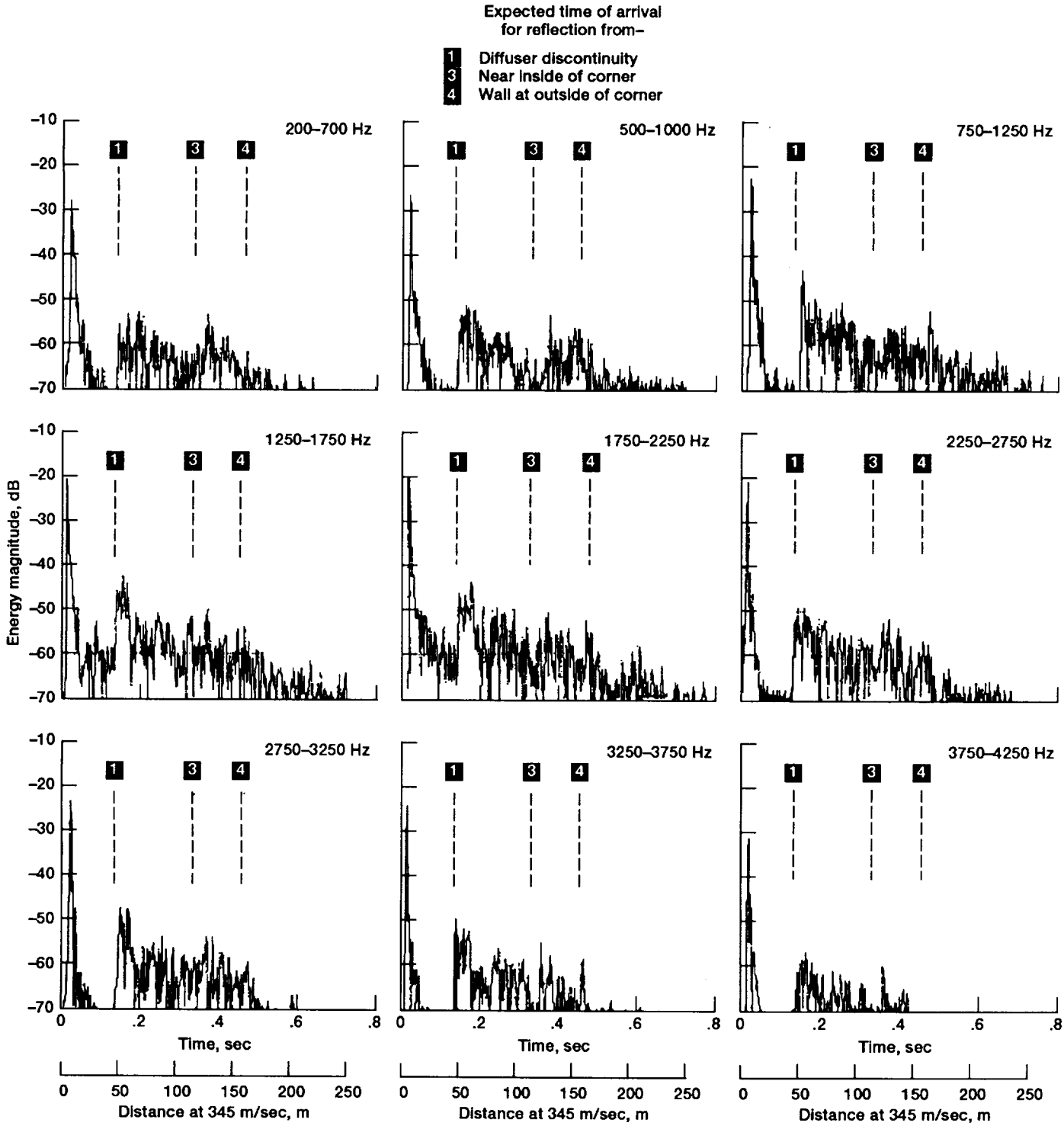

Figure 25.—Time domain measurements in 500 Hz intervals of late reflections from downstream of test section using setup 10.

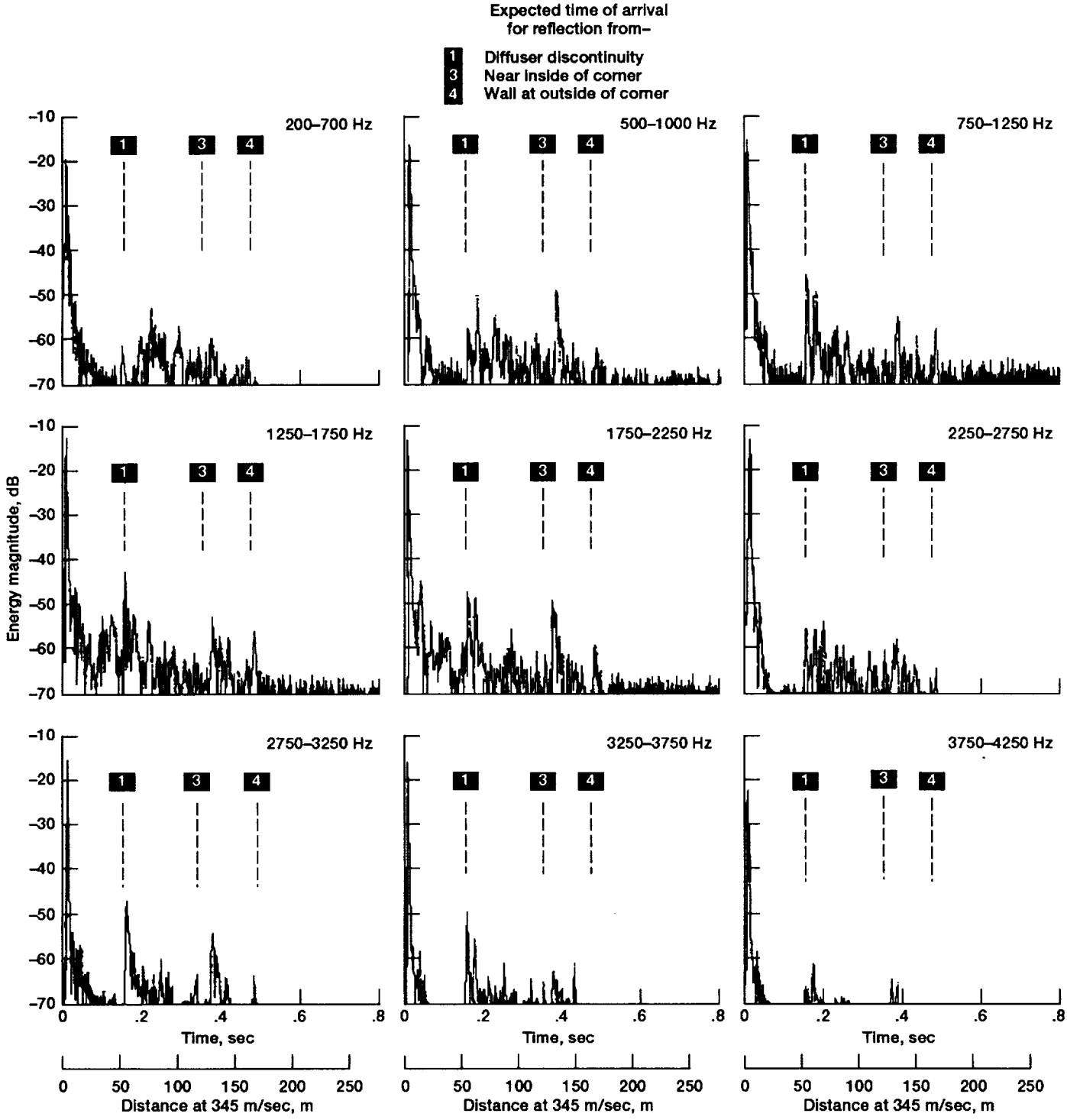

Figure 26.—Time domain measurements in 500 Hz intervals of late reflections from downstream of test section using setup 11.

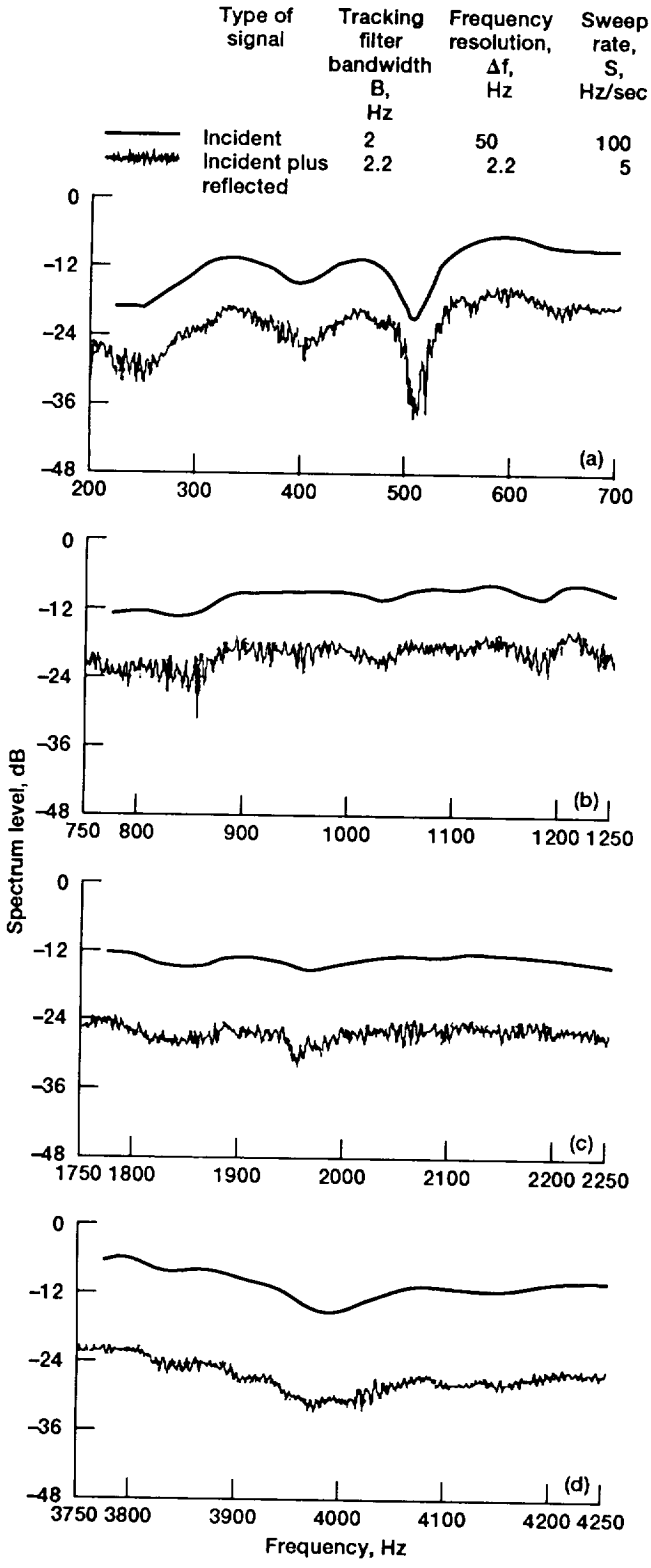

(a) Center frequency, 450 Hz.
(b) Center frequency, 1000 Hz.
(c) Center frequency, 2000 Hz.
(d) Center frequency, 4000 Hz.

Figure 27.—Frequency domain measurements in selected 500 Hz intervals of late reflections from downstream of test section using setup 10.

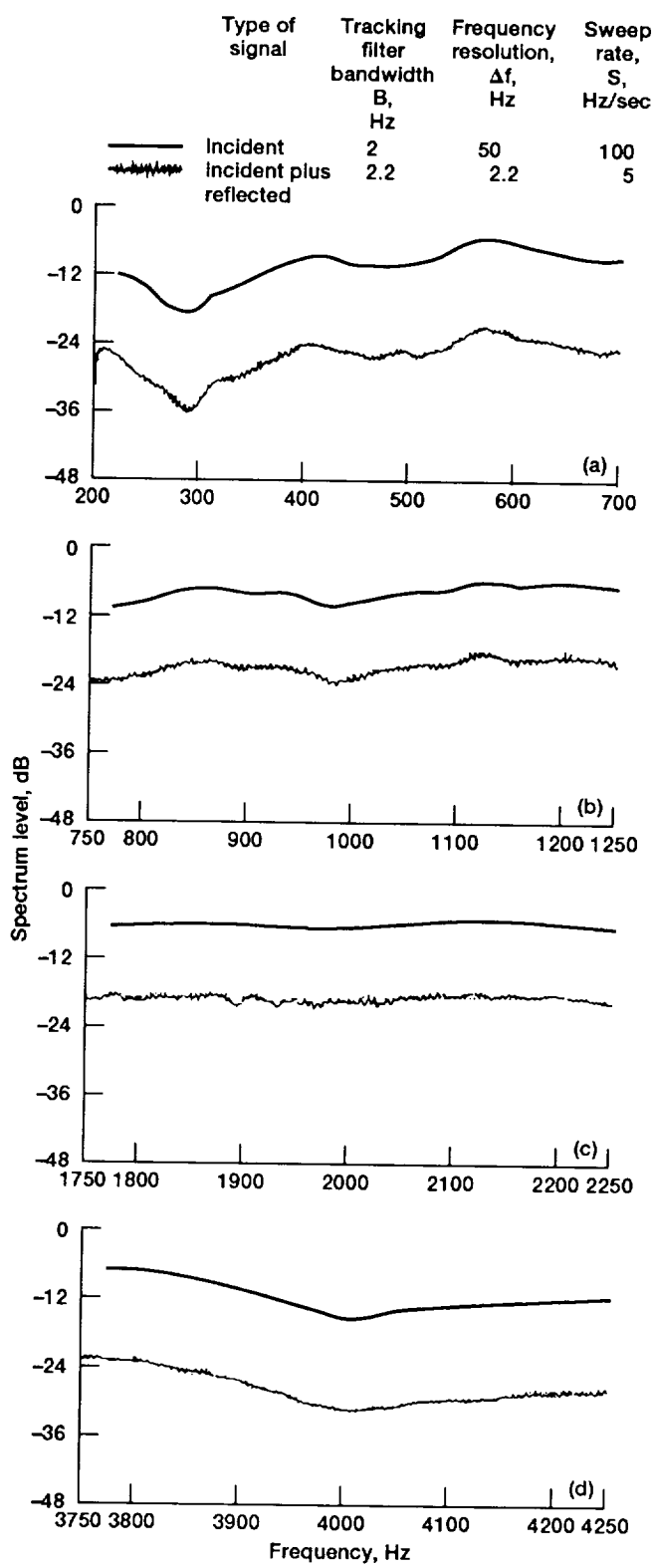

(a) Center frequency, 450 Hz.
(b) Center frequency, 1000 Hz.
(c) Center frequency, 2000 Hz.
(d) Center frequency, 4000 Hz.

Figure 28.—Frequency domain measurements in selected 500-Hz intervals of late reflections from downstream of test section using setup 11.

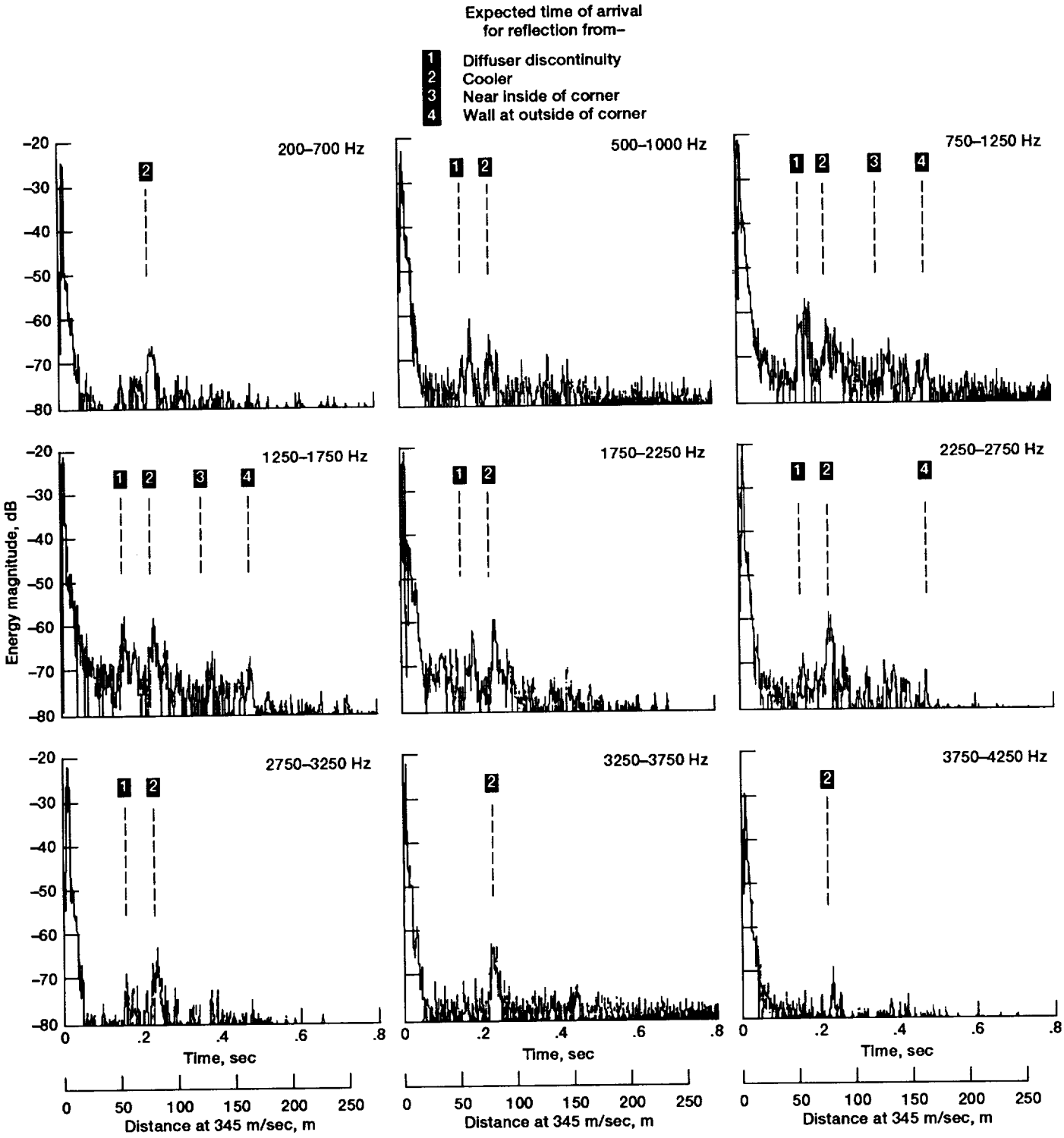

Figure 29.—Time domain measurements in 500-Hz intervals of late reflections using setup 1.

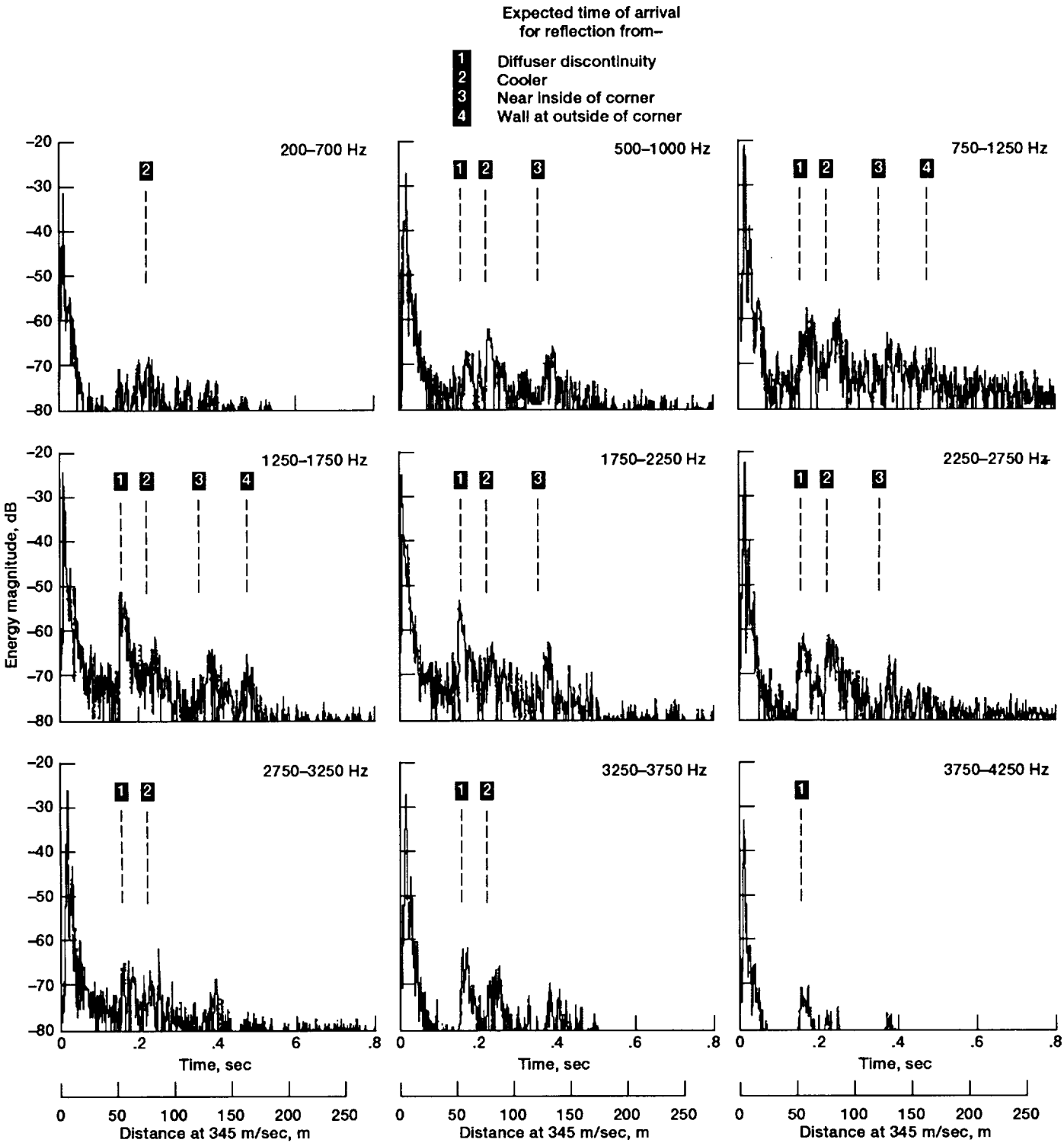

Figure 30.—Time domain measurements in 500 Hz intervals of late reflections using setup 2.

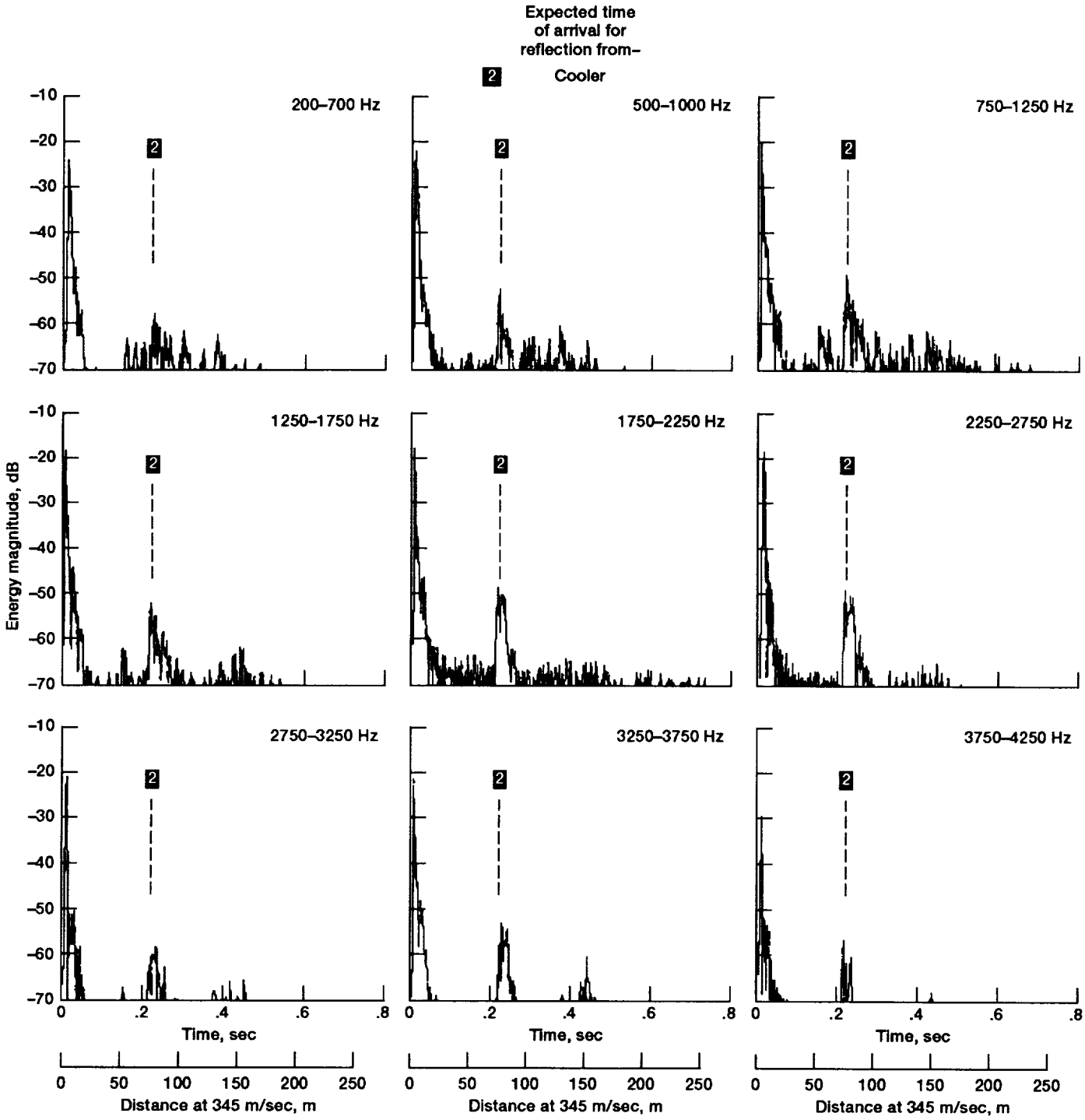

Figure 31.—Time domain measurements in selected 500 Hz intervals of late reflections from upstream of test section using setup 3.

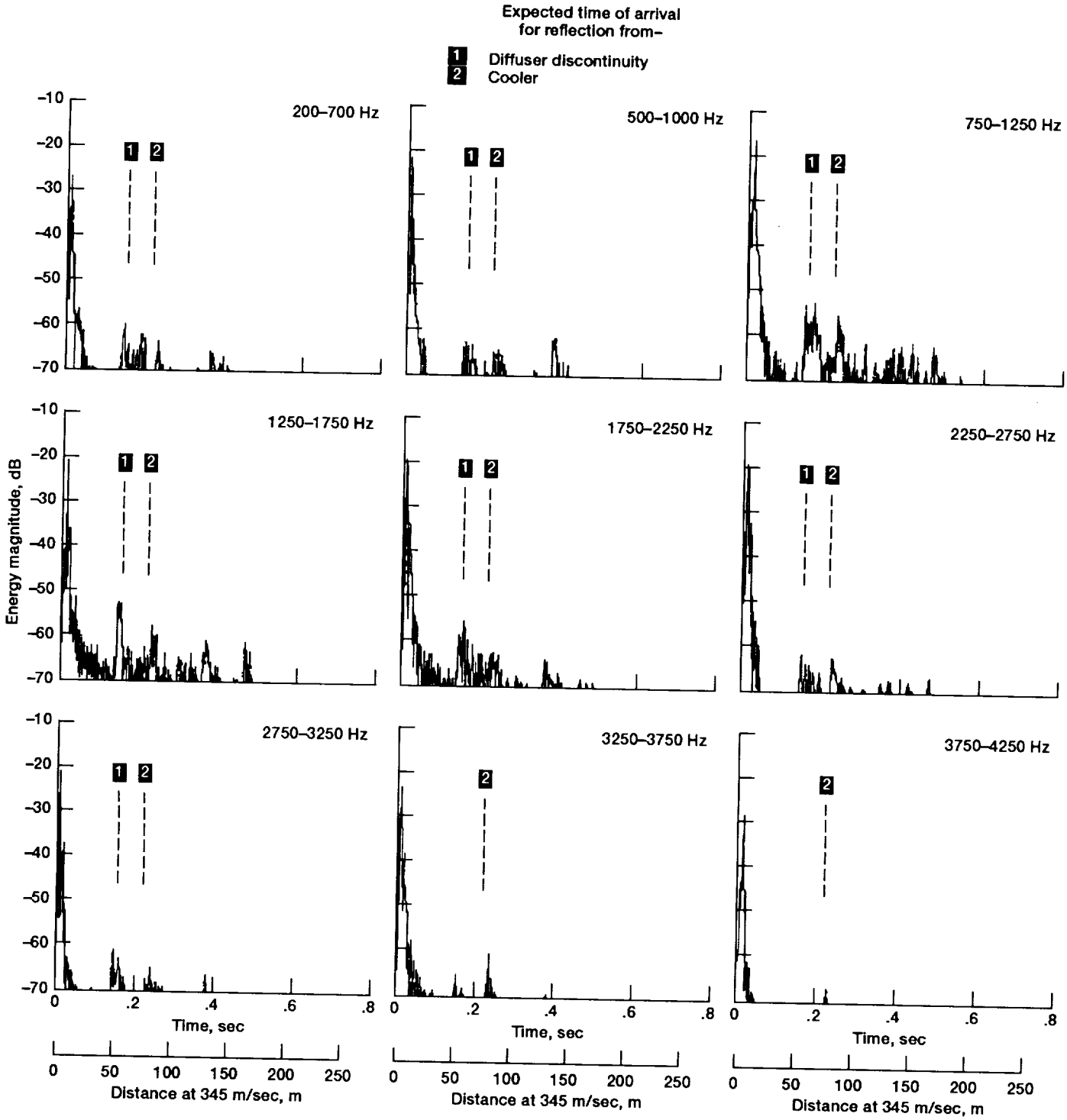

Figure 32.—Time domain measurements in selected 500 Hz intervals of late reflections using setup 4.

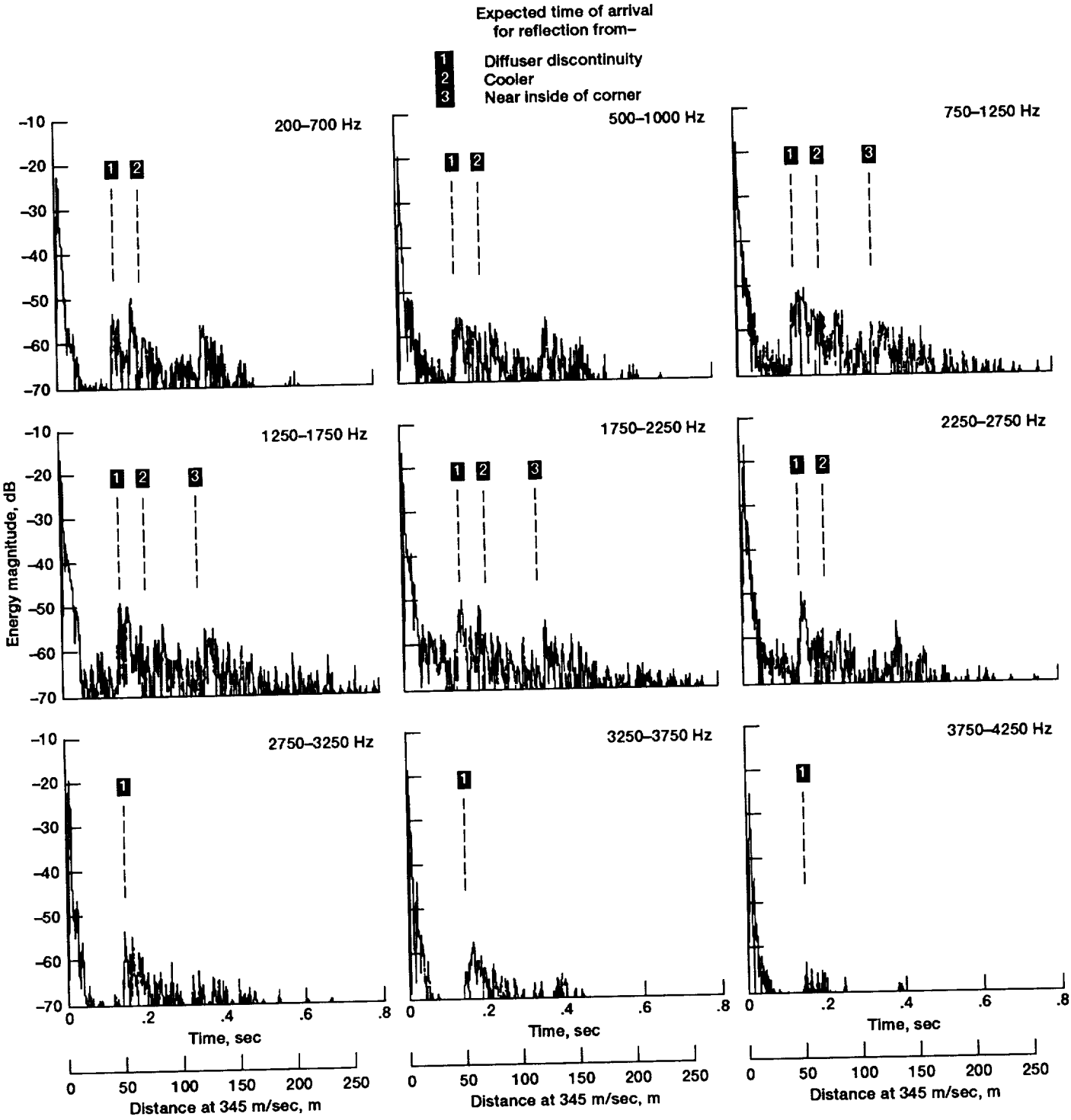

Figure 33.—Time domain measurements in selected 500 Hz intervals of late reflections using setup 5.

In figure 26, these reflections stand out a little more clearly at the center of the test section, since other reflected or scattered signals have been attenuated by the treatment. Selected frequency response plots are shown in figures 27 and 28. The interference ripple at the end of the test section is up to 6.2 dB, not as high as the upstream reflected interference ripple.

The effects of late reflection were also measured using setups 1 to 5 (previously shown in figs. 4 to 8). The time domain plots are shown for all five setups in figures 29 to 33. The setups with the microphone nearer the center of the test section (setups 1, 2, and 4) have late reflections (figs. 29, 30, and 32) from both upstream and downstream. Setup 3 (fig. 31), which has the microphone in a typical upstream sideline position, has mostly reflections from upstream of the test section. In a typical downstream sideline position, setup 5 has reflections coming from downstream (fig. 33). In all these cases, the late reflection energy peaks are small and, especially for the typical sideline measurement setups 3 to 5, about 30 dB less than the incident energy signal. The frequency response plots show this low level of late reflected energy as the amount of interference ripple in the incident-plus-reflection measurements. Figures 34 to 36 show selected frequency response plots for sideline setups 3 to 5. The maximum interference ripple for late reflections is about 2 dB and, as can be seen in the figures, the average ripple would be much less since on most of the plots, the ripple is barely detectable even with the expanded y-scale. Finally, the effects of late reflections for all the measurement setups used are given in table III in terms of the maximum interference ripple in each of four selected frequency ranges. The results indicate that the late reflections will interfere within about a 2-dB range of the incident signal for measurements of the incident signal away from the ends of the treated test section. The average effect of late reflections will be discussed later. Setups 8 and 10 in the table show large interference ripple effects since in both of these setups the microphone is located near the start or the exit of the test section.

Acoustic Evaluation—Decay With Distance

The second set of acoustic evaluations measured the extent of the acoustic free field for an acoustic source in the test section. The decay of sound with distance was measured for different steady acoustic sources along horizontal radial lines from the source and at various angles to the direction of airflow in the test section, as schematically shown in figure 37. These horizontal lines are labeled 30°, 45°, 60°, 75°, 90°, 105°, and 135° for the angle that the line makes with the direction of airflow. A microphone was traversed along these lines to measure the sound field. Using an acoustic driver connected to a horn with directional characteristics, measurements of the decay of sound away from the source were made both on and off the major axis of the source. For on-axis measurements,

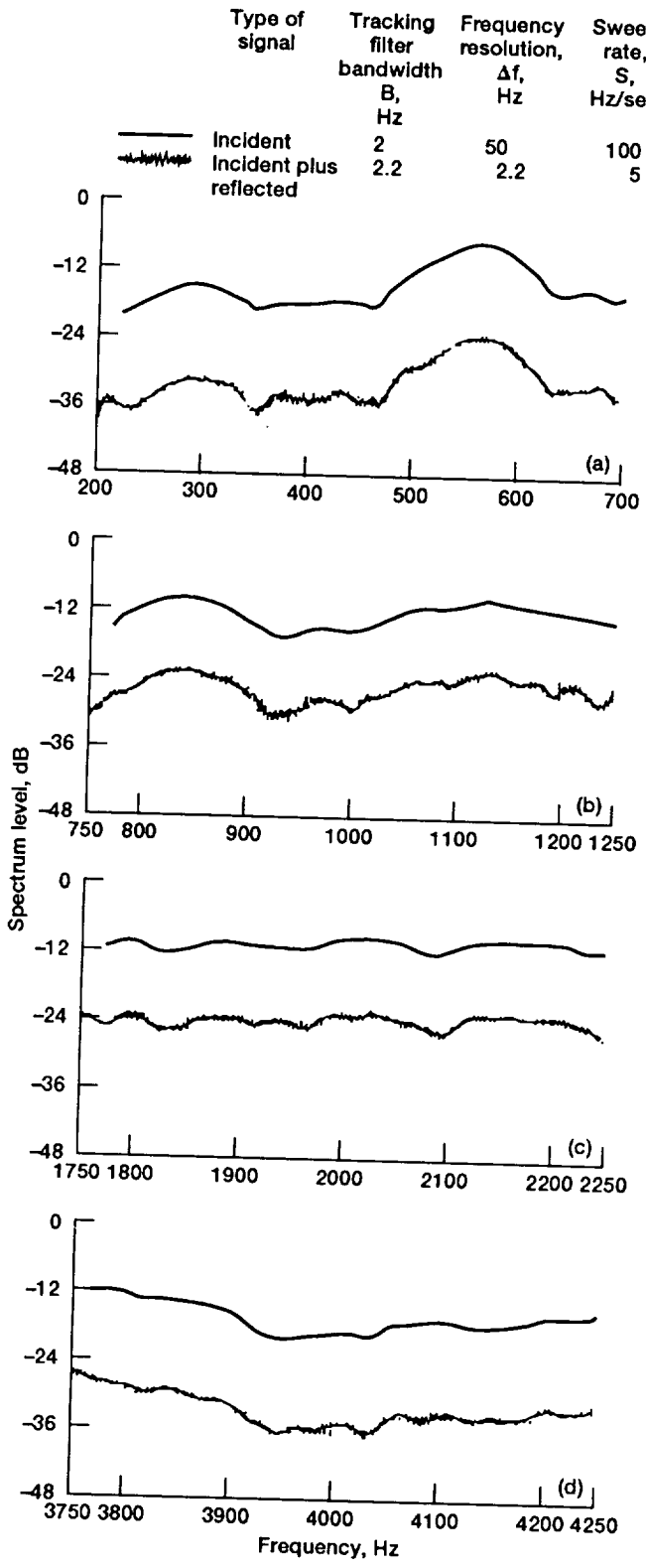

(a) Center frequency, 450 Hz.
(b) Center frequency, 1000 Hz.
(c) Center frequency, 2000 Hz
(d) Center frequency, 4000 Hz.

Figure 34.—Frequency domain measurements in selected 500 Hz intervals of late reflections using setup 3.

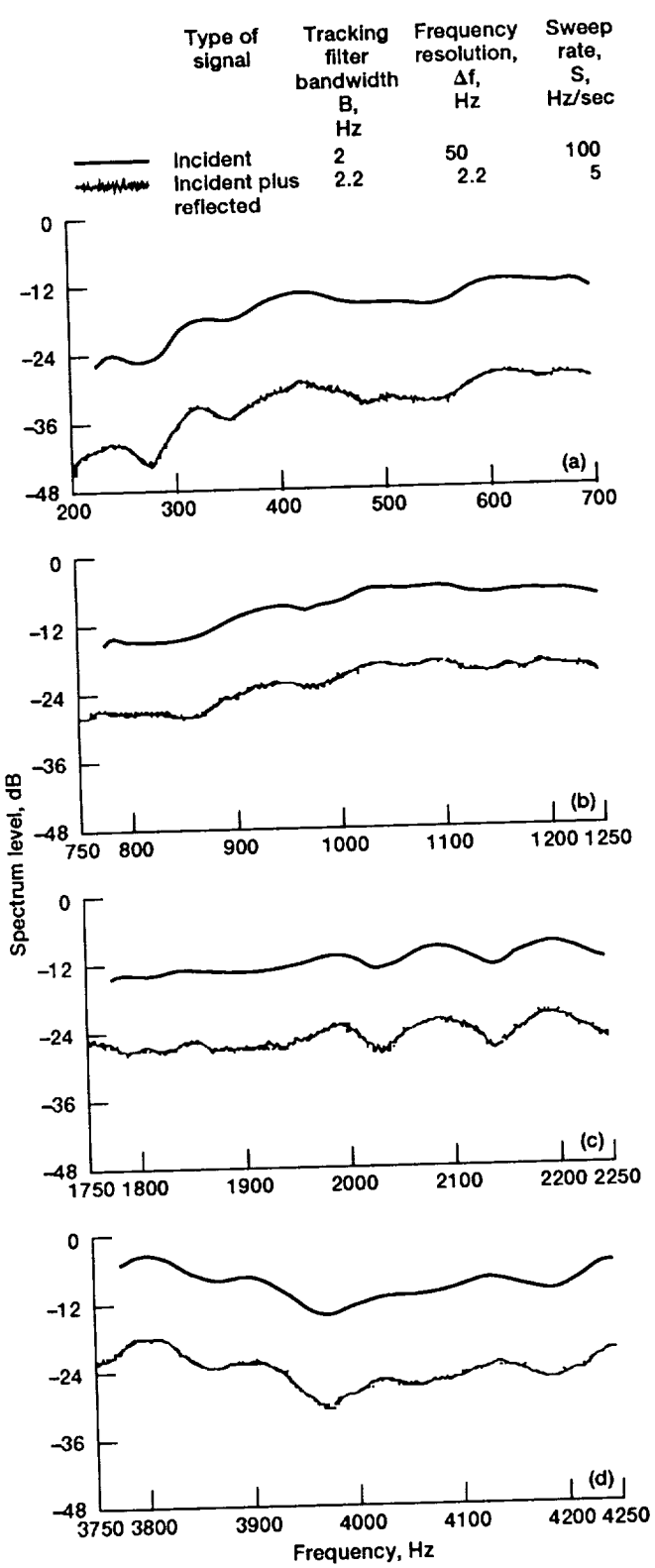

(a) Center frequency, 450 Hz.
(b) Center frequency, 1000 Hz.
(c) Center frequency, 2000 Hz.
(d) Center frequency, 4000 Hz.

Figure 35.—Frequency domain measurements in selected 500 Hz intervals of late reflections using setup 4.

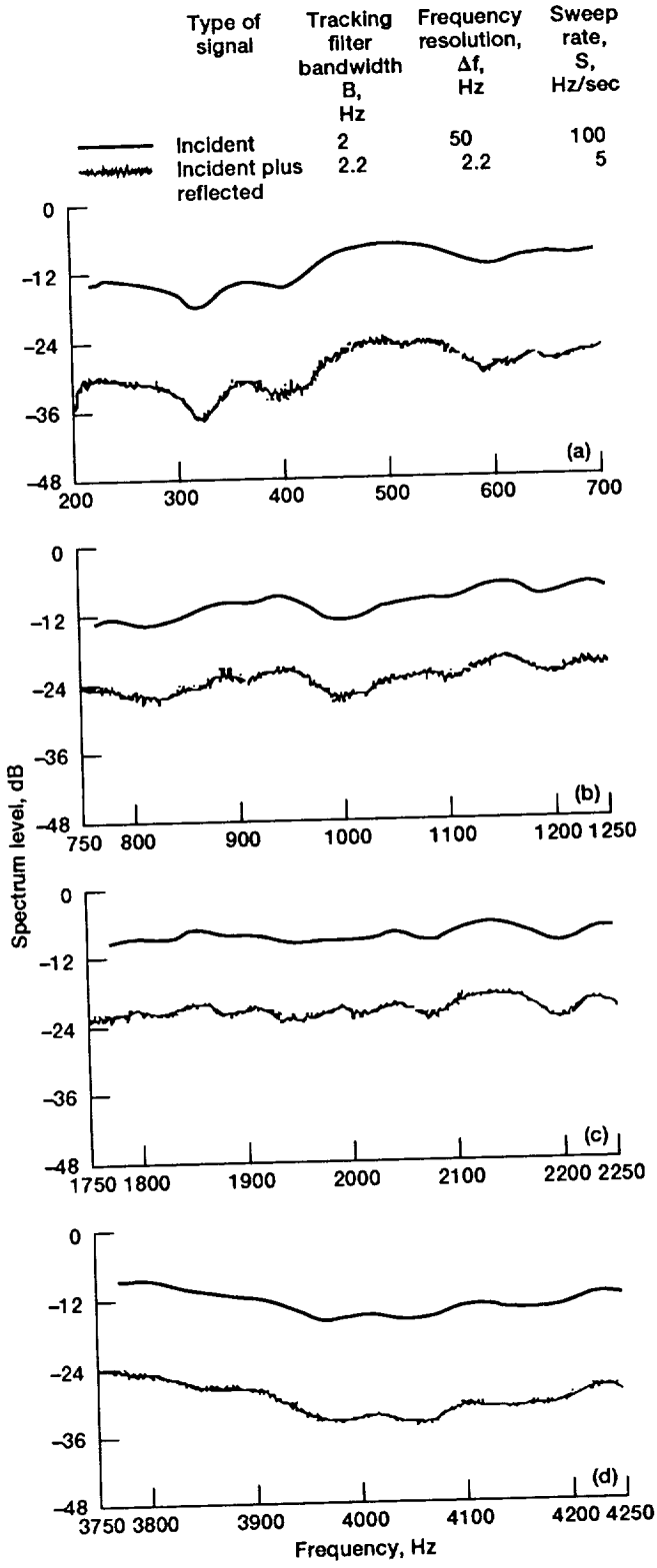

(a) Center frequency, 450 Hz.
(b) Center frequency, 1000 Hz.
(c) Center frequency, 2000 Hz.
(d) Center frequency, 4000 Hz.

Figure 36.—Frequency domain measurements in selected 500 Hz intervals of late reflections using setup 5.

ORIGINAL PAGE
BLACK AND WHITE PHOTOGRAPH

TABLE III.—SUMMARY OF LATE REFLECTION EFFECTS

Setup number	Maximum measured interference ripple in given frequency range, 20 log (max. level/min. level), dB, at—			
	200–700 Hz	750–1250 Hz	1750–2250 Hz	3750–4250 Hz
1	0.6	0.6	0.6	0.4
2	1.8	2.2	1.6	1.2
3	1.8	2.0	1.0	1.4
4	1.6	0.8	1.4	0.4
5	2.0	1.8	1.6	0.8
8	10.8	4.4	4.6	6.1
9	2.2	0.8	0.6	0.8
10	4.8	6.2	4.2	4.0
11	2.0	1.2	1.8	0.6

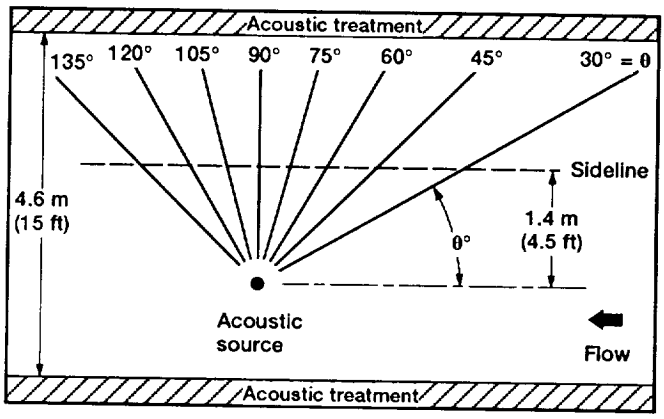

Figure 37.—Schematic showing source and traverse locations for decay with distance measurements.

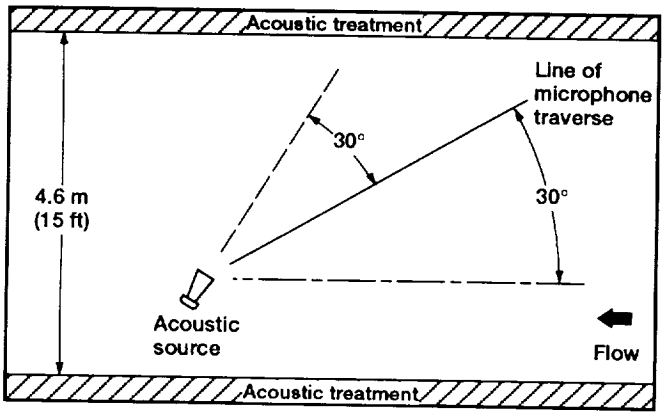

Figure 38.—Example schematic for the off-axis measurement of the decay with distance from the acoustic source.

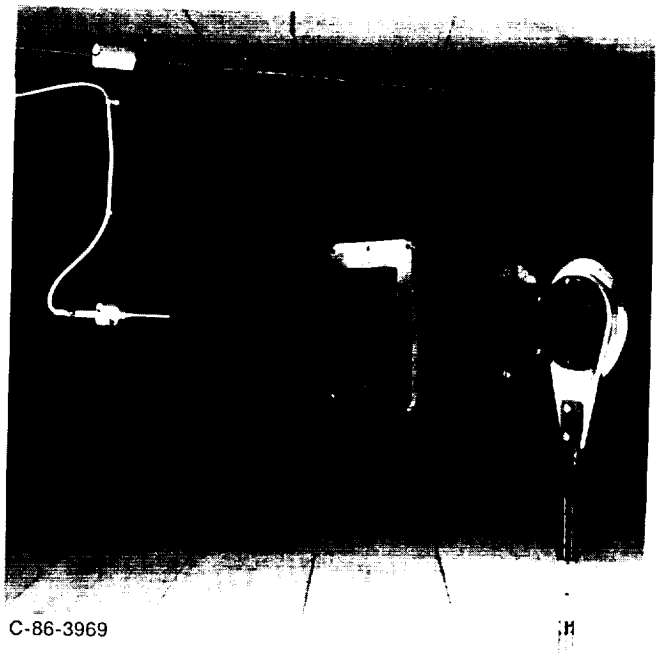

Figure 39.—Close-up view of acoustic driver with horn and microphone mountings for decay with distance measurements.

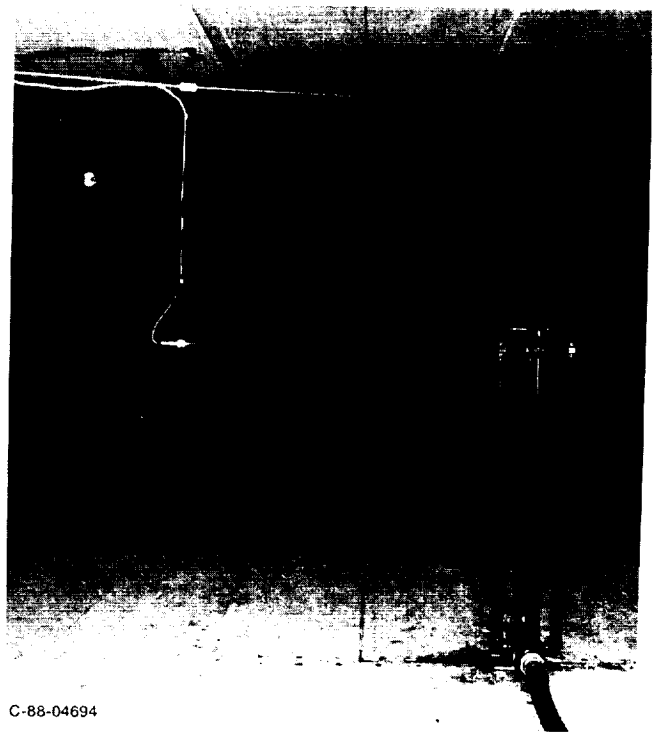

Figure 40.—Air source consisting of crossing jets used as broadband omnidirectional source for decay with distance measurements.

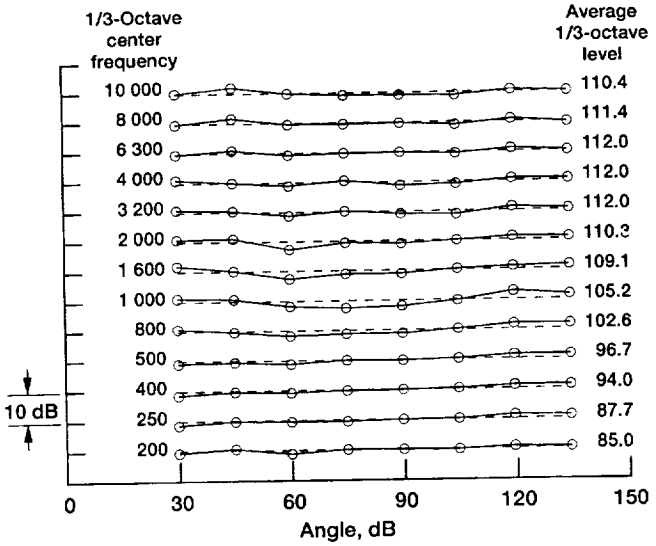

Figure 41.—Omnidirectional characteristics of air source measured at radius 45.7 cm from source center in the horizontal plane.

the axis of the acoustic horn was pointed along the line traversed by the microphone. Figure 38 shows an example schematic drawing of an off-axis measurement where the horn is pointing 30° towards the wall from the measurement line, which is 30° to the flow direction. A closeup of this acoustic source and the microphone mounted on the traversing cable are shown in figure 39. Both pure tones and white noise were used as acoustic signals. In addition, an air source consisting of crossing jets (fig. 40) was used as a broadband, omnidirectional source (ref. 15). The 2.54-cm diameter jets were designed for a peak frequency of about 2500 Hz. Measurements taken 45.7 cm from the center of this air source confirmed the omnidirectional characteristics in the horizontal plane (fig. 41). For all the decay with distance measurements, the acoustic source was located at the same position as listed for setup 3 in table I.

With the steady acoustic source in continuous operation, the microphone measured data at fixed positions along the traversing cable from a point near the source to a point near the wall. The measured levels for either one-third-octave band analysis of the broadband noise or pure tones at each position were converted to decibels and plotted versus the common logarithm of the distance from the source to the microphone. All the plots of the decay with distance data are given in appendixes A, B, and C. Ideally, in an acoustic free field, the acoustic level should decrease 6 dB for a factor of 2 increase in the distance between the source and the microphone (a 6-dB decay of sound per doubling of the distance). In general, the data show that the free-field behavior extends to at least the sideline position shown in figure 37 and that, in most instances, the free-field behavior extended 20 percent farther along the radius of the traverse. Beyond this point and closer to the wall, reflections off the wall more strongly influence the measurement. Excluding data near the source and near the wall, where near the wall is defined as those locations farther than 1.2 times the sideline location along the radial traverse line, the data were compared with this ideal characteristic decay line. The maximum deviations of the data from a 6-dB decay line fitted to the data in a least-squares error sense were determined and tabulated in table IV for the broadband omnidirectional source (air source), table V for the broadband directional acoustic source, and in table VI for the pure-tone directional source.

Table IV shows the maximum deviations from the free-field 6-dB decay line for data measured from the broadband omnidirectional source (appendix A). The data were measured along traverses at eight angles (see fig. 37) and analyzed into 13 one-third-octave bands. For the 400-Hz one-third-octave band and higher, the maximum deviations were no greater than ±2 dB from the ideal 6-dB decay line. The two lowest one-third-octave bands had slightly larger deviations. These results are reflected in the summary statistics shown at the bottom of the table. The average deviation from the ideal 6-dB decay line over all frequency bands and angles was ±1.1 dB. When the two lowest bands were deleted from the average, the average deviation reduced to ±1.0 dB.

TABLE IV.—MEASURED FREE-FIELD MAXIMUM DEVIATIONS FROM A 6-dB DECAY LINE FOR A BROADBAND OMNIDIRECTIONAL ACOUSTIC SOURCE

Angle	1/3-Octave band, Hz												
	200	250	400	500	800	1000	1600	2000	3200	4000	6300	8000	10 000
	Free field maximum deviation, dB												
30	1.9, −1.4	2.9, −1.9	1.8, −0.8	1.7, −0.8	1.2, −0.6	1.1, −1.1	1.8, −1.5	1.6, −1.6	1.3, −1.3	1.4, −1.7	1.6, −2.0	1.3, −1.8	1.5, −1.6
45	0.9, −1.3	1.8, −1.6	1.2, −1.0	1.1, −0.9	0.3, −0.4	0.7, −0.7	1.5, −0.9	0.8, −1.1	1.2, −0.6	1.0, −0.9	1.1, −0.8	1.0, −0.7	1.3, −1.2
60	1.8, −1.7	1.9, −1.0	1.2, −1.0	1.2, −1.2	1.0, −1.1	1.3, −1.2	0.9, −1.6	1.3, −1.8	0.6, −1.0	0.6, −1.0	0.8, −1.3	0.9, −1.3	0.5, −1.2
75	1.3, −1.3	1.9, −1.0	1.2, −1.3	1.0, −0.7	0.5, −0.4	1.0, −1.2	0.8, −0.9	1.1, −0.8	1.0, −0.8	0.8, −0.8	0.6, −0.6	0.6, −0.7	0.8, −0.8
90	3.9, −2.9	1.6, −1.3	0.9, −0.8	1.0, −0.6	0.5, −0.5	1.2, −1.5	0.9, −0.9	1.4, −1.3	0.9, −0.7	0.9, −0.9	0.9, −0.6	1.1, −0.7	0.7, −0.6
105	1.6, −1.4	1.6, −1.0	0.9, −0.7	0.8, −0.7	0.5, −0.7	0.7, −0.6	0.7, −1.5	1.0, −1.2	1.0, −1.4	0.7, −1.3	0.7, −1.4	0.8, −1.2	0.9, −1.1
120	1.0, −0.8	1.8, −1.6	1.4, −1.2	1.6, −0.8	0.6, −0.5	1.2, −1.4	0.6, −0.8	1.3, −1.7	0.6, −0.9	0.8, −1.2	0.8, −0.8	0.6, −0.9	0.7, −0.8
135	1.3, −1.1	2.2, −1.3	1.7, −1.3	1.0, −0.6	0.2, −0.6	0.9, −1.8	0.9, −1.2	0.7, −0.6	0.9, −1.0	0.7, −1.4	0.6, −1.4	0.5, −1.6	0.4, −1.5

Summary statistics	Average	1 Standard deviation
All bands	1.1, −1.1	0.5, 0.4
400-Hz band and up	1.0, −1.0	0.3, 0.4

TABLE V.—MEASURED FREE FIELD MAXIMUM DEVIATIONS FROM A 6-dB DECAY LINE FOR A BROADBAND DIRECTIONAL ACOUSTIC SOURCE

Angle	1/3-Octave band, Hz												
	200	250	400	500	800	1000	1600	2000	3200	4000	6300	8000	10 000
	Free-field maximum deviation, dB												
[a]30	2.8, −2.4	3.3, −5.3	1.4, −2.2	2.1, −2.3	1.4, −1.6	1.4, −2.2	0.9, −1.4	1.3, −1.4	1.3, −1.3	0.8, −1.3	1.8, −1.5	1.8, −1.3	1.8, −1.4
[a]45	2.1, −1.8	2.5, −2.9	0.7, −0.8	1.3, −3.2	1.4, −1.3	0.9, −1.3	1.0, −0.9	0.8, −1.3	0.8, −1.1	1.5, −1.2	1.9, −1.9	1.3, −1.4	1.4, −1.4
[a]60	1.7, −2.0	2.1, −2.8	1.2, −0.6	2.1, −2.1	1.2, −1.2	1.0, −1.3	0.9, −0.8	1.5, −1.1	1.1, −0.6	1.3, −0.9	1.6, −1.5	1.4, −1.0	1.4, −1.7
[a]75	4.2, −1.4	2.4, −2.0	1.4, −1.5	1.5, −1.7	1.7, −1.9	1.5, −0.8	1.0, −0.9	1.0, −1.1	1.0, −1.3	0.7, −0.9	2.3, −1.1	1.5, −1.6	1.9, −1.5
[a]90	1.8, −1.2	1.6, −1.2	0.8, −1.4	0.8, −1.1	1.9, −1.3	1.7, −1.3	1.1, −1.0	1.1, −0.6	0.8, −0.8	0.8, −1.3	2.0, −2.9	1.5, −1.8	1.5, −1.2
[a]105	2.0, −1.2	3.3, −1.9	1.4, −1.1	1.9, −1.9	1.3, −1.9	1.0, −1.5	0.7, −0.9	0.8, −1.6	0.8, −0.9	0.6, −0.8	2.2, −3.1	2.0, −2.7	1.6, −1.2
[a]120	1.4, −1.7	2.3, −2.1	1.4, −1.0	1.7, −1.5	1.5, −1.2	1.0, −1.1	0.5, −1.1	0.6, −0.6	0.5, −0.8	0.8, −0.8	1.1, −1.0	1.3, −1.3	1.4, −1.7
[a]135	2.4, −2.2	2.8, −2.3	1.7, −1.4	2.0, −1.7	1.5, −2.0	0.9, −1.2	1.1, −1.4	1.0, −1.0	1.3, −1.7	1.3, −1.5	1.9, −2.3	1.9, −2.1	1.6, −1.8
[b]30	2.1, −1.7	2.7, −1.7	2.2, −1.5	1.6, −1.0	1.0, −1.5	1.7, −1.5	0.9, −1.9	2.0, −2.3	2.2, −2.2	3.2, −1.1	1.7, −2.0	2.4, −2.5	1.5, −2.2
[b]60	1.7, −1.7	1.6, −1.2	1.0, −1.9	1.0, −0.7	0.6, −0.5	1.1, −1.2	1.1, −1.3	1.7, −1.2	1.0, −1.9	1.6, −1.0	1.5, −0.8	1.3, −1.0	1.0, −1.5
[b]135	2.9, −2.1	2.6, −1.8	1.1, −0.9	1.4, −1.2	1.1, −0.8	1.5, −1.6	1.1, −0.8	1.6, −1.0	1.3, −1.4	1.1, −1.2	1.3, −1.9	1.7, −1.8	1.6, −1.9

Summary statistics	Average	1 Standard deviation
On axis		
All bands	1.5, −1.5	0.6, 0.7
400-Hz band and up	1.3, −1.4	0.4, 0.5
Off axis		
All bands	1.6, −1.5	0.6, 0.5
400 Hz band and up	1.5, −1.4	0.5, 0.5

[a]On axis.
[b]Off axis.

TABLE VI.—MEASURED FREE-FIELD MAXIMUM DEVIATIONS FROM A 6-dB DECAY LINE FOR A PURE-TONE DIRECTIONAL ACOUSTIC SOURCE

Angle	Frequency, Hz				
	250	500	1000	2000	4000
	Free-field maximum deviation, dB				
[a]30	3.7, −2.6	4.4, −3.5	2.3, −1.2	1.1, −0.9	1.9, −2.5
[a]60	2.6, −2.8	2.6, −2.4	1.6, −1.3	0.8, −0.9	0.8, −1.3
[a]90	2.3, −3.6	1.8, −2.3	2.2, −1.6	2.4, −2.9	1.9, −1.3
[a]135	2.6, −2.4	1.9, −6.7	1.9, −1.2	2.0, −2.3	2.0, −1.4
[b]30	4.1, −3.1	4.9, −4.3	2.8, −5.4	2.4, −3.2	2.6, −5.1
[b]60	2.9, −2.2	2.1, −1.4	2.6, −2.1	4.1, −3.9	2.4, −1.6
[b]135	2.7, −2.0	2.3, −4.7	1.2, −1.4	2.4, −1.5	2.9, −3.0

Summary statistics	Average	1 Standard deviation
On axis		
All frequencies	2.1, −2.2	0.8, 1.3
1, 2, and 4 kHz	1.7, −1.6	0.6, 0.6
Off axis		
All frequencies	2.8, −3.0	0.9, 1.4
1, 2, and 4 kHz	2.6, −3.0	0.7, 1.5

[a]On axis.
[b]Off axis.

When the broadband acoustic source has directional characteristics, the maximum deviations (as shown in table V) get typically larger than the maximum deviations for the omnidirectional source. The on-axis measurements (appendix B, fig. 43) were made with the source pointed in the direction of the traverse. The off-axis measurements (appendix B, fig. 44) were made with the source pointed 30° toward the wall from the line of the traverse. In general, the off-axis data for the broadband directional source had maximum deviations that were no larger than the on-axis data. This is clearly seen in the summary statistics given in table V. Again, the two lowest one-third-octave bands had the largest maximum deviations and the average deviation was reduced when these values were deleted from the average. Combining both on- and off-axis average deviations for the 400-Hz frequency band and above, the average deviation from the 6-dB decay line for the broadband acoustic source was then about ± 1.4 dB.

Using a pure-tone source restricts the results to a single frequency. This tends to excite a standing wave in the test section, which more prominently displays the reinforcement and cancellation effects from reflections. As a consequence, larger variations in the acoustic field are measurable. The maximum deviations from the ideal 6-dB decay line for five frequencies are shown in table VI for the data in appendix C, (fig. 45). These pure-tone deviation values are, indeed, typically larger than the previous broadband deviation values, and the summary statistics reflect this trend, also. Part of the reason for this situation lies in the choice of the sideline location (fig. 37). This sideline location was a common reference in all the decay with distance data, and the maximum deviations were determined after excluding the data from locations 20 percent beyond the sideline location as described previously. In general, then, the result of using this common sideline location is that this location was too close to the wall for acoustic free-field measurement of the pure-tone source. This is especially evident in the 1-, 2-, and 4-kHz data shown in figures 45(c) to (e). If the sideline location was moved closer to the source, then, in general, the maximum deviations would have been less and free-field measurements of the pure-tone source could be made at these three higher frequencies within the same accuracy as the broadband data.

Discussion

In general, many measurements could be made to acoustically evaluate the tunnel test section. Some measurements may be better suited to determining the acoustical characteristics of the test section for a particular model test than other

types of measurements. The suitability of the measurements depends on such test parameters as source type, microphone placements, treatment configuration (some boxes may be replaced by a solid panel for some tests), test model placement and size, and solid surfaces on test model and model support structures. A user of the test section must be aware of these conditions when taking acoustical measurements. The results presented here are for an empty test section where the size of the acoustic source is relatively small compared with the size of the test section and where the microphone mounting hardware is minimal. Further, to satisfy the original motivation for installing this treatment, the tunnel test section was evaluated for turboprop acoustic measurements (refs. 13 and 14). Thus, source and microphone placements tended to be similar to those used for turboprop measurements, and most of the data were taken at frequencies below 5 kHz.

Given all the data from the two types of measurement (time delay spectrometry analysis of early and late reflections and steady decay with distance measurements), how do all the results compare?

Early reflection results showed interference ripples due to reflections in measurements of the incident signal that varied on average from 1.7 to 3.2 dB from the minimum to the maximum of the interference pattern. These measurements were made at individual locations within the test section and, in each case, the major axis of the source was pointed at those measurement locations.

Next, the effect of late reflections was measured to have, at most, a 2-dB interference ripple and, at most frequencies, much less than a 2-dB interference ripple on the incident signal in addition to the interference due to early reflections. This result assumed that the microphone position was away from the ends of the test section. Any microphone location between the test section axial positions given for setups 3 and 5 (table I) would be away from the ends of the test section. It should be noted that it took a fine frequency resolution (2.2 Hz) to detect late reflection interference. Also note that acoustic data taken in the test section during a particular model test are typically spectrum analyzed with frequency resolutions greater than 2.2 Hz. If the frequency resolution is greater than about 10 Hz, then it is doubtful that these low level late reflections would be resolved as having any effect on incident signal measurements taken well within the test section.

Because late reflections are not a problem for measurements within the test section, the decay with distance results show the effects of reflections from within the test section (early reflections) only. These results are spatial wave patterns that vary about the ideal 6-dB decay line. Using the same directional acoustic source as was used for the early reflection measurements, the spatial wave patterns averaged a 3-dB variation from minimum to maximum level, or about ± 1.5 dB, about the ideal 6-dB decay line. This result was an average from both on- and off-axis measurements for one-third-octave band analysis of broadband noise at 400 Hz and higher, and at 1, 2, and 4 kHz when the source used pure tones and was measured on-axis. An omnidirectional source had typically less variation in the spatial wave pattern. Recall that the early reflection interference ripple result was determined from averages over frequency at specific locations within the test section. Whereas the decay with distance result was, in essence, determined from averaging over both space and frequency. Thus, the decay with distance value represents how well the test section simulates an acoustic free field within the spatial region of measurement. Specific locations within this region will be slightly more or less than this 3-dB variation, as can be determined from the early reflection results and the decay with distance data plots.

Now that we have considered the measured characteristics of the acoustic field in the test section, we can determine if they are consistent with what would be expected for the acoustic field characteristics based on the impedance and absorption coefficient measurements (ref. 3) of the installed treatment in the tunnel test section. It is these absorptive characteristics of the treatment that determine the early reflection interference pattern and the decay with distance variations. Reference 3 states that the measured absorption coefficient for the full depth treatment was greater than 0.95 over the frequency range 250 to 4 kHz. This was the frequency range where the treatment had high absorption. Reference 3 included data at higher frequencies, where absorption was less than 0.95, and we must use these data since this paper reports results of acoustic field measurements to 10 kHz. The absorption coefficient in reference 3 was shown to be decreasing above 4 kHz until at 10 kHz the absorption coefficient was about 0.8. Since the average acoustic free-field variations become larger when the treatment absorption coefficient is lower, we will use the 0.8 value for the absorption coefficient for a worst-case example of the effects of reflections off the treatment on the acoustic free field. First, let a plane wave reflect off the treatment. The resulting spatial standing-wave pattern associated with this plane wave would be 8.4 dB from minimum to maximum level. Next, if spherical spreading were included, the standing-wave pattern would be less than this value because of the path length difference between incident and reflected waves. However, this result depends on the position of the microphone within the acoustic field in the test section. We examine two setups: (1) the 30° setup (fig. 6) and (2) the 90° setup (fig. 7). The resulting spatial standing wave, including spherical spreading, at these locations are (1) 4.3 dB and (2) 2.4 dB, respectively. As the absorption coefficient increases toward 1.0, both of these standing-wave values will decrease. Thus, for a relatively compact acoustic source with low directivity characteristics, an average variation of 3 dB in the acoustic free field is within expectation, given that we are including a frequency range from 250 Hz to 10 kHz and that the treatment absorption coefficient is greater than 0.8 over that range.

If the source is highly directional, there may be source-microphone configurations where the lower level incident signal is contaminated by a large reflection. This was shown

in some of the early reflection results (see, for example, fig. 17). However, this problem did not show up in the steady decay with distance measurements. The TDS measurements did a good job identifying reflections, the general locations of the reflection points, and their apparent effects in a narrow time window using a directional source activated by a sweeping pure tone. But those measurements may not be a good indicator of results for a broadband source analyzed in one-third-octave bands (Or perhaps one-third-octave band analysis hides the effects of reflections that may appear in a narrow band analysis). The off-axis pure-tone results (table VI) show some wider variations in the decay with distance data than the off-axis results for a broadband source (table V). Thus, measurements made off-axis from the major lobe of a source directivity pattern should be analyzed for reflections, perhaps cepstrum analysis may be useful for broadband sources (refs. 16 and 17).

The general result of the acoustic evaluation reported herein is that the reflections off the treatment were reduced enough that simulated free-field measurements of an acoustic source were possible over the frequency range 400 Hz to 10 kHz and within a typical accuracy of ± 1.5 dB of only the incident signal. If the source is not highly directional, then the free-field variations are typically much smaller. The data also show that the choice of measurement location is a factor in the accuracy of free-field measurements. Even though this tunnel treatment was designed for the measurement of lower frequency acoustic sources, it is sometimes desirable to measure sources with higher frequency content. To extrapolate these results higher than 10 kHz, the effects of atmospheric absorption have to be considered. A brief discussion of these effects and how they may affect the results of acoustic measurements in the test section is given in appendix D.

Conclusions

1. The effect of early reflections from within the test section was to create interference patterns in the incident signal. The interference ripple about the incident signal for five measurement setups varied on average from 1.7 to 3.2 dB wide from minimum to maximum level for on-axis measurements over the frequency range from 500 to 5150 Hz. These effects were measured using time delay spectrometry, which can identify the location on the treatment that reflected the measured reflected signals. As a consequence, the early reflection results depend on the local behavior of the surface at the points of reflection of the incident acoustic wave.

2. Late reflections from upstream and downstream of the test section due to a source in the test section come from two dominant points: (a) the wind tunnel cooler upstream of the test section, (b) the diffuser discontinuity downstream of the test section.

3. Late reflections are insignificant for acoustic measurements taken within the test section between axial locations of about 3 to 7 m from the start of the test section if the frequency resolution of the measurement is greater than 10 Hz.

4. Decay with distance measurements in the test section for an acoustic source with low directivity characteristics show that free-field data can be measured on average with an accuracy of ± 1.5 dB or better. This result was an average from both on- and off-axis measurements for 1/3-octave band analysis of broadband noise at 400 Hz and higher, and at 1, 2, and 4 kHz when the source used pure tones and was measured on-axis. An omnidirectional source had typically less variation in the spatial wave pattern. Specific locations within the region where decay with distance measurements were made may have slightly more or less than this variation as can be determined from the early reflection results and the decay with distance data plots.

Lewis Research Center
National Aeronautics and Space Administration
Cleveland, Ohio, July 23, 1991

Appendix A—Decay with Distance Data for Broadband Omnidirectional Source

Figure 42 shows the measured decay with distance for the broadband omnidirectional source (air source) shown in figure 40. Each plot shows measurements along the eight radial microphone traverse lines (fig. 37), for a single 1/3-octave band. The sideline markers in each figure represent the sideline positions for each angle as shown in figure 37. The data were compared with the 6-dB decay line and the deviations from this line are listed in table IV.

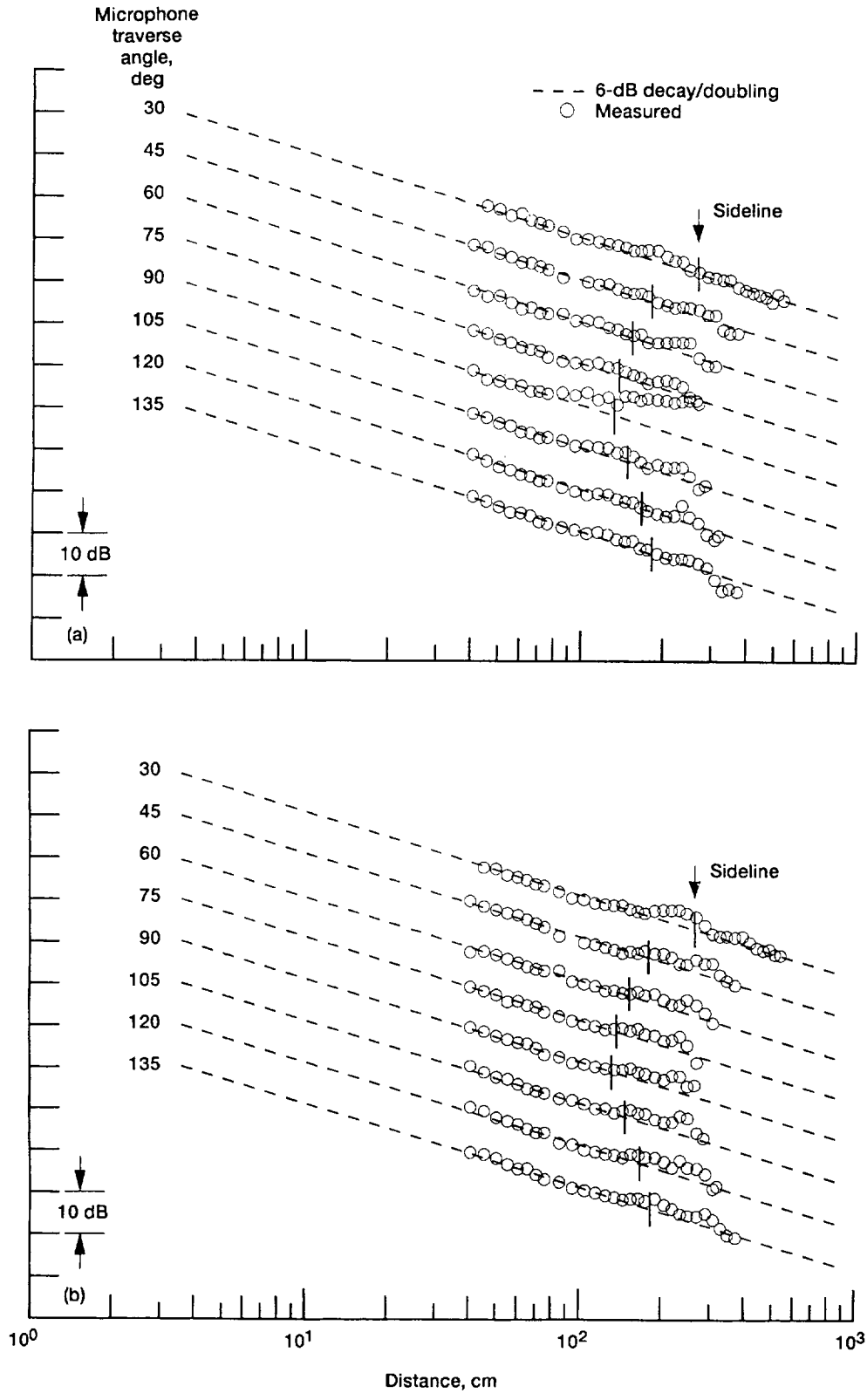

(a) 200-Hz 1/3-octave band.
(b) 250-Hz 1/3-octave band.

Figure 42.—Measured decay with distance from a broadband omnidirectional source.

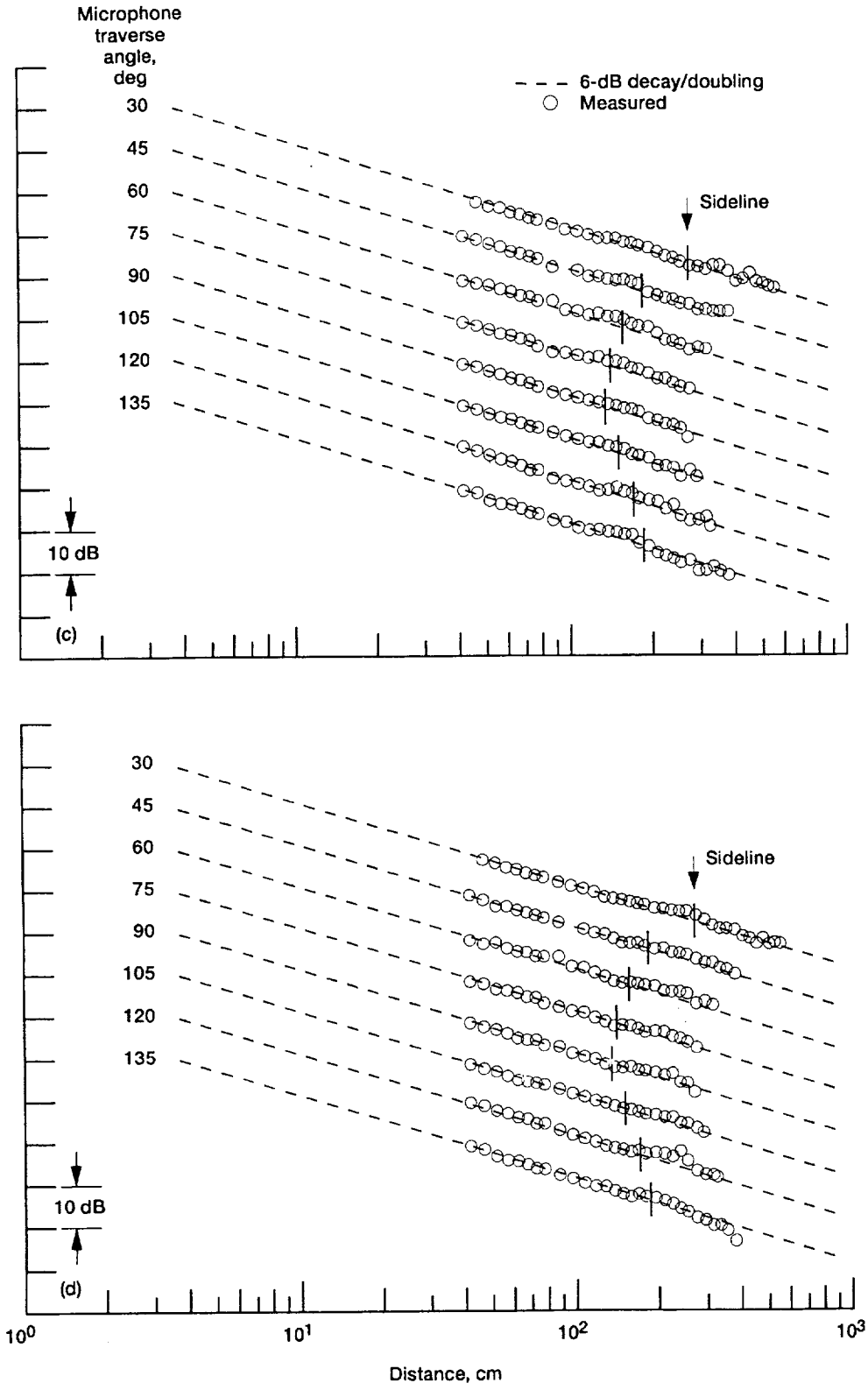

(c) 400-Hz 1/3-octave band.
(d) 500-Hz 1/3-octave band.

Figure 42.—Continued.

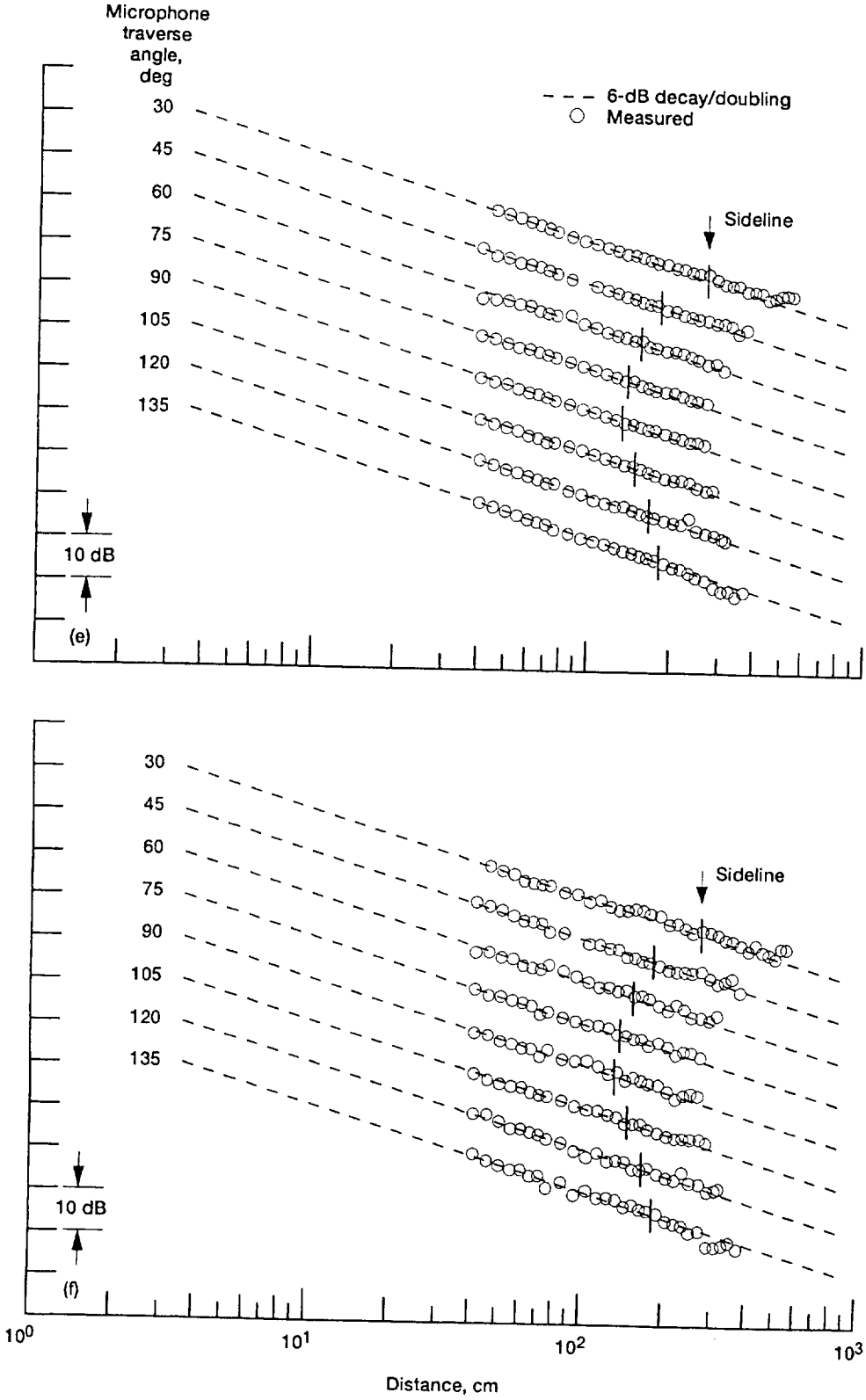

(e) 800-Hz 1/3-octave band.
(f) 1000-Hz 1/3-octave band.

Figure 42.—Continued.

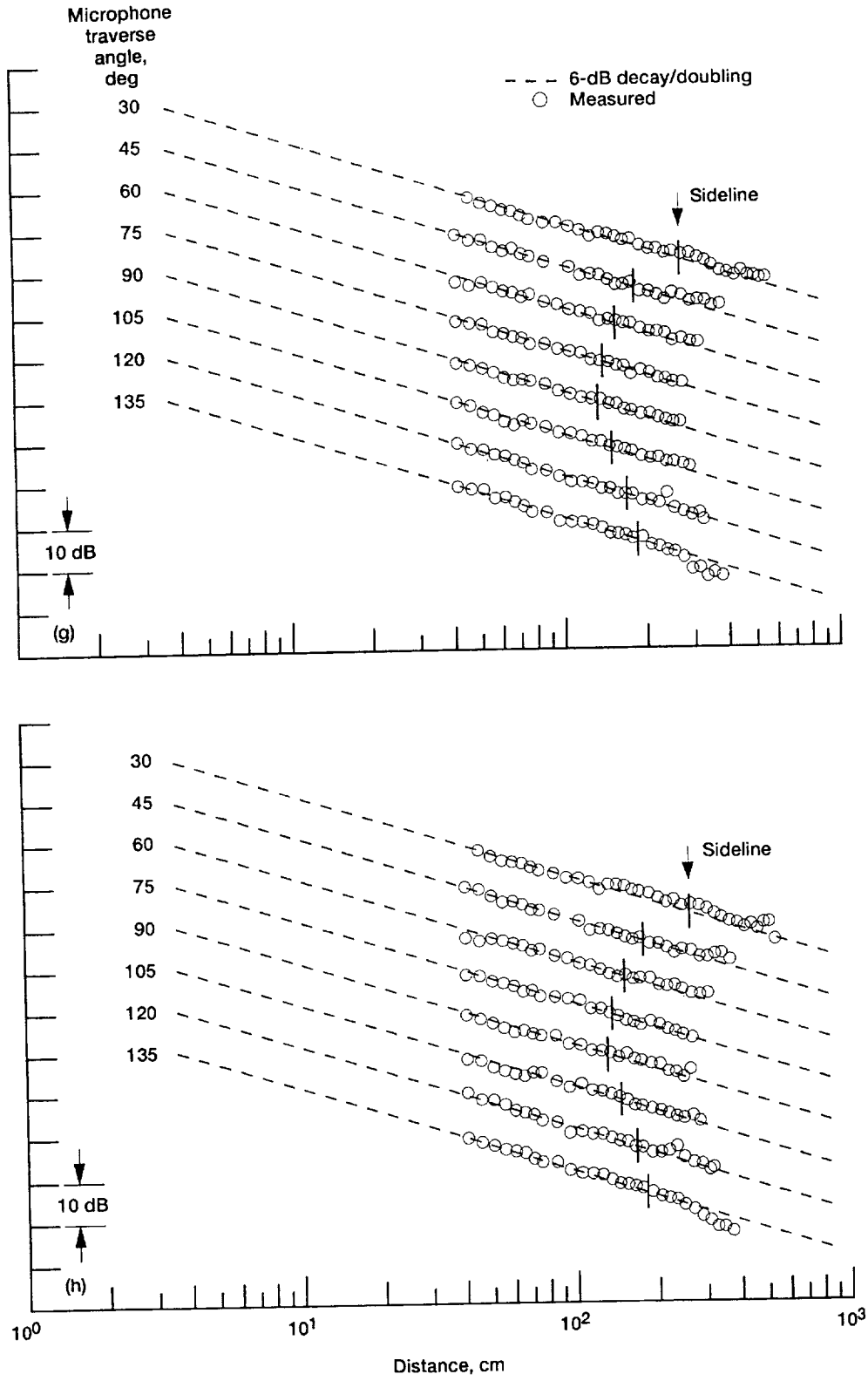

(g) 1600-Hz 1/3-octave band.
(h) 2000-Hz 1/3-octave band.

Figure 42.—Continued.

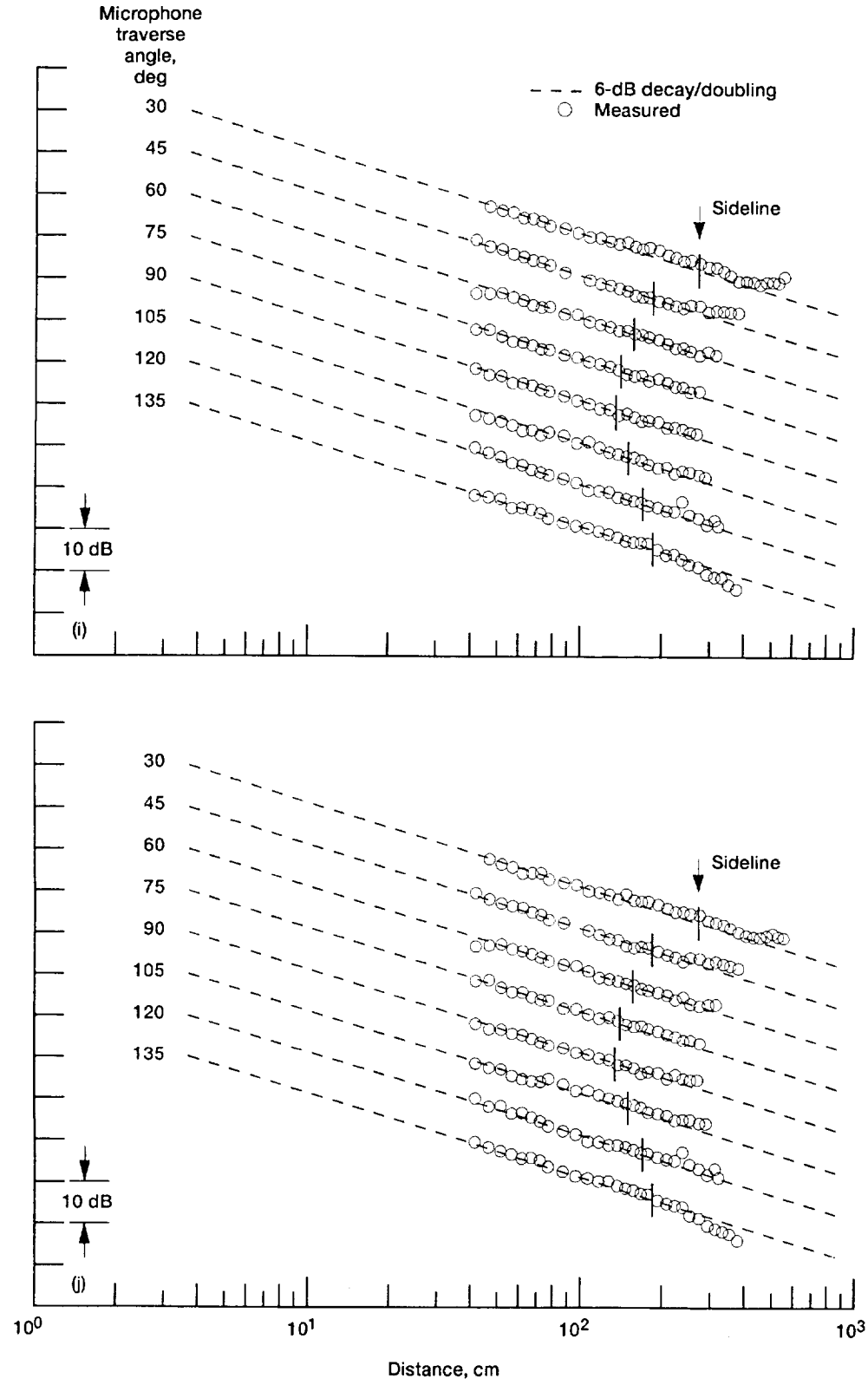

(i) 3200-Hz 1/3-octave band.
(j) 4000-Hz 1/3-octave band.

Figure 42.—Continued.

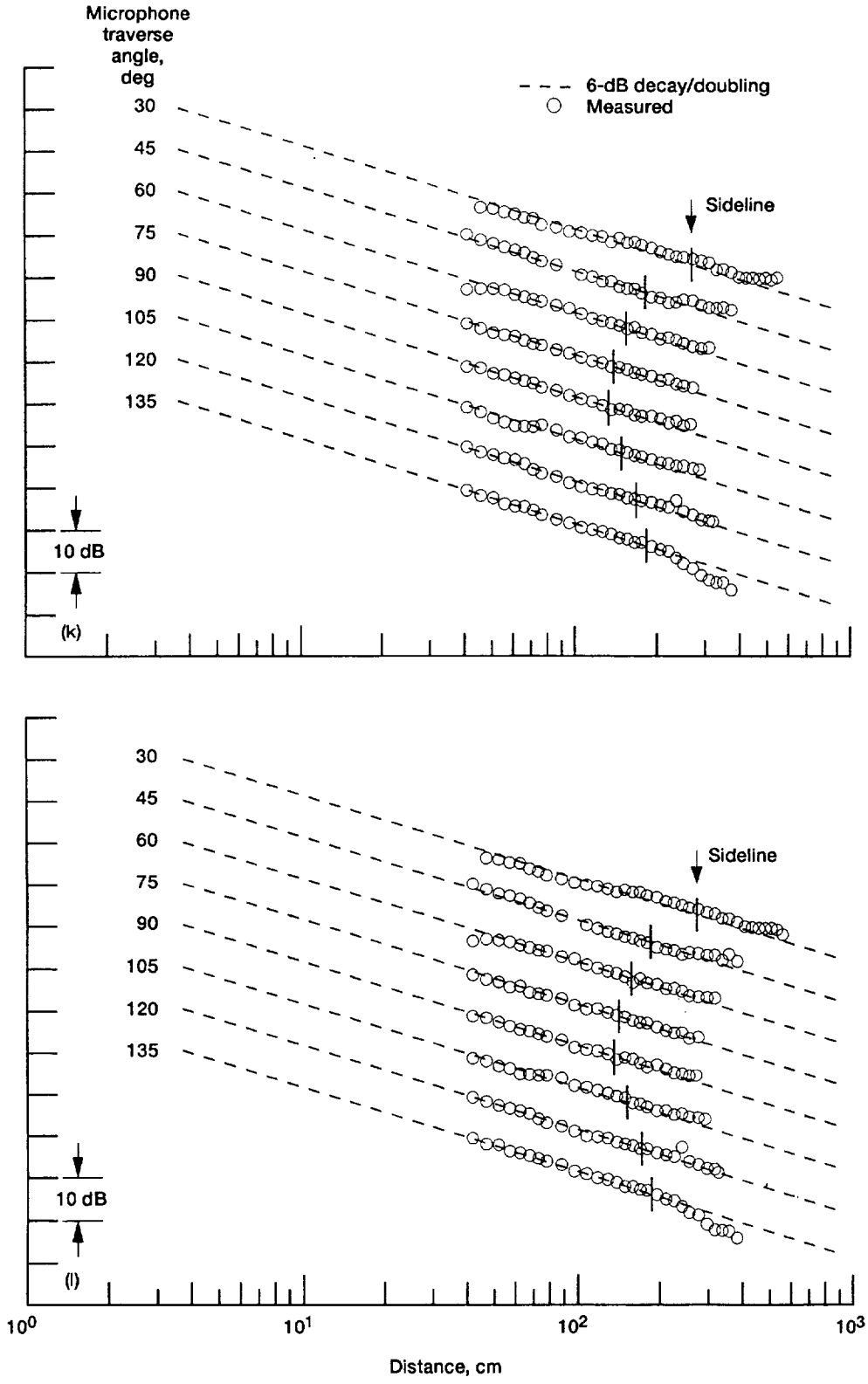

(k) 6300-Hz 1/3-octave band.
(l) 8000-Hz 1/3-octave band.

Figure 42.—Concluded.

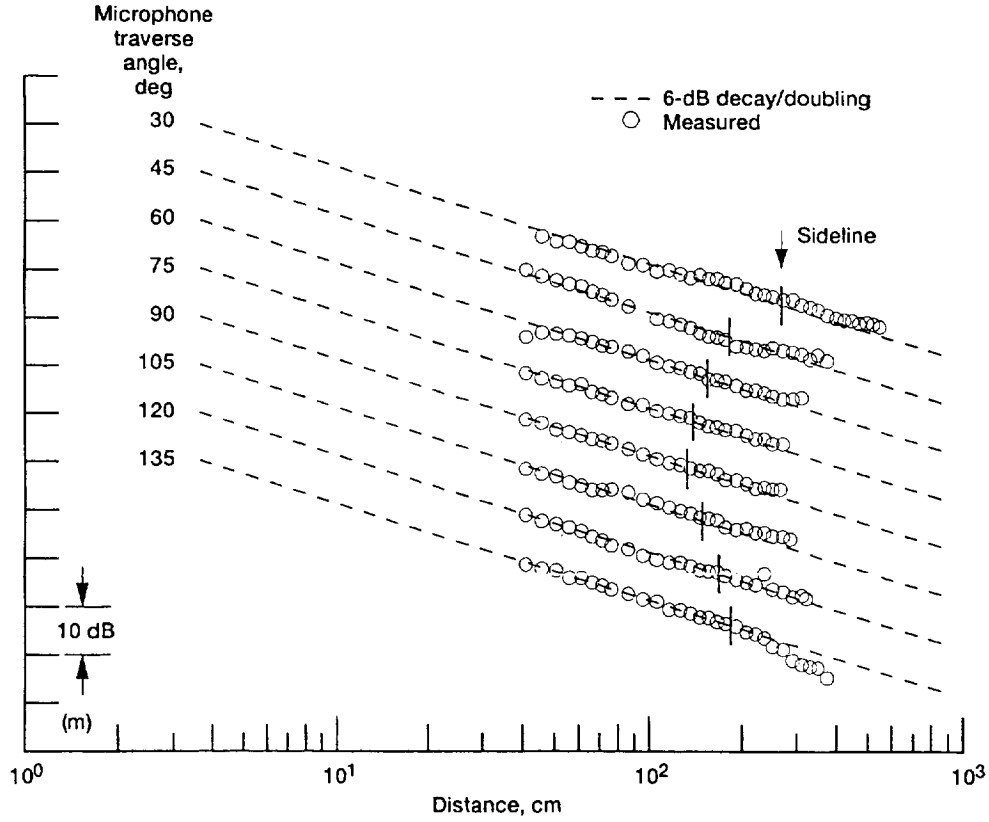

(m) 10 000-Hz 1/3-octave band.

Figure 42.—Concluded.

Appendix B—Decay with Distance Data for Broadband Directional Source

Figure 43 shows the measured decay with distance for the broadband directional source (Fig. 39) when the measurements were taken along each of the eight radial microphone traverse lines shown in figure 37 and the axis of the source was pointed along the microphone traverse line. Each plot of figure 43 shows measurements at eight angles for a single octave band. Decay with distance measurements off the major axis of the source are shown in figure 44, where comparisons with on-axis measurements are also shown. An off-axis measurement setup is illustrated in figure 38. The angle label for each data line in the plots refers to the direction of the microphone traverse line. For off-axis measurements, the angle of the source axis is given in the figure sublegends. The sideline markers in each plot represent the sideline positions for each angle as shown in figure 37. The data were compared with the 6-dB decay line, and the deviations from this line are listed in table V.

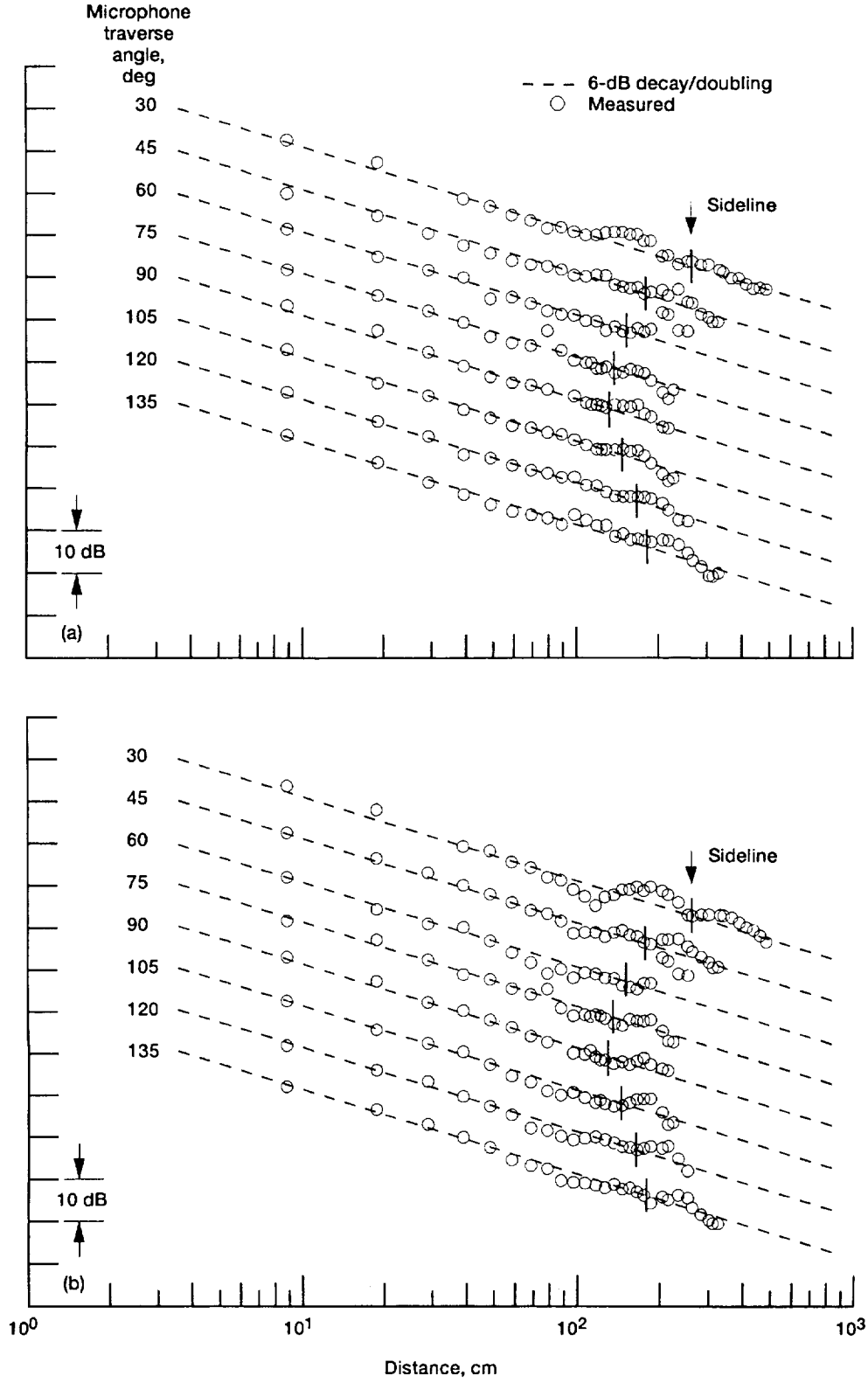

(a) 200-Hz 1/3-octave band.
(b) 250-Hz 1/3-octave band.

Figure 43.—Measured decay with distance on-axis from a broadband directional source.

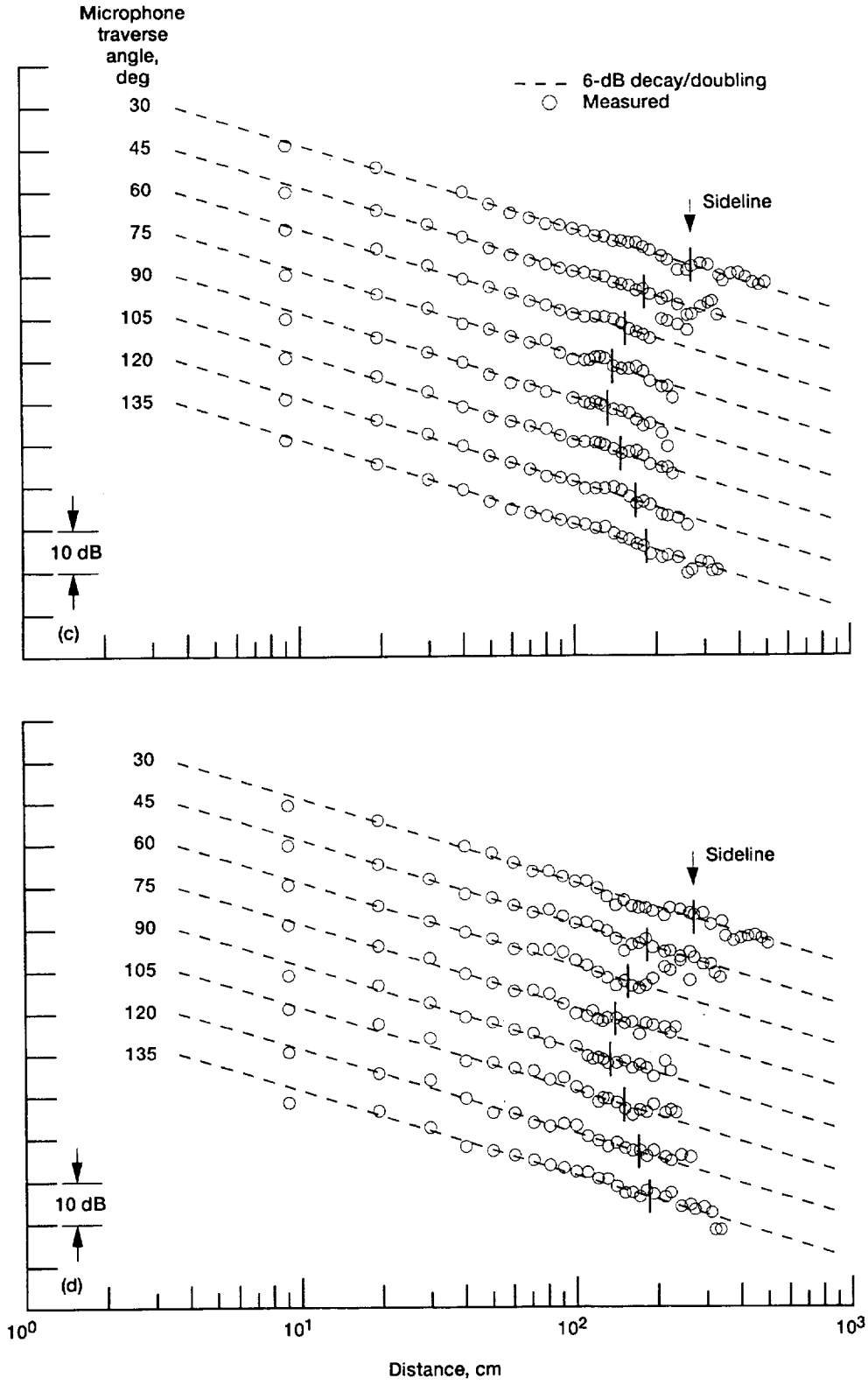

(c) 400-Hz 1/3-octave band.
(d) 500-Hz 1/3-octave band.

Figure 43.—Continued.

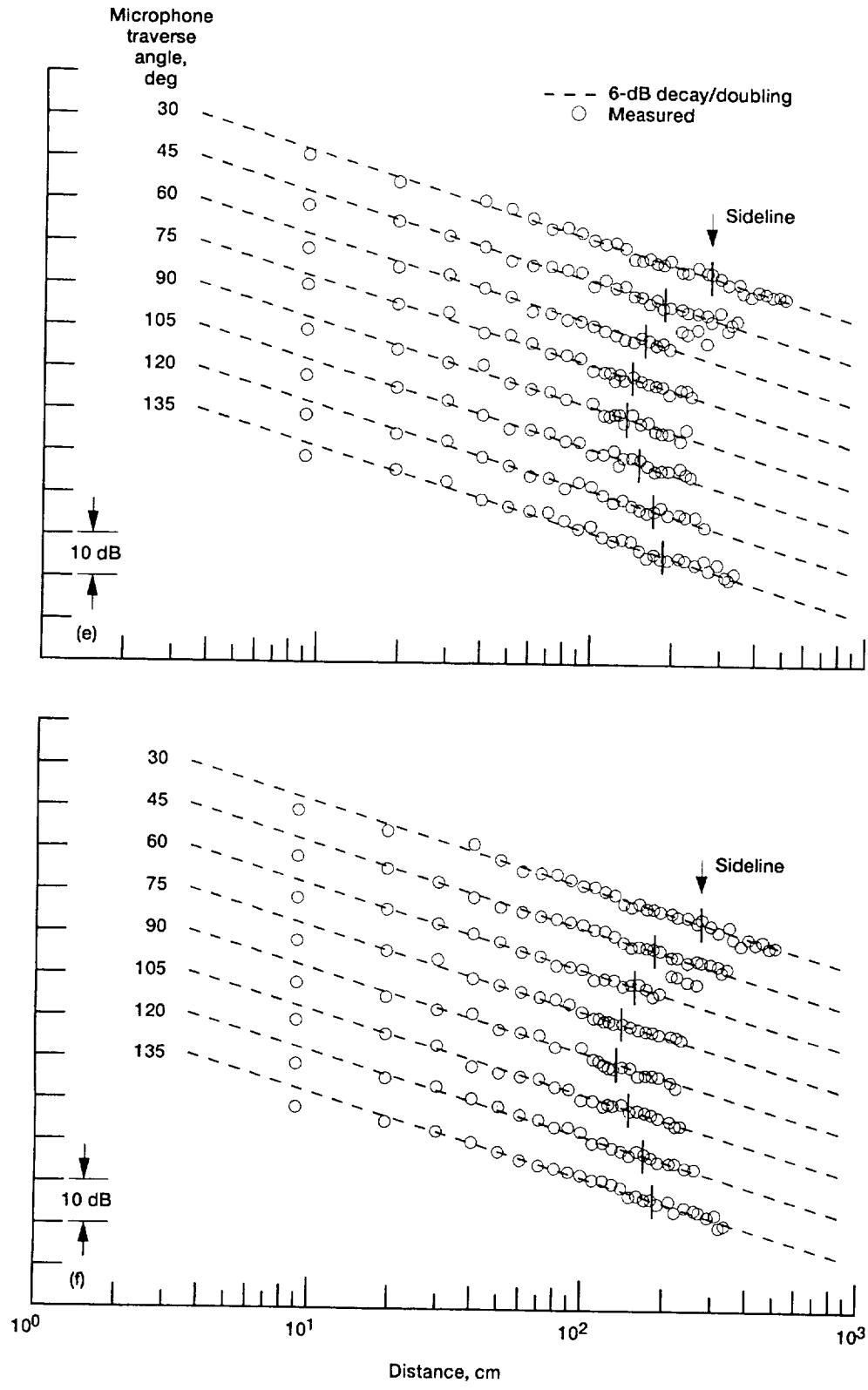

(e) 800-Hz 1/3-octave band.
(f) 1000-Hz 1/3-octave band.

Figure 43.—Continued.

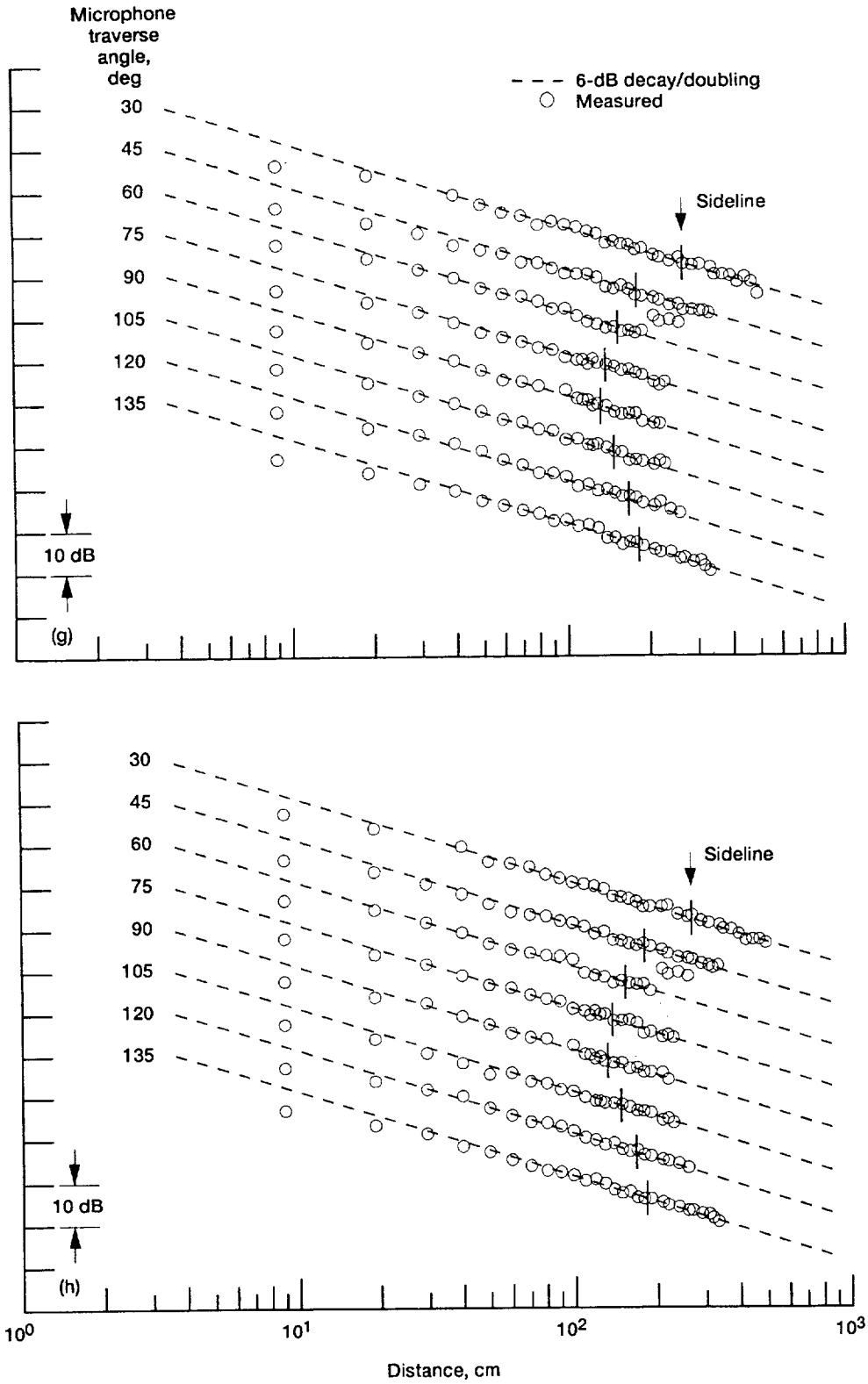

(g) 1600-Hz 1/3-octave band.
(h) 2000-Hz 1/3-octave band.

Figure 43.—Continued.

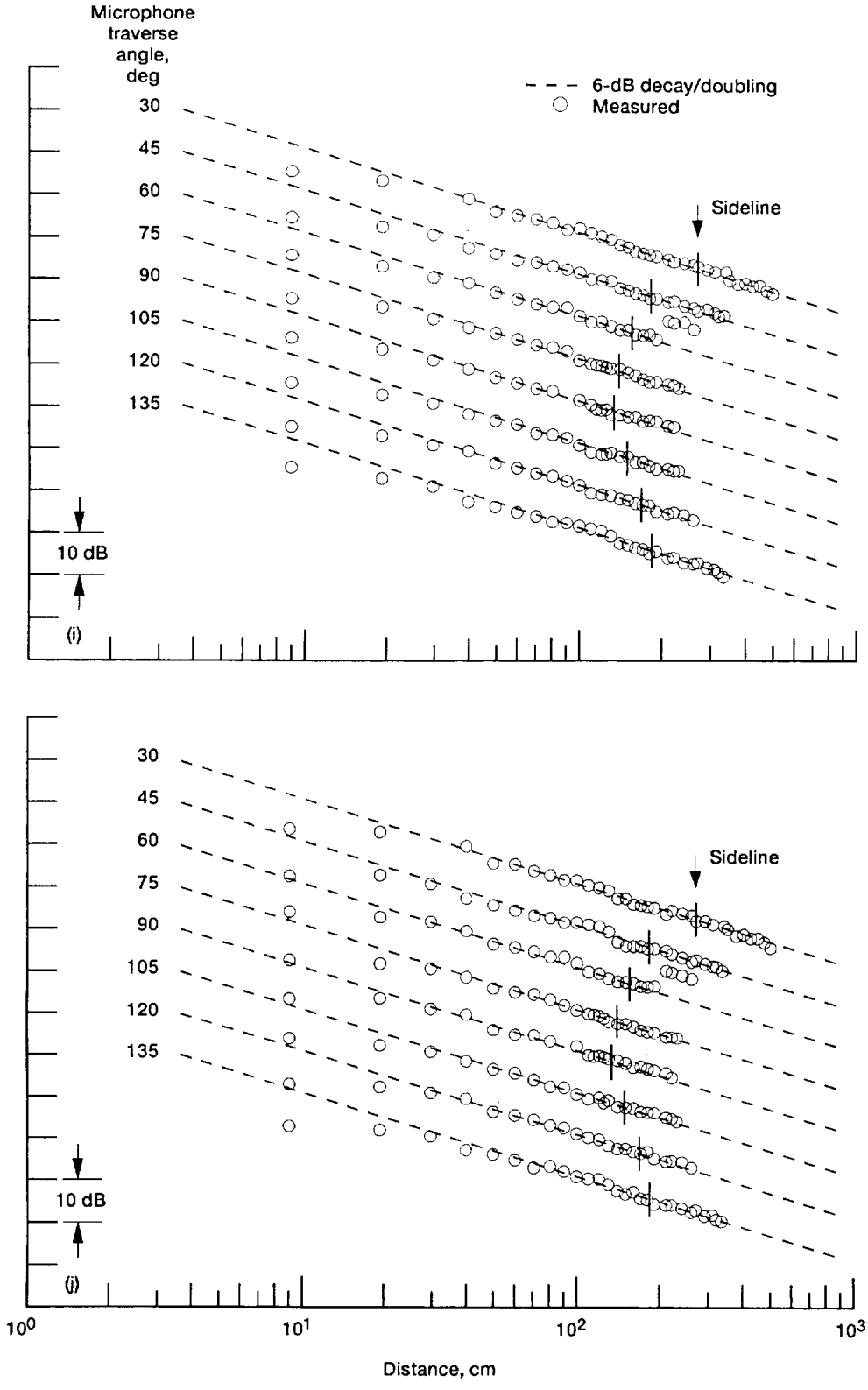

(i) 3200-Hz 1/3-octave band.
(j) 4000-Hz 1/3-octave band.

Figure 43.—Continued.

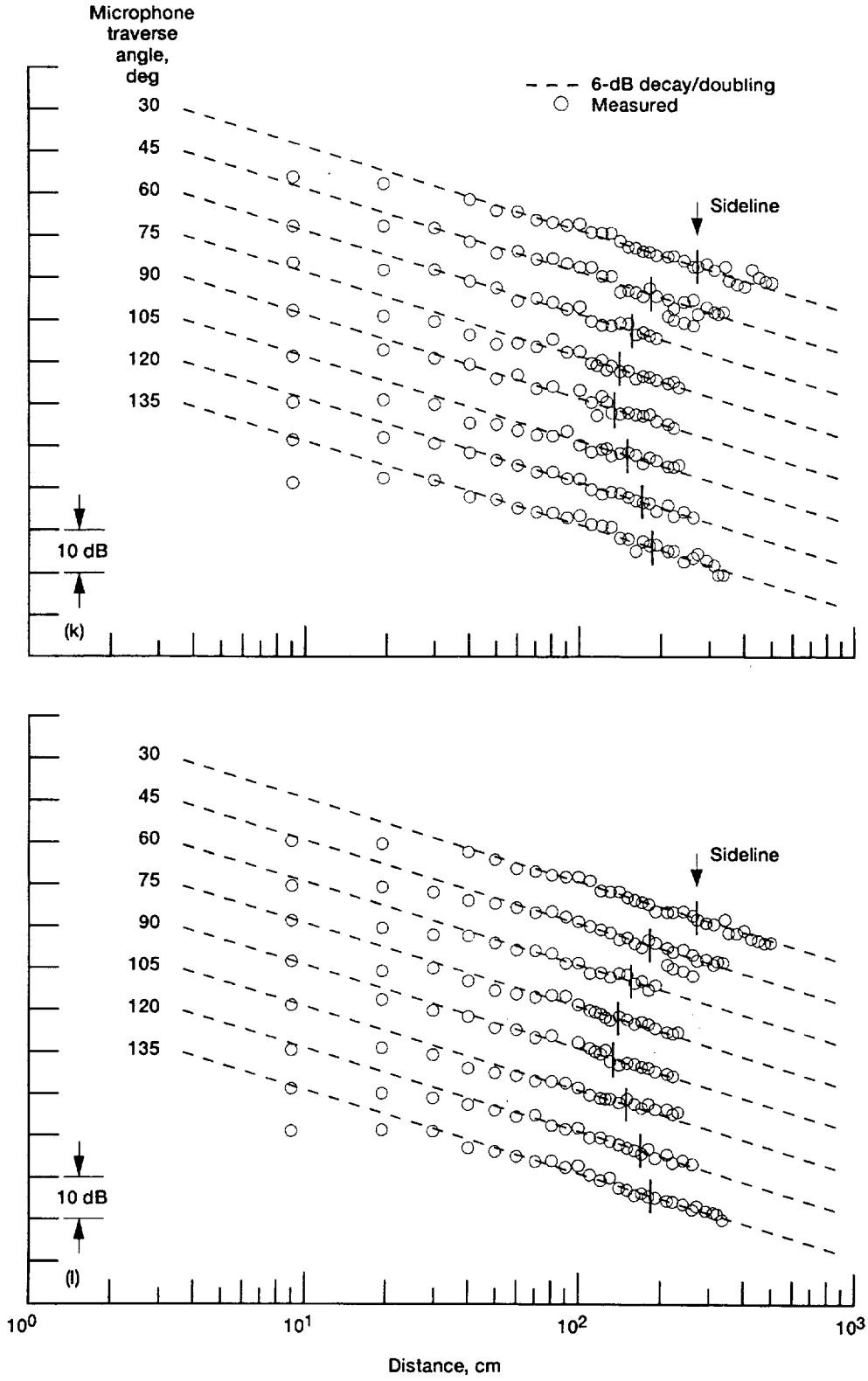

(k) 6300-Hz 1/3-octave band.
(l) 8000-Hz 1/3-octave band.

Figure 43.—Continued.

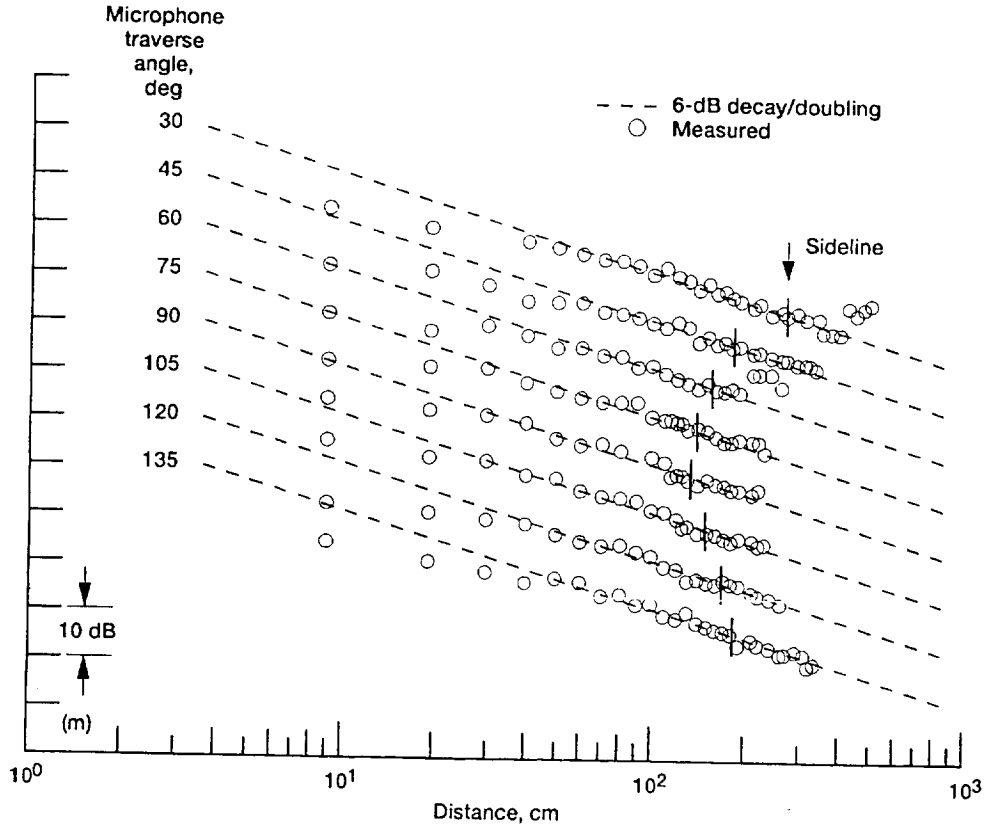

(m) 10 000-Hz 1/3-octave band.

Figure 43.—Concluded.

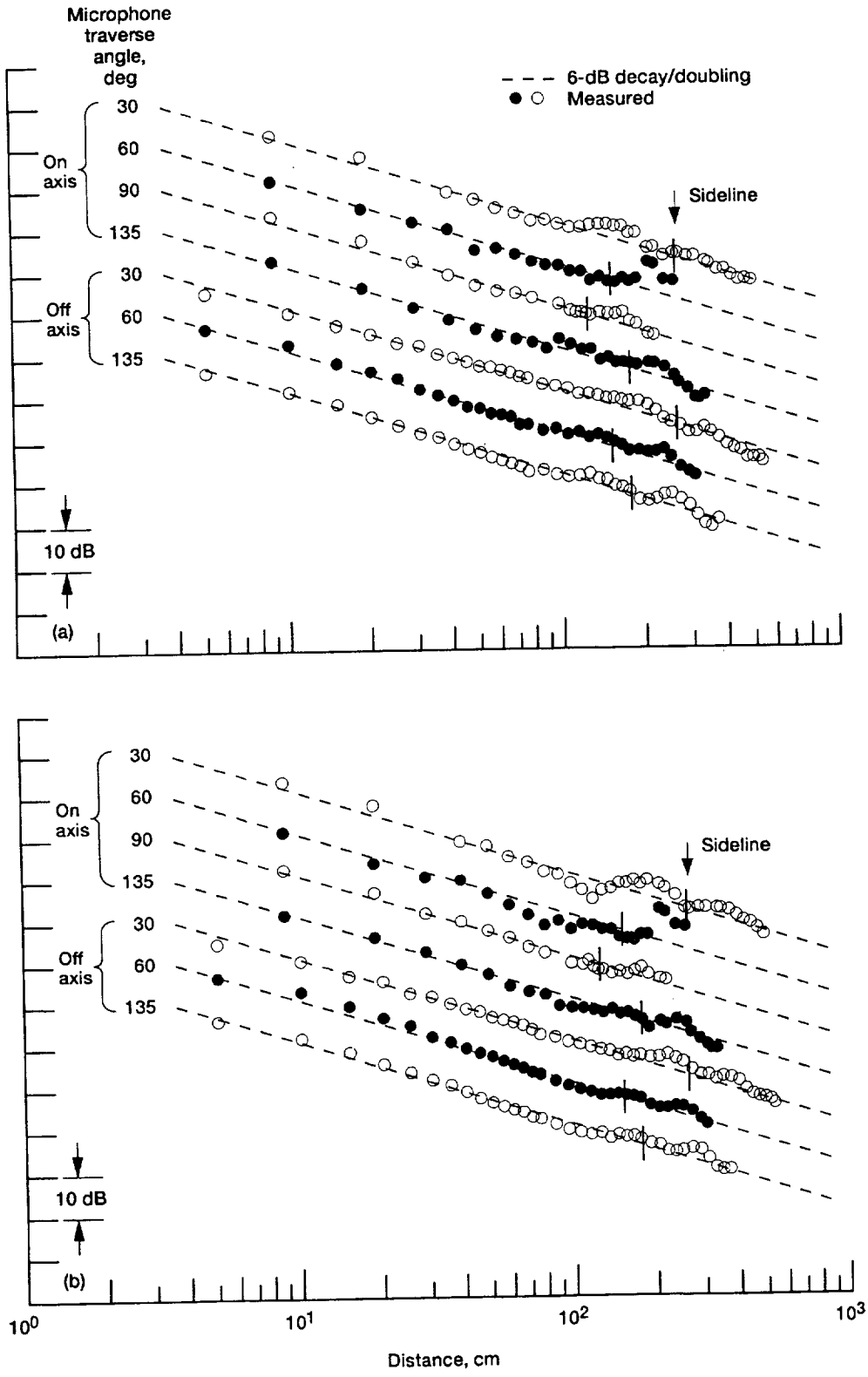

(a) 200-Hz 1/3-octave band.
(b) 250-Hz 1/3-octave band.

Figure 44.—Measured decay with distance from a broadband directional source; comparison between on- and off-axis measurements. Angle of source major axis for off-axis measurements: 30, source 60; 60, source 90; 135, source 105.

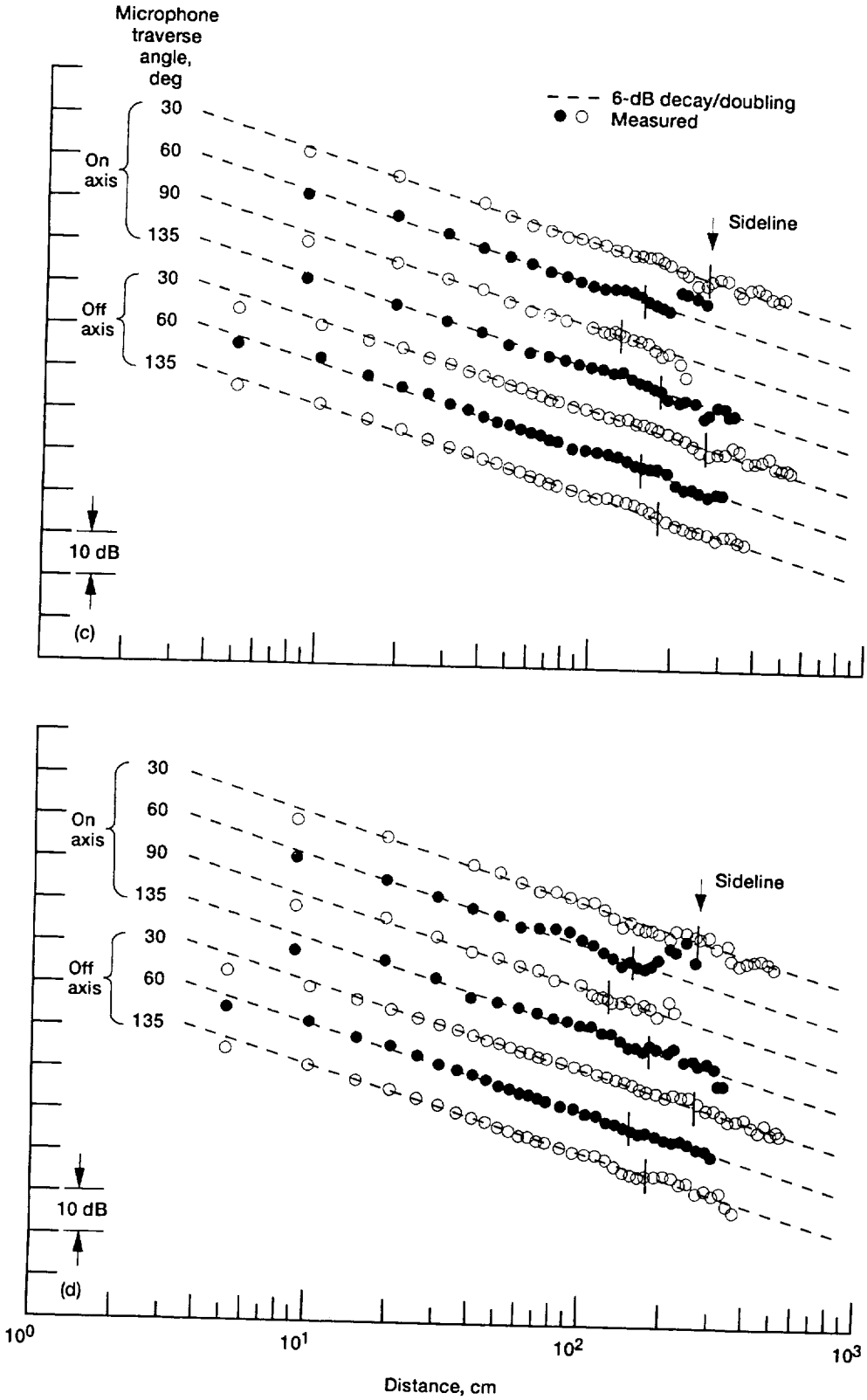

(c) 400-Hz 1/3-octave band.
(d) 500-Hz 1/3-octave band.

Figure 44.—Continued.

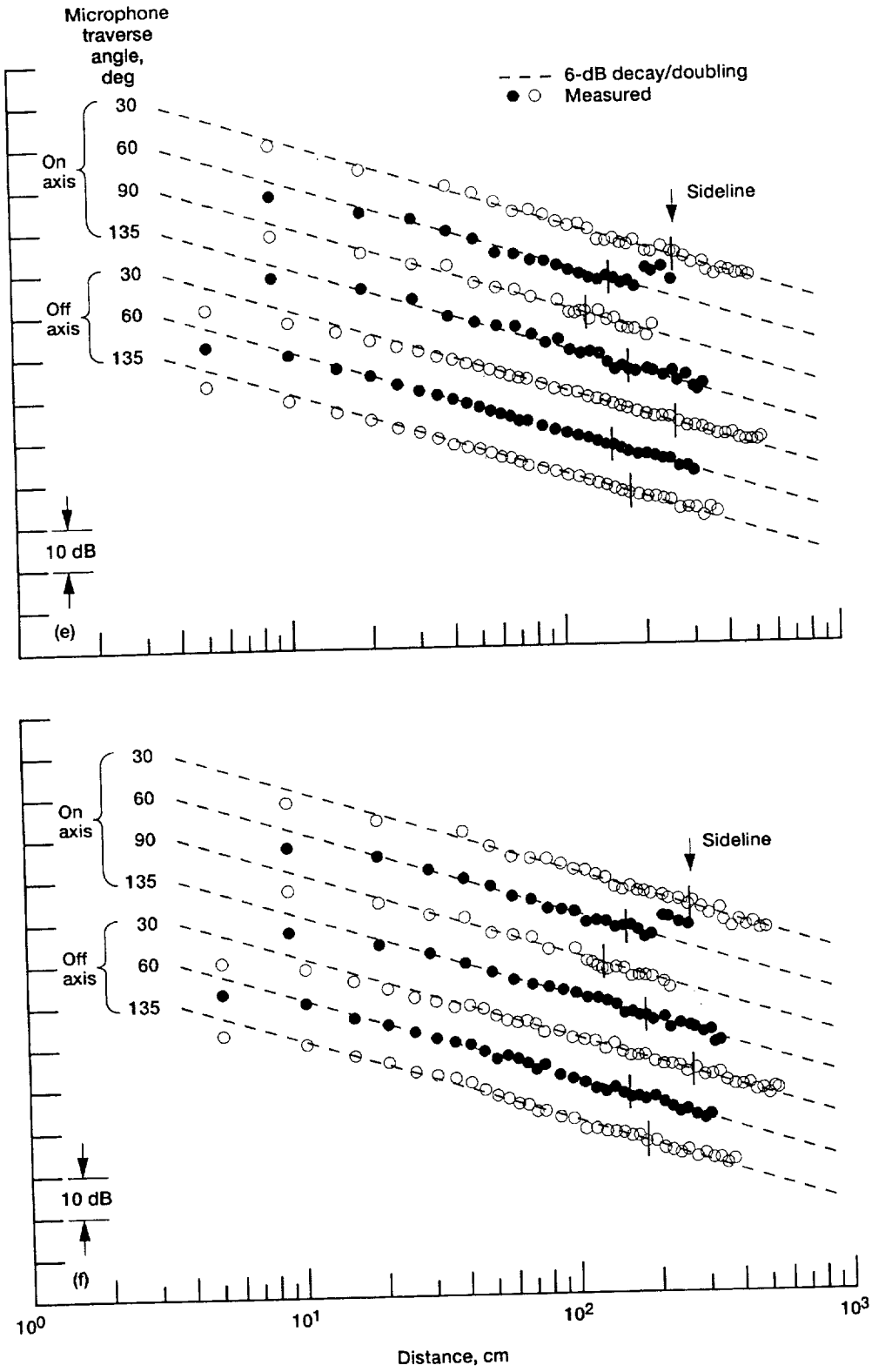

(e) 800-Hz 1/3-octave band.
(f) 1000-Hz 1/3-octave band.

Figure 44.—Continued.

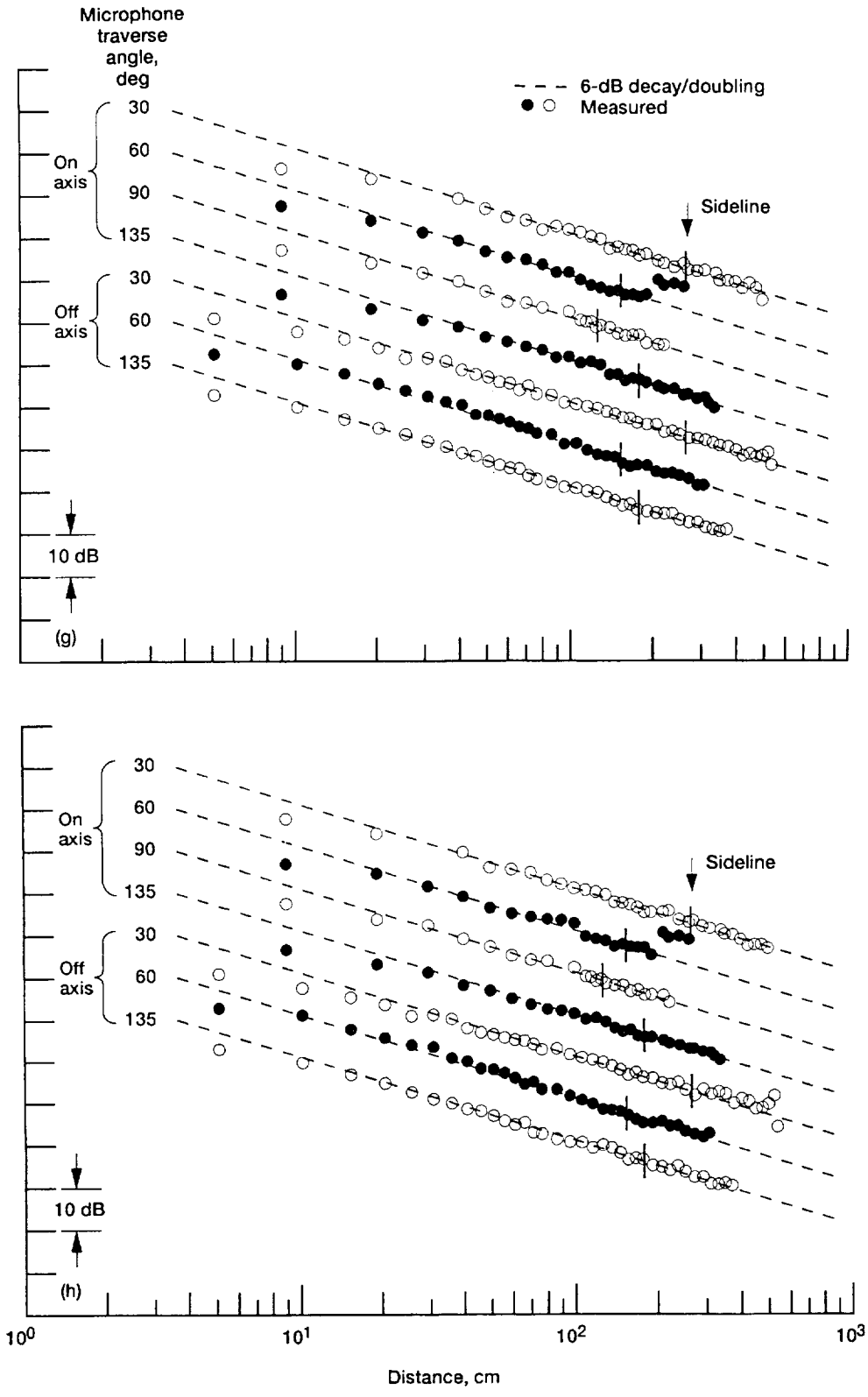

(g) 1600-Hz 1/3-octave band.
(h) 2000-Hz 1/3-octave band.

Figure 44.—Continued.

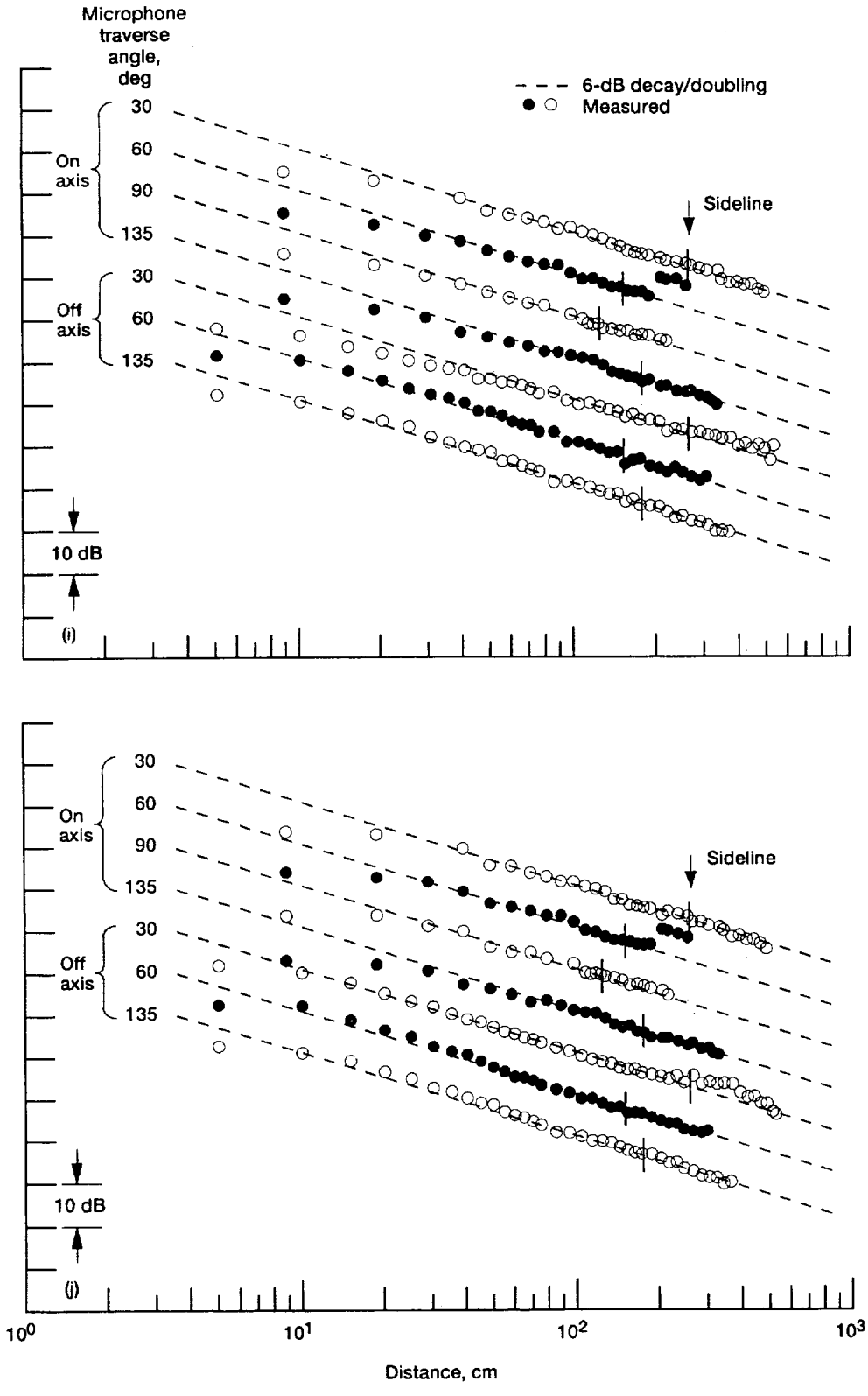

(i) 3200-Hz 1/3-octave band.
(j) 4000-Hz 1/3-octave band.

Figure 44.—Continued.

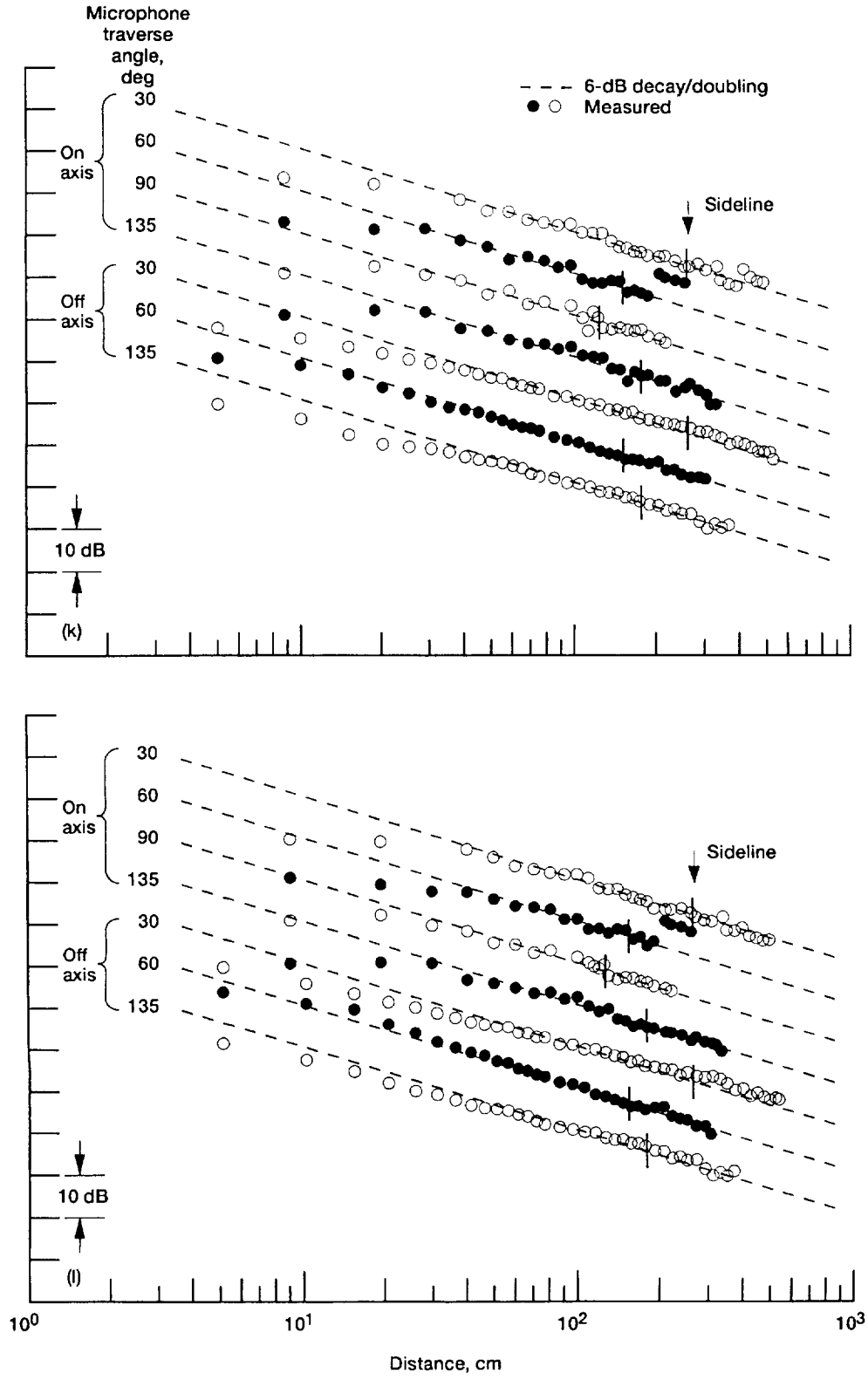

(k) 6300-Hz 1/3-octave band.
(l) 8000-Hz 1/3-octave band.

Figure 44.—Continued.

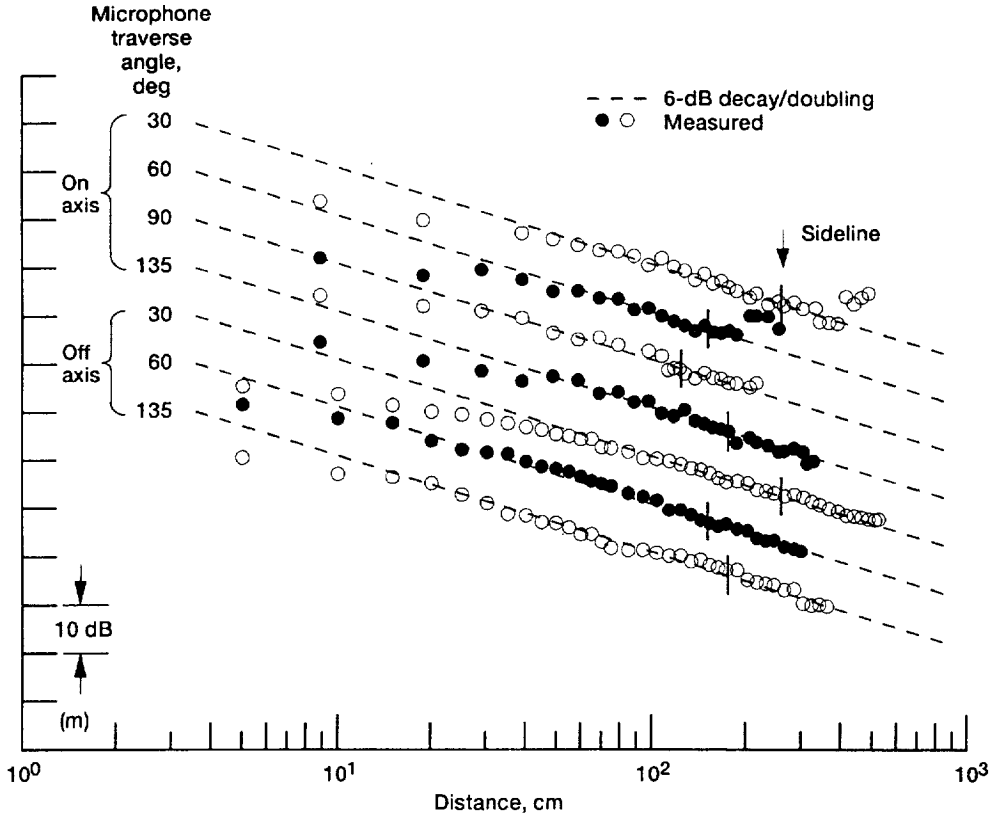

(m) 10 000-Hz 1/3-octave band.

Figure 44.—Concluded.

Appendix C—Decay with Distance Data for Pure-Tone Directional Source

Decay with distance measurements on and off the major axis are shown in figure 45 for the directional source excited by pure tones. The methodology of taking the on- and off-axis measurements with pure tones is the same as that described for broadband noise in appendix B. Each plot compares the data at a single frequency. The sideline markers in each plot represent the sideline positions for each angle as shown in figure 37. The data were compared with the 6-dB decay line and the deviations from this line are listed in table VI.

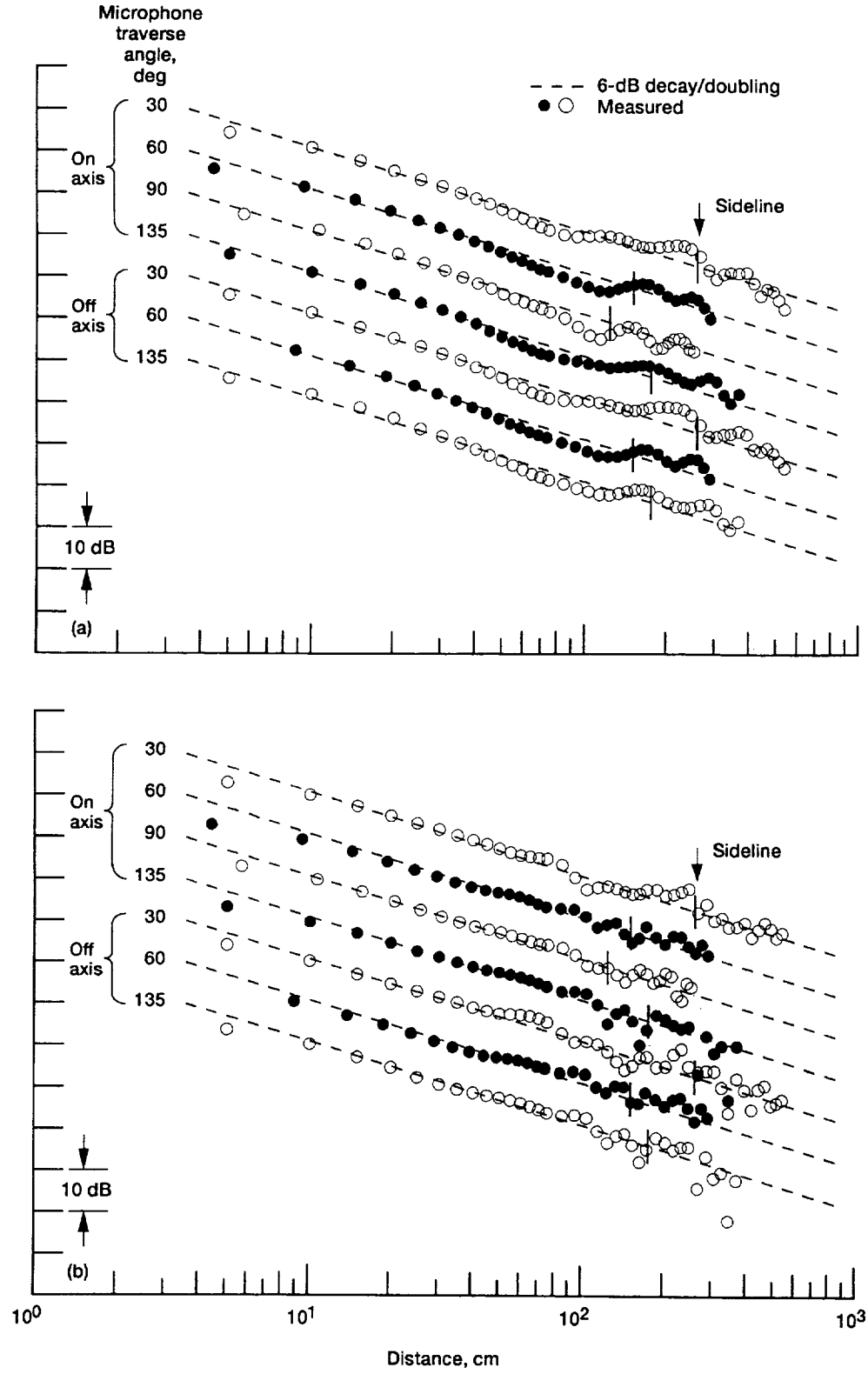

(a) 250-Hz pure tone.
(b) 500-Hz pure tone.

Figure 45.—Measured decay with distance from a pure-tone directional source; comparison between on- and off-axis measurements. Angle of source major axis for off-axis measurements: 30, source 60; 60, source 90; 135, source 105.

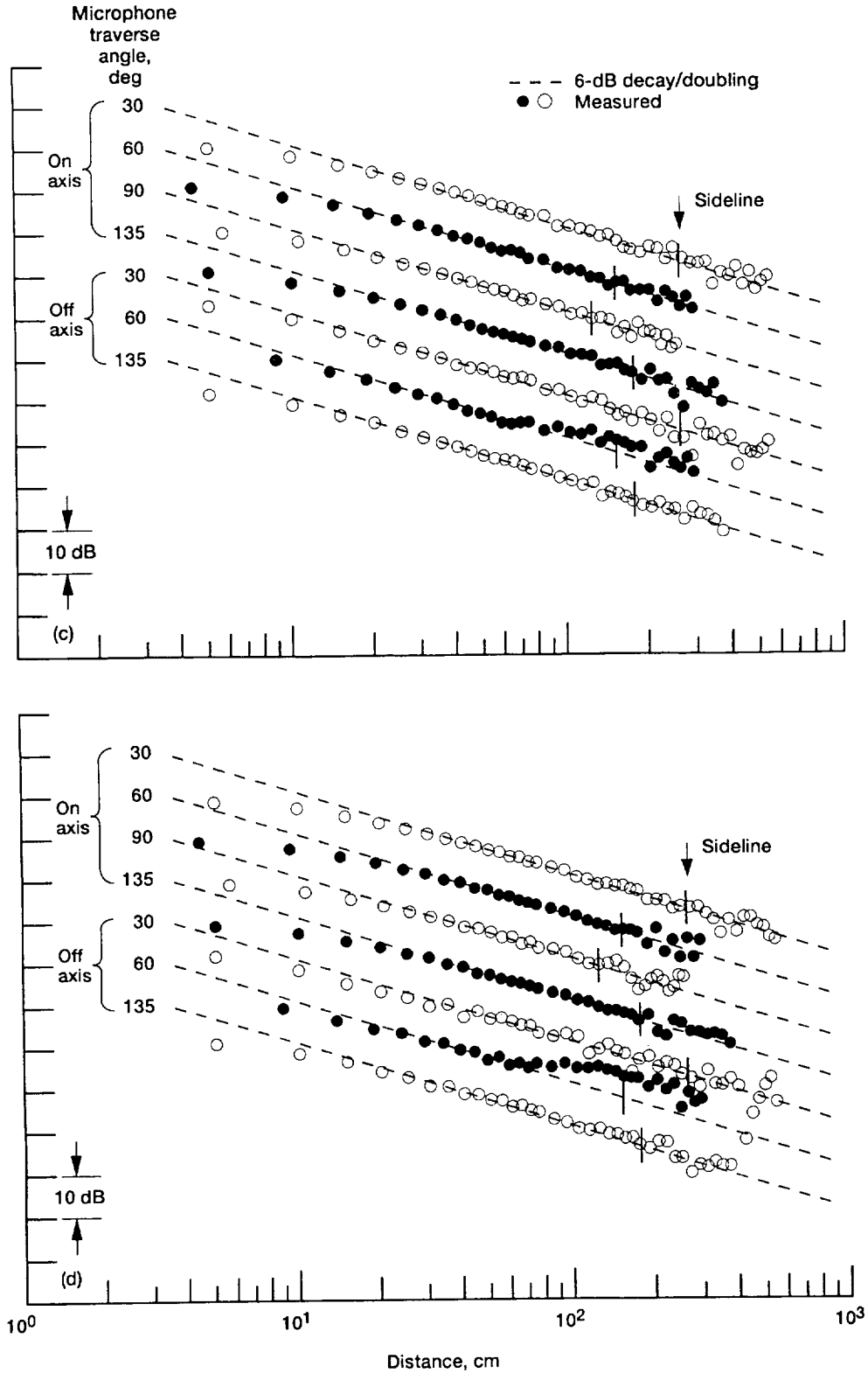

(c) 1000-Hz pure tone.
(d) 2000-Hz pure tone.

Figure 45.—Continued.

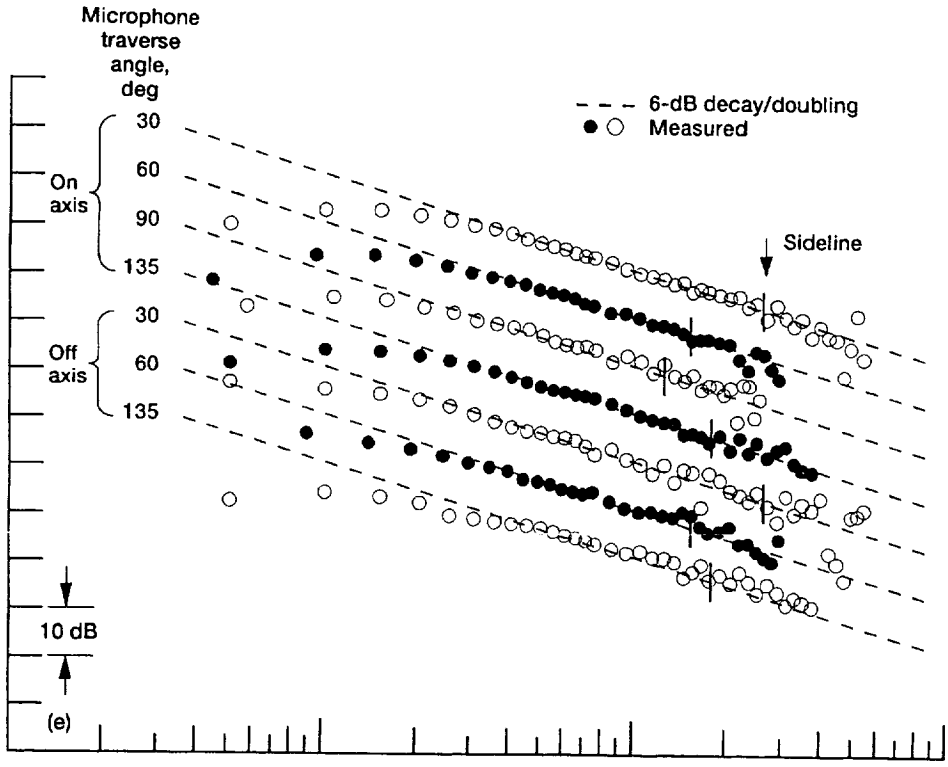

(e) 4000-Hz pure tone.

Figure 45.—Concluded.

Appendix D—Effects of Atmospheric Absorption at High Frequencies

The effects of atmospheric absorption become important at high frequencies and/or large distances. For lower frequency sound sources in the tunnel test section, such as the turboprop models (refs. 13 and 14), these effects were not important. Since the test section evaluation measurements were designed with these lower frequency sources in mind and since the frequencies were less than 10 kHz and the distances were on the order of a few meters, the data in this study were not affected by atmospheric absorption. However, more recent measurements have been made in the tunnel test section where frequencies above 10 kHz are important (ref. 18). Without making test section evaluation measurements at higher frequencies, we can note what effects atmospheric absorption may have on acoustic measurements in the test section.

There is a standard method for the calculation of atmospheric absorption (ref. 19). A summary of the calculation method is given by Shields and Bass (ref. 20) along with a method for calculating the effects of atmospheric absorption in fractional-octave bands. Bass et al. have since modified the atmospheric absorption calculations with better expressions for the vibrational relaxation times of oxygen and nitrogen (ref. 21). (It should be noted that eq. (5) in ref. 21 is incorrect. It is correctly given in eq. (3.19) of ref. 20.) Given that the atmospheric absorption of sound is a function of frequency, distance, relative humidity, ambient temperature, and ambient pressure, a complete survey of all these parameters was not possible. Calculations were conducted for a select number of 1/3-octave bands, according to the procedure outlined in reference 20, for the following parameters: relative humidity, 70 percent; ambient temperature, 293.15 K; and ambient pressure, 1 atm. In addition, the calculations assumed that the acoustic power spectral density of the source goes as f^m over any 1/3-octave band where f is the frequency and m is an integer. We chose m to equal -2 since the source would then have the high-frequency characteristics of a subsonic jet (ref. 22). Figure 46 shows decay with distance calculations with and without the effects of atmospheric absorption in six one-third-octave bands. The effects of atmospheric absorption are obvious at the higher frequencies and large distances.

Finally, we can estimate the effects of atmospheric absorption on high-frequency measurements in the treated tunnel test section. This analysis also includes the effects of treatment absorption and the effects of spherical spreading. The analytical treatment model, given in reference 3, assumes that the acoustic wavelength is much larger than any of the physical dimensions of the treatment such as fiber diameter, perforate hole diameter, perforate hole spacing, and perforated plate thickness. Thus, there is a limit to which the treatment model is accurate at high frequencies, and 40 kHz is found to be marginally within this limit. Reference 3 shows that the

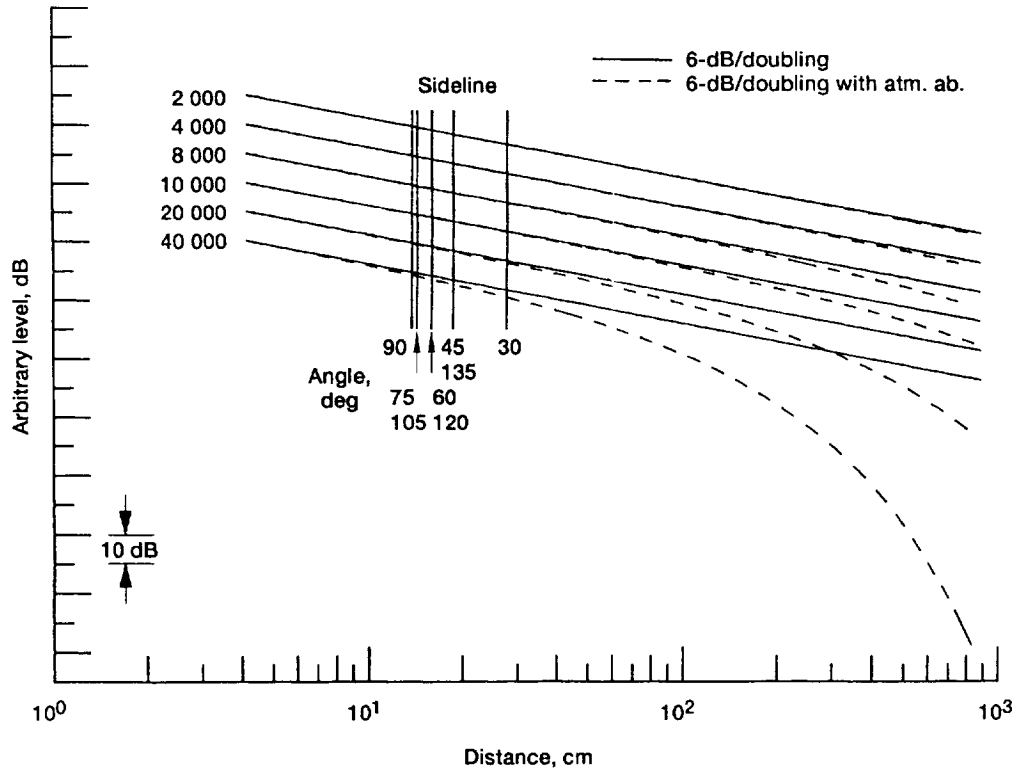

Figure 46.—Decay with distance calculations in selected 1/3-octave bands with and without atmospheric absorption.

treatment model predicts the absorption coefficient to be decreasing as the frequency approaches 10 kHz. This was supported by data. The trend continues to 40 kHz.

The incident and reflected acoustic signals, p_i and p_r respectively, at a microphone located within the test section are given by

$$p_i = \frac{A}{R_i} e^{jkR_i} e^{-aR_i} \tag{1}$$

$$p_r = \frac{A}{R_r} R_n e^{jkR_r} e^{-aR_r} \tag{2}$$

where A is the amplitude characteristic of the source, R_i is the incident path length, R_r is the reflection path length, R_n is the normal reflection coefficient, k is the wavenumber $(= 2\pi f/c)$, j is $(-1)^{1/2}$, and a is the atmospheric absorption factor. The reflected signal will interfere with the incident signal to some level, depending on the amplitude and phase of the reflected signal relative to the incident signal. This result will depend on the position where measurements are made within the test section. An estimate of the possible range of interference at a particular position is given as

$$dB_{\text{inf}} = 20 \log \frac{p_{\max}}{p_{\min}} = 20 \log \frac{|p_i| + |p_r|}{|p_i| - |p_r|} \tag{3}$$

Calculations were made for the 90° and the 30° sideline positions indicated in figure 37. The results are shown in table VII where the relation, $|R_n|^2 = 1 - \alpha$, was used to calculate R_n.

For selected individual frequencies from 10 to 40 kHz, table VII shows the decrease in absorption coefficient, as predicted, resulting in an increasing interference pattern for the plane wave. The effect of spherical spreading significantly reduces the reflection interference at the two sideline measurement locations. This effect is greatest at 90°. With angles away from 90°, the effect of spherical spreading is less along the sideline since the path length difference between the incident and reflected signals is decreasing. When atmospheric absorption is included, it has very little effect at 10 kHz. The atmospheric absorption increases until, for this case, it tends to balance out the decrease in wall absorption in the 25- to 40-kHz frequency range.

In summary, this analysis shows that high-frequency acoustic measurements, to at least 40 kHz, are possible in the tunnel treated test section to within the worst-case accuracy given for lower frequencies in the conclusions of this report. However, these results for two locations and one atmospheric condition should not be generally applied to all other possible measurement conditions in the test section.

TABLE VII.—CALCULATED RESULTS OF REFLECTION INTERFERENCE INCLUDING EFFECTS OF ATMOSPHERIC ABSORPTION

Frequency, f, kHz	Normal absorption coefficient α	Plane wave reflection interference, dB_{int} dB	Reflection interference at $a = 0$, dB_{inf}, dB		Atmospheric absorption factor, a, Np/m	Reflection interference for $a \neq 0$, dB_{inf}, dB	
			Sideline location			Sideline location	
			90°	30°		90°	30°
10	0.91	5.4	1.6	2.8	0.0136	1.5	2.7
15	.81	8.1	2.3	4.2	.0288	2.1	3.9
20	.69	10.9	3.0	5.4	.0485	2.5	4.8
25	.58	13.4	3.5	6.3	.0713	2.8	5.3
30	.48	15.8	3.9	7.1	.0961	2.8	5.6
35	.40	17.9	4.4	7.7	.122	2.8	5.6
40	.33	20.0	4.4	8.2	.148	2.7	5.6

Appendix E—Symbols

A acoustic source characteristics parameter

a atmospheric absorption factor

B measurement tracking filter bandwidth

c speed of sound

ΔdB total attenuation, $= dB_r - dB_i$

dB_{inf} level of reflection interference in, dB

d_{ij} path length difference between path i and path j

F sweep frequency range

f frequency

Δf frequency resolution

Δf_{int} frequency interval in reflection interference pattern (table II), Hz

Δf_{ij} frequency shift between signals i and j

i incident signal or incident signal path

j $(-1)^{1/2}$ in appendix D

k wavenumber

m positive or negative integer

n positive integer

p_i incident acoustic signal

p_{max} maximum signal level, eq. (3)

p_{min} minimum signal level, eq. (3)

p_r reflected acoustic signal

R_i incident path length

R_n normal reflection coefficient

R_r reflection path length

r reflected signal or reflected signal path

S sweep rate, Hz/sec

T measurement time window

t_i time for signal to travel incident path i

t_r time for signal to travel reflected path r

Δt time resolution

α normal absorption coefficient

Subscripts:

i incident signal or incident signal path

r reflected signal or reflected signal path

References

1. Rentz, P.E.: Softwall Acoustical Characteristics and Measurement Capabilities of the NASA Lewis 9×15 Foot Low Speed Wind Tunnel. (BBN-3176, Bolt, Beranek and Newman Inc.; NASA Contract NAS3-19410), NASA CR-135026, 1976.
2. Dahl, M.D.; and Rice, E.J.: Measured Acoustic Properties of Variable and Low Density Bulk Absorbers. NASA TM-87065, 1985.
3. Dahl, M.D.; and Woodward, R.P.: Comparison Between Design and Installed Acoustic Characteristics of the NASA Lewis 9- by 15-Foot Low Speed Wind Tunnel Acoustic Treatment. NASA TP-2996, 1990.
4. Diedrich, J.H.; and Luidens, R.W.: Measurement of Model Propulsion System Noise in a Low-Speed Wind Tunnel. NASA TM X-71845, 1976.
5. Ver, I.L.: Acoustical Evaluation of the NASA Langley V/STOL Wind Tunnel. NASA CR-145087, 1976.
6. Theobald, M.A.: Evaluation of the Acoustic Measurement Capability of the NASA Langley V/STOL Wind Tunnel Open Test Section with Acoustically Absorbent Ceiling and Floor Treatments. NASA CR-165796, 1978.
7. Rennison, D.C.; Wilby, J.F.; and Gordon, C.G.: Design Concepts for Sound Absorbing Linings in the Test Section of the NASA Ames 80 × 120 Foot Wind Tunnel. (BBN—3707, Bolt, Beranek, and Newman, Inc.,; NASA Contract NAS2-9549), NASA CR-152155, 1978.
8. Trebble, W.J.G.: The Acoustic Characteristics of the RAE 1.5 m Wind Tunnel. RAE Technical Report 79002, Royal Aircraft Establishment, 1979.
9. Block, P.J.W.; and Gentry, G.L.: Evaluation of the Langley 4- by 7-Meter Tunnel for Propeller Noise Measurements. NASA TM-85721, 1984.
10. Bengelink, R.L.; Doerzbacher, R.P.; and Krynytzky, A.J.: The Development and Calibration of an Acoustic Wall Transonic Test Section. AIAA Paper 86-0759, Mar. 1986.
11. Yuska, J.A.; Diedrich, J.H.; and Clough, N.: Lewis 9- By 15-Foot V/STOL Wind Tunnel. NASA TM X-2305, 1971.
12. Heyser, R.C.: Acoustical Measurements by Time Delay Spectrometry. J. Audio Eng. Soc., vol. 15, no. 4, Oct. 1967, pp. 370-382.
13. Woodward, R.P.: Measured Noise of a Scale Model High Speed Propeller at Simulated Takeoff/Approach Conditions. AIAA Paper 87-0526, Jan. 1987 (also, NASA TM-88920).
14. Woodward, R.P.; and Hughes, C.E.: Noise of a Model Counterrotation Propeller with Simulated Fuselage and Support Pylon at Takeoff/Approach Conditions. AIAA Paper 89-1143, Apr. 1989 (also, NASA TM-101996).
15. Ver, I.L.: Some Acoustical Characteristics of a Crossing-Jet Noise Source. J. Acoust. Soc. Am., vol. 57, no. 5, May 1975, pp. 1205-1206.
16. Childers, D.G.; Skinner, D.P.; and Kemerait, R.C.: The Cepstrum: A Guide to Processing. Proc. IEEE, vol. 65, no. 10, Oct. 1977, pp. 1428-1443.
17. Syed, A.A.; Brown, J.D.; Oliver, M.J.; and Hills, S.A.: The Cepstrum: A Viable Method for the Removal of Ground Reflections. J. Sound Vib., vol. 71, no. 2, July 22, 1980, pp. 299-313.
18. Krejsa, E.A.; Cooper, B.A.; Hall, D.G.; and Khavaran, A.: Noise Measurements from an Ejector Suppressor Nozzle in the NASA Lewis 9- by 15-Foot Low Speed Wind Tunnel. AIAA Paper 90-3983, Oct. 1990 (also, NASA TM-103628).
19. ANSI S1.26-1978 (R-1989): American National Standard Method for the Calculation of the Absorption of Sound by the Atmosphere. American National Standards Institute, New York, 1978.
20. Shields, F.D.; and Bass, H.E.: Atmospheric Absorption of High Frequency Noise and Application to Fractional-Octave Bands. NASA CR-2760, June 1977.
21. Bass, H.E.; Sutherland, L.C.; and Zuckerwar, A.J.: Atmospheric Absorption of Sound: Update. J. Acoust. Soc. Am., vol. 88, no. 4, Oct. 1990, pp. 2019-2021.
22. Crighton, D.G.: Basic Principles of Aerodynamic Noise Generation. Prog. Aerospace Sci., vol. 16, no. 1, Mar. 1975, pp. 31-96.